CHARLES UNIVERSITY

FACULTY OF SCIENCE

Study programme: Physical Geography and Geoecology

Mgr. Blanka Gvoždíková

RELATIONSHIP AMONG MOISTURE FLUX ANOMALIES, EXTREME PRECIPITATION, AND FLOODS IN CENTRAL EUROPE

VZTAH ANOMÁLIÍ TOKŮ VLHKOSTI, EXTRÉMNÍCH SRÁŽEK A POVODNÍ VE STŘEDNÍ EVROPĚ

Doctoral thesis

Supervisor: RNDr. Miloslav Müller, Ph.D.

Praha, 2021

I declare that I have written this doctoral thesis independently and cited all information sources and literature. The work, either in full or in part, has not been previously submitted for any other academic degree.

Prohlašuji, že jsem tuto disertační práci zpracovala samostatně a že jsem uvedla všechny použité informační zdroje a literaturu. Tato práce ani její část nebyly předloženy k získání jiného nebo stejného akademického titulu.

Praha, 28 January 2021

.....

Acknowledgements

The completion of my dissertation would not have been possible without the support of my supervisor, Dr. Miloslav Müller, to whom I am extremely grateful for the guidance throughout the studies and for valuable advice and suggestions that greatly increased the clarity of my scientific work.

Thanks should also go to the Department of Physical Geography and Geoecology of Charles University for the opportunity to complete my study here and to the Institute of Meteorology at Free University of Berlin, where I could spend several months on a traineeship supported by Erasmus+ programme. I very much appreciate the help from Prof. Stephan Pfahl and others in his working group, who encouraged me to new research perspectives and assisted with programming and the technical issues in processing reanalysis and forecast data.

For the data provided, I would like to acknowledge the European Centre for Medium-Range Weather Forecasts (ECMWF), the Global Runoff Data Centre (GRDC), the European Climate Assessment & Dataset project (ECA&D), and national hydrometeorological institutes in the Czech Republic (CHMI), Poland (IMGV), Germany (DWD), Austria (ZAMG), France (Météo-France) and Switzerland (MeteoSwiss).

Finally, many thanks to my family for all the support you have shown me.

Abstract

Floods associated with extreme precipitation are one of the most serious natural hazards, which produce substantial human and socio-economic losses in central Europe. One way to reduce the impact of flooding is by increasing preparedness with better flood forecasts and warnings, which is not possible without a proper understanding of physical processes leading to a flood hazard. However, frequent research on floods in relation to causal precipitation and synoptic conditions is usually carried out regionally, although some events often affect areas of a size of entire countries or even larger.

The thesis was focused exactly on these large-scale precipitation and flood events that occurred in the second half of the 20th century and then until 2013, for which the size of the affected area is as crucial in the extremity assessment as the magnitude of flood discharges or precipitation totals. The extremity indices used for the assessment of extreme precipitation and flood events connected both aspects. The larger area of interest defined within central Europe allowed examining the spatial structure of events, the differences between them, and their relation to conditions in the atmosphere. To connect the extremes of precipitation with extremes in atmospheric conditions, the causal circulation was evaluated quantitatively, based on the characteristics of the moisture flux at 850 hPa isobaric level in the area of extra high upward vertical velocity, which are both important ingredients for the occurrence of extreme precipitation in central Europe.

As a result, the different types of moisture flux conditions corresponded perfectly with specific seasonal and spatial patterns of extreme precipitation. There were only two main types of extreme precipitation events in central Europe, the difference between them can be explained by the seasonal distribution of anomalies of moisture flux from the respective sectors: (i) warm half-year events with prevailing northern moisture flux and affecting mainly eastern central Europe, and (ii) events with prevailing western moisture flux occurring in the west and exclusively from September to March.

Only in case of events with northern moisture flux, a close connection existed between moisture flux anomalies and precipitation extremeness. This fact allowed to consider the application of moisture flux anomalies from the northern sector in forecasting and extreme weather warnings. However, the question remained whether the predictability of moisture flux anomalies is good enough to support the correct prediction of extreme precipitation events. The results showed that the general use is probably not possible due to worse vertical velocity forecast; the approach based on moisture flux anomalies could be applied only to the largest summer precipitation events, for which the forecast was good and stable. Therefore, predicting moisture flux anomalies potentially could help to increase preparedness for the same type of precipitation events that produced the most damaging central European summer floods, such as in July 1981 and 1997, August 2002 or June 2013.

Keywords: floods, extreme precipitation, extremity index, moisture flux, predictability, central Europe

Abstrakt

Povodně spojené s extrémními srážkami jsou jedněmi z nejzávažnějších přírodních ohrožení ve střední Evropě, které mají značné ekonomické dopady na společnost. Jedním ze způsobů, jak dopady zmírnit, je zvyšovat připravenost pomocí lepších předpovědí a včasných varování před povodněmi, což ale není možné bez dokonalého pochopení fyzikálních procesů, které k povodňovému ohrožení vedou. Mnoho studií se věnuje výzkumu povodňových událostí ve vztahu k příčinným srážkám a synoptickým podmínkám, často je ale tento výzkum zaměřen jen regionálně, ačkoli některé události postihují oblasti srovnatelné s rozlohou samostatných států nebo dokonce i větší.

Tato práce byla zaměřena právě na tyto rozsáhlé srážkové a povodňové události druhé poloviny 20. století a dále až do roku 2013, u nichž je pro hodnocení extremity stejně důležitá plocha zasažené oblasti jako velikost povodňových průtoků nebo úhrny srážek. Indexy extremity použité pro hodnocení extrémních srážkových a povodňových událostí kombinovaly oba aspekty. Větší zájmové území v rámci střední Evropy umožnilo zkoumat prostorovou strukturu událostí, rozdíly mezi různými typy událostí a jejich vztah k podmínkám v atmosféře. Aby bylo možné určit souvislost mezi srážkovými extrémy a anomálními cirkulačními podmínkami v atmosféře, byla cirkulace hodnocena kvantitativně na základě charakteristik toku vlhkosti v izobarické hladině 850 hPa v místech s mimořádnou rychlostí vzestupných pohybů vzduchu, což jsou důležité složky pro vznik extrémních srážkových událostí ve střední Evropě.

Různé podmínky toku vlhkosti ve výsledku dokonale odpovídaly konkrétním sezónním a prostorovým charakteristikám extrémních srážek. V zásadě se ve střední Evropě vyskytují dva hlavní typy extrémních srážkových událostí, které lze definovat na základě sezónního rozložení anomálií toku vlhkosti z příslušných sektorů: (i) události teplého půlroku s převládajícím severním tokem vlhkosti, které postihují hlavně východ střední Evropy, a (ii) události s převládajícím západním tokem vlhkosti, které se vyskytují spíše na západě a výlučně v období od září do března.

Pouze v případě událostí se severním tokem vlhkosti existovala úzká souvislost mezi anomáliemi toku vlhkosti a extrémy srážek, což by mohlo mít potenciální využití v předpovědích a ve vydávání výstražných informací před extrémními srážkovými a povodňovými událostmi. Otázkou ale zůstává, jestli předpověď anomálií toku vlhkosti je dostatečně kvalitní, abychom jí mohli podpořit předpověď extrémních srážkových událostí. Z výsledků vyplývá, že obecné využití zřejmě není možné vzhledem k horší prediktabilitě vertikálních rychlostí; přístup založený na anomáliích toku vlhkosti lze aplikovat jen v případě největších letních srážkových událostí, kdy je předpověď anomálií toku vlhkosti stabilní. Potenciálně to může znamenat zlepšení připravenosti na tento typ srážkových událostí, které vždy vyústily ve velké středoevropské povodně, jakými byly události v červenci 1981 a 1997, srpnu 2002 nebo červnu 2013.

Klíčová slova: povodně, extrémní srážky, index extremity, tok vlhkosti, prediktabilita, střední Evropa

Table of contents

1 Introduction 6
1.1 Motivation and literature review 6
1.2 Aims of the study 9
1.2 Structure of the thesis 10

2 Study area, data and methods 12
2.1 Study area 12
2.2 Data 12
2.3 Methods 13
2.3.1 Evaluation of extensive floods 13
2.3.2 Evaluation of precipitation extremes
Paper I: Novel indices for the comparison of precipitation extremes and floods: an example from the Czech territory 14
2.3.3 Evaluation of moisture flux anomalies 27
2.3.4 Predictability assessment 27

3 Extensive floods
Paper II: Evaluation of extensive floods in western/central Europe **28**

4 Extreme precipitation events
Paper III: Spatial patterns and time distribution of central European extreme precipitation events between 1961 and 2013 ..... **40**

5 Moisture flux anomalies
Paper IV: Moisture fluxes conducive to central European extreme precipitation events **57**

6 Application in forecasting
Paper V: Predictability of moisture flux anomalies indicating central European extreme precipitation events **72**

7 Main results and discussion 90
7.1 Extreme large-scale hydrometeorological events 90
7.2 Circulation causes 91
7.3 Predictability of events 92

8 Conclusions 94
References 96

1 Introduction

1.1 Motivation and literature review

In the last 40-year period, weather- and climate-related extremes generated the majority of total losses caused by natural hazards in European countries. While heatwaves were responsible for most fatalities, windstorms along with floods caused by extreme precipitation resulted in higher economic damage (EEA, 2019). The frequency and intensity of extreme precipitation events have likely increased in Europe in last decades (IPCC, 2014; van den Besselaar et al., 2013), although the signal varies by seasons (Łupikasza, 2017), and scientists expect the rising trend to continue in the future (IPCC, 2014). It may imply a greater risk of flooding in some river basins, although there is less confidence about it because flooding also depends on factors other than precipitation. Nevertheless, the flood-related costs constantly increase but this may be the effect of increasing exposure of people and assets (IPCC, 2014). Better preparedness could reduce the impact on humans either by implementing flood protection measures that modify the event itself or by changing human behaviour and reducing vulnerability (Smith, 2004). The latter option is significantly less expensive than the construction of large dams. Besides raising hazard awareness, good flood forecasts and warnings are important, which is not possible without a sufficient skill of the quantitative precipitation forecast. However, the forecast often fails in case of extreme precipitation events due to high spatial and temporal variability of precipitation (Sukovich et al., 2014).

In central Europe, both river and flash floods are responsible for many casualties and serious economic losses. The differences between the two types of floods are in the size of the affected area and the main triggers: flash floods are locally restricted and relate to convective systems of sub-synoptic scale, while river floods are the result of rather large-scale precipitation or its combination with melting snow in winter or spring. This work primarily focused on large-scale events that often hit different basins or even countries at the same time, and therefore usually cause much more damage than flash floods (Barredo, 2007). Within river floods, those caused by extreme large-scale rainfall were of major concern, so they could be directly connected to causal synoptic-scale circulation.

Extreme precipitation and floods are rare events, which go far into the tail of the probability distribution of daily data (Zhang et al., 2011). The extremity of both the precipitation and floods can be evaluated based on point measurements, either by monitoring the exceedance of certain fixed threshold for daily precipitation totals and maximum discharges at individual gauges (Ustrnul et al., 2014) or using percentile-based threshold or return periods (Keef et al., 2009; Łupikasza, 2017), i.e. applying the concept of rarity. Both approaches appear in the literature but generally greater suitability for the spatial comparison of extremes is the advantage of using percentiles and return periods (Zhang et al., 2011). However, apart from event magnitude, there are other aspects of the extremity: duration and particularly the spatial extent of the event (Müller and Kašpar, 2014; Ren et al., 2012), which is essential for the evaluation of large-scale events, which are of special interest here. The involvement of the affected area in the evaluation of the event extremity is common even in case of other meteorological phenomena, for example, heatwaves (Lhotka and Kyselý, 2014; Valeriánová et al., 2017) or windstorms (Roberts et al., 2014; Kašpar et al., 2017). Only the sensitivity to the choice of the study area and its extent may be a disadvantage of regional evaluation techniques (Konrad, 2001). That is why Müller and Kašpar (2014) presented an event-adjusted method of evaluation of precipitation extremes, which does not depend on a certain area extent, but it optimizes the considered area, as well as the event duration.

In the case of extreme floods, one of the older methods that took into account the aspect of the affected area was presented by Francou and Rodier (1967). Among others, the method was used to evaluate the largest floods in the World Catalogue of Maximum Observed Floods compiled by Herschy (2003). However, the obtained flood extremity value related to the most affected catchment and did not consider the affected area cumulatively. In contrast, the flood extremity index recently presented by Uhlemann et al. (2010) and then by Schröter et al. (2015) considers the heterogeneous spatial extent, as it always looks at the length of the affected rivers. The list of major floods in Germany made by Uhlemann et al. (2010) included mainly floods of the cold half-year and only a few summer events, although these were sometimes the most catastrophic floods of recent decades, as was the flood in August 2002 (Ulbrich et al., 2003a) or June 2013, which was evaluated later by Schröter et al. (2015). However, the information about the extremity of these floods may be incomplete, because both affected also the Czech Republic or Austria (Blöschl et al., 2013; Ulbrich et al., 2003b; Valeriánová et al., 2013), which was not taken into account. Another, well-known summer flood from July 1997 no longer appeared in the list of Uhlemann et al. (2010), as the flood affected the area further east, especially the Oder and Vistula river basins (Kundzewicz et al., 1999).

Still, the above-mentioned summer floods arose from quite similar atmospheric conditions, when a cyclone followed the Vb track (van Bebber, 1891) or similar. During the Vb events, cyclones move from the region of Genoa to the northeast and bring Mediterranean air into central Europe. The warm and moist air turns around the centre of the cyclone, so we actually experience moisture flux from the north or the northeast (Müller and Kašpar, 2010). Simultaneously, the Alps and other west-east oriented mountains in central Europe act as an orographic barrier, which additionally forces condensation of the water vapour and enhances precipitation (Wypych et al., 2018). These conditions

are the most relevant for large-scale summer extreme precipitation and floods over large parts of central Europe (Messmer et al., 2015; Hofstätter et al., 2017) and especially significant parts of the Elbe, Oder and Danube basins (Kyselý, 2009; Nissen et al., 2014). However, the event of 2013 did not have the classic Vb character as in 2002 and 1997, multiple cyclones tracked rather westward into central Europe, affecting mainly the Elbe and Danube basins (Grams et al., 2014). Nevertheless, a persistent northern moisture flux was a common feature for the development of heavy precipitation even in 2013. A similar situation occurred during the historical floods in September 1890 or July 1903 (Brázdil et al., 2005; Elleder, 2007; Mudelsee et al., 2004) and in July 1954 (Blöschl et al., 2013). All of these historical and recent extreme events occurred in the summer half of the year and affected mainly Danube, Elbe, and/or Oder basins. Although the soil saturation also played a role in the magnitude of the flood response (Blöschl et al., 2013), exceptional precipitation in a given river basin always gave the main impulse for the catastrophic large-scale summer floods in central Europe.

Towards the west, the frequency of events due to Vb cyclones decreases, although similar but strongly deviated tracks were reported with extreme precipitation arising, for example, in the Vosges Mountains (Minářová et al., 2018). But in general, the causes of extreme precipitation and floods, as well as their seasonal distribution, change as we approach the Atlantic Ocean. Western Europe experiences extreme precipitation and flooding primarily during the cold half of the year due to zonal westerly circulation patterns associated with Atlantic frontal systems (Beurton and Thieken, 2009; Caspary, 1995; Jacobeit et al., 2003). Known cases of extreme precipitation that have resulted in a strong hydrological response include the events of December 1993, January 1995 (Kundzewicz et al., 2013; Ulbrich and Fink, 1995) or October/November 1998, which development was similar to the winter floods in the area (Müller et al., 2009a).

Central Europe thus forms a kind of transitional zone between the more frequent winter hydrometeorological extremes in the west and summer extremes in the east. These are probably the two main groups of large-scale precipitation and flood extremes in central Europe, which completely differ in their causes when the events are associated with moisture supply either from the Atlantic or Mediterranean (Sodemann and Zubler, 2010; Hofstätter et al., 2017). However, when going into details, some studies suggest larger variability of synoptic-scale patterns that induce extreme precipitation and floods in the area (Jacobeit et al., 2006; Kašpar and Müller, 2010; Wypych et al., 2018).

The connection between hydrometeorological extremes in central Europe and synoptic types is relatively well discussed in the literature (e.g. Jacobeit et al., 2006; Ustrnul and Czekierda, 2001). There are many synoptic type classifications of subjective, mixed or objective character (Huth et al., 2008). In connection with extreme precipitation and floods, the classifications are often qualitative, i.e. the circulation patterns are classified by similar fields of sea level pressure or geopotential height (Jacobeit et al., 2003; Ustrnul and Czekierda, 2001), backward air trajectories (Seibert et al., 2007), cyclone tracks (Hofstätter et al., 2017), etc. However, when associated with extreme events, Müller and Kašpar (2010) emphasized the need to add a quantitative aspect to the classification process,

which allows expressing the extremity of circulation conditions at different places. There are two reasons why they found quantitative classification more appropriate: first, a certain synoptic type (e.g. of Hess and Brezowsky, 1952) often occurs also on other days than those with precipitation extremes, and second, the identified circulation pattern may produce quite different weather over individual parts of the study area.

Such a quantitative evaluation of the synoptic–dynamical conditions can be based on anomalies of some meteorological variables, including potential vorticity, vertical velocity, or moisture flux, which appear in the literature in connection with the occurrence of hydrometeorological extremes (Froidevaux and Martius, 2016; Martius et al., 2006). Sometimes a combination of several anomalous variables was considered (Kašpar and Müller, 2014; Müller et al., 2009b). Most notably the transport of moisture seems to be essential for the emergence of precipitation and flood extremes in central Europe. A close relationship between extreme floods and intense moisture transport has been demonstrated in the Alps by Froidevaux and Martius (2016), who examined the vertically integrated variable, and by Müller and Kašpar (2011), who focused on the moisture flux at single isobaric levels. However, the moisture supply is probably not sufficient because only sustained ascent of moist air provides suitable conditions for extreme precipitation (Doswell et al., 1998; Giannakaki and Martius, 2015).

In any case, if some circulation anomalies are connected to extreme precipitation and floods, they can be used also for forecasting those events. Given that some circulation anomalies, e.g. moisture flux, are related to a larger-scale circulation, we can assume that their predictability will be better than in the case of precipitation, which is driven by more complex small-scale atmospheric processes (Lavers et al., 2016). There has been already evidence from previous studies that integrated vapour transport is more predictable than precipitation (Lavers et al., 2014), so it could support extreme precipitation forecasts even at longer lead times and improve preparedness for precipitation and flood extremes.

1.2 Aims of the study

The general aim of this work was to study hydrometeorological extremes in complex from the consequences, i.e. floods, to meteorological causes including heavy precipitation and anomalies of meteorological variables related to them. The thesis thus mentally followed the work of J. Hladný, who emphasized the need to investigate the causal synoptic conditions in the atmosphere, the induced precipitation field and the runoff response together in the so-called hydro-synoptic continuum (Hladný, 2007). Traditionally, the works on this topic concerned a certain river basin in the Czech Republic (e.g. Čekal, 2005; Šmídová, 2009), although a flood event usually affected a larger area. In contrast, the presented work examined a study area of five main river basins in central Europe so that the entire event or its substantial part could be captured. The focus was on the large-scale flood and precipitation extremes that occurred in the second half of the 20th century and at the beginning of the 21st century and that affected an area often crossing national borders in central Europe. The causal

synoptic conditions were studied in relation to extreme precipitation, which means that the synoptic causes were considered only for floods, where large-scale extreme precipitation was the main trigger.

The other part of the work was more practically focused on the predictability of precipitation and flood extremes. It is necessary to realize that precipitation forecast is the main source of uncertainty in extreme precipitation and flood warnings. Therefore, the aim was also to use the acquired knowledge about circulation causes in forecasting extreme precipitation and floods and possibly improve preparedness for these events.

Altogether, the thesis had several partial objectives:

(i) Compilation of the list of extreme flood events in central Europe, objectively evaluated by an extremity index combining the discharge magnitudes with lengths of the affected rivers. Assessment of the effect of the index settings on the results. Determination of the spatial and temporal distribution of extreme flood events.

(ii) Compilation of the list of extreme precipitation events in central Europe, objectively evaluated by an extremity index with respect to the areal precipitation extremity. Comparison of the lists of extreme floods and precipitation events. Evaluation of the precipitation events hierarchically, on different spatial levels, in order to cluster the events according to spatial patterns of precipitation. Assessment of whether the detected clusters differ significantly from each other also in terms of the seasonal occurrence of precipitation events.

(iii) Explanation of the circulation causes of extreme precipitation events in central Europe by the combined evaluation of anomalies of the atmospheric moisture flux and the upward vertical velocity, which are both important ingredients required for the extreme precipitation occurrence. Comparison of the types of events obtained with regard to similar circulation anomalies with the event clusters generated according to spatial patterns of precipitation.

(iv) Verification of the ability to use moisture flux anomalies as an additional forecasting tool, which could potentially help to predict the occurrence of extreme precipitation events in central Europe.

1.2 Structure of the thesis

The thesis is structured in the same way as the research went from consequences, i.e. floods, to the causes. It is presented as a collection of five research articles, one of which is part of the methodology section and the others form individual chapters according to the stated goals.

The following Chapter 2 defines the study area of central Europe, describes the data used during the whole study and introduces the methodology for evaluating extreme floods, precipitation, circulation causes and assessing their predictability. Within Section 2.3.2, **Paper I** describes the evaluation method of the extremity of precipitation, based on event-adjusted weather extremity

index, which combines the information about the rarity of precipitation totals, the area affected by precipitation and the duration of the event. The paper also compares different methods for assessing the extremity of precipitation and floods:

> **Paper I:** Müller, M., Kašpar, M., Valeriánová, A., Crhová, L., Holtanová, E., Gvoždíková, B., 2015. Novel indices for the comparison of precipitation extremes and floods: an example from the Czech territory. Hydrology and Earth System Sciences, 19, 4641–4652. https://doi.org/10.5194/hess-19-4641-2015.

The following are three chapters, each addressing consecutively one of the objectives (i) to (iii) and therefore presenting a different phenomenon: floods, precipitation, and moisture fluxes. The chapters refer to individual **Papers II** to **IV**:

> **Paper II:** Gvoždíková, B., Müller, M., 2017. Evaluation of extensive floods in western/central Europe. Hydrology and Earth System Sciences, 21, 3715–3725. https://doi.org/10.5194/hess-21-3715-2017.
>
> **Paper III:** Gvoždíková, B., Müller, M., Kašpar, M., 2019. Spatial patterns and time distribution of central European extreme precipitation events between 1961 and 2013. International Journal of Climatology, 39, 3282−3297. https://doi.org/10.1002/joc.6019.
>
> **Paper IV:** Gvoždíková, B., Müller, M., 2021. Moisture fluxes conducive to central European extreme precipitation events. Atmospheric Research, 248. https://doi.org/10.1016/j.atmosres.2020.105182.

Chapter 6 then informs about the potential application of moisture flux anomalies in forecasting extreme precipitation and floods. It refers to **Paper V** and addresses objective (iv):

> **Paper V:** Gvoždíková, B., Müller, M. Predictability of moisture flux anomalies indicating central European extreme precipitation events. Submitted to Quarterly Journal of the Royal Meteorological Society.

2 Study area, data and methods

2.1 Study area

Central Europe is quite a heterogeneous region in terms of extreme precipitation and floods. As mentioned above, this area is characterized by a noticeable shift in the seasonal distribution of flood and precipitation extremes in a west-to-east direction. It has natural boundaries: the Alps to the south, the Carpathian Mountains and Lesser Poland Upland to the east and the coasts of the North and Baltic seas to the northwest and the north, respectively. However, the area had to be adapted to certain hydrometric profiles to be able to assess the areal extremity of floods. Therefore, the study area of central Europe was rather defined by six main river basins: Rhine, Ems, Weser, Elbe, Oder, and Danube up to Bratislava. Hydrometric profiles enclosing our area of interest were selected as close as possible to the mouth of the rivers. The area then remained identically defined for the evaluation of extreme precipitation and circulation conditions.

2.2 Data

The data used in the thesis were of four types: hydrological and precipitation station data used for assessing the extremity of events, reanalysis and prognostic fields describing circulation conditions. Within this section, the data are described only briefly, for a more detailed description, see the data and methodology section of individual Chapters 3 to 6.

For the evaluation of extensive floods, the time series of mean daily discharge values was used for selected stations between 1951 and 2013, when most measurements were available. The data were from seven countries: the Czech Republic, Slovakia, Poland, Austria, Switzerland, Germany and the Netherlands, but they were mostly obtained from the database of the Global Runoff Data Centre (GRDC, 2020), an international archive of monthly and daily discharges. The time series was incomplete in some cases, so additional data were collected from national hydrological yearbooks, the Czech Hydrometeorological Institute (CHMI), the Austrian server eHYD (2021) and the Polish Institute of Meteorology and Water Management – National Research Institute (IMGW-PIB, 2021).

Similarly, the daily precipitation totals at selected rain gauges were collected from national hydrometeorological institutes in the Czech Republic (CHMI), Poland (IMGV), Germany (DWD – Deutscher Wetterdienst), Austria (ZAMG – Zentralanstalt für Meteorologie und Geodynamik), France (Météo-France) and Switzerland (MeteoSwiss). A large part of the data was also obtained from the European Climate Assessment & Dataset project (ECA&D; Klein Tank et al., 2002). However, due to less data coverage in the period up to the end of 1960, the evaluation of large-scale extreme precipitation was carried out only from 1961.

The period considered was further shortened during the evaluation of moisture flux anomalies, as the reanalysis data were available only from 1979. Reanalyses are gridded meteorological datasets, which provide a quite complete picture of the state of the atmosphere in the past. We can use it instead of observations, where the direct measurements are not possible. However, reanalyses are produced by a combination of observations with forecasting models (Parker, 2016). Our study employed new ERA5 reanalysis data (Copernicus Climate Change Service, 2017) from the European Centre for Medium-Range Weather Forecasts (ECMWF), which should be extended back to 1950 in the future. For the purposes of this work, reanalysis of the vertical velocity at the isobaric level of 700 hPa and air temperature, specific humidity, the zonal and meridional components of wind at the 850 hPa level were retrieved. The data from 850 hPa level were required for the calculation of the zonal and meridional moisture fluxes. The original 6-h-resolution data with a horizontal grid spacing of 0.25° was replaced by daily means from 06, 12, 18 UTC and 00 UTC of the following day to make it comparable with daily precipitation totals (from 06 to 06 UTC) used during the evaluation of extreme precipitation events.

For assessing the predictability of moisture flux, the prognostic data were not available for ERA5, but the earlier ERA-Interim model (Dee et al., 2011) had to be used instead. The same variables as for ERA5, only with lower spatial and temporal resolution, were also retrieved for reanalysis and forecast of ERA-Interim. So that it was easier to compare the "observations" and forecasts of moisture flux anomalies, but also the results for two different reanalyses. Although the reanalysis and forecast data were obtained for the period 1979 to 2018, we again focused mainly on events up to 2013, as was previously limited by the selection of flood and precipitation extremes.

2.3 Methods

2.3.1 Evaluation of extensive floods

The methodology for the identification of extreme large-scale floods was primarily based upon the approach of Uhlemann et al. (2010), when both the spatial extent of floods and the aspect of the discharge magnitudes were incorporated into an extremity index, which evaluated flood events.

The whole process consisted of several steps, which are described in more detail within methodology section of Chapter 3. Here the steps are presented in a simplified way. (i) At first, flood

peak discharges exceeding some threshold had to be identified at individual stations. A two-year return period was determined as the basic threshold. (ii) As a flood event was defined as a group of time-related flood peaks, we needed to search for simultaneously occurring significant discharge peaks at individual gauge stations in time span of several days according to the overall extent of the study area. The duration of the event was defined by the temporal distance between the individual flood peaks. (iii) The normalized peak discharges of a single event were weighted by the length of the affected river segments upstream from the respective stations and the overall extremity index was derived from the cumulative weighted discharges.

2.3.2 Evaluation of precipitation extremes

Paper I: Müller, M., Kašpar, M., Valeriánová, A., Crhová, L., Holtanová, E., Gvoždíková, B., 2015. Novel indices for the comparison of precipitation extremes and floods: an example from the Czech territory. Hydrology and Earth System Sciences, 19, 4641–4652. https://doi.org/10.5194/hess-19-4641-2015.

Hydrol. Earth Syst. Sci., 19, 4641–4652, 2015
www.hydrol-earth-syst-sci.net/19/4641/2015/
doi:10.5194/hess-19-4641-2015
© Author(s) 2015. CC Attribution 3.0 License.

Hydrology and Earth System Sciences
Open Access
EGU

Novel indices for the comparison of precipitation extremes and floods: an example from the Czech territory

M. Müller[1,2], M. Kašpar[1], A. Valeriánová[3], L. Crhová[3], E. Holtanová[3], and B. Gvoždíková[2]

[1]Institute of Atmospheric Physics AS CR, Prague, Czech Republic
[2]Faculty of Science, Charles University, Prague, Czech Republic
[3]Czech Hydrometeorological Institute, Prague, Czech Republic

Correspondence to: M. Müller (muller@ufa.cas.cz)

Received: 2 December 2014 – Published in Hydrol. Earth Syst. Sci. Discuss.: 9 January 2015
Revised: 3 November 2015 – Accepted: 5 November 2015 – Published: 24 November 2015

Abstract. This paper presents three indices for evaluation of hydrometeorological extremes, considering them as areal precipitation events and trans-basin floods. In contrast to common precipitation indices, the weather extremity index (WEI) reflects not only the highest precipitation amounts at individual gauges but also the rarity of the amounts, the size of the affected area, and the duration of the event. Furthermore, the aspect of precipitation seasonality was considered when defining the weather abnormality index (WAI), which enables the detection of precipitation extremes throughout the year. The precipitation indices are complemented with the flood extremity index (FEI) employing peak discharge data. A unified design of the three indices, based on return periods of station data, enables one to compare easily interannual and seasonal distributions of precipitation extremes and large floods.

The indices were employed in evaluation of 50 hydrometeorological extremes of each type (extreme precipitation events, seasonally abnormal precipitation events, and large floods) during the period 1961–2010 in the Czech Republic. A preliminary study of discrepancies among historic values of the indices indicated that variations in the frequency and/or magnitude of floods can generally be due not only to variations in the magnitude of precipitation events but also to variations in their seasonal distribution and other factors, primarily the antecedent saturation.

1 Introduction

Precipitation is extensively studied due to its impacts on the hydrology, geomorphology, and economy of a given region. Precipitation extremes are of special interest because impacts rapidly increase with the precipitation extremity. There are three main concepts of extremity: severity, intensity, and rarity (Stephenson, 2008). Evaluation of the extremity of past events enables one to determine return periods of heavy precipitation and to estimate the probable maximum precipitation (Řezáčová et al., 2005b). Currently, the main challenge in precipitation climatology is understanding past and possible future changes in the frequency and/or magnitude of precipitation extremes (e.g., Alexander et al., 2006). These changes could alter the frequency and/or magnitude of consequent floods. To properly assess this linkage, we need to define quantitative indices to investigate the coupling between precipitation extremes and flood events.

Floods are frequently evaluated by their severity, which can be defined as the amount of socioeconomic loss or number of casualties. For example, Barredo (2007) selected 23 flash floods and 21 river floods during the period of 1950–2005 in Europe based on two criteria: losses exceeding 0.005 % of EU GDP and/or more than 70 casualties. In contrast, severity can hardly be used for evaluation of precipitation events because the damage is usually not directly produced by the precipitation but by subsequent phenomena (floods, landslides, etc.). Moreover, factors of exposure and vulnerability can produce serious discrepancies between causes and consequences.

The concept of intensity better corresponds to physical causes; thus, it is more convenient for comparison between precipitation extremes and floods. Rodier and Roche (1984) and lately Herschy (2003) assessed the world's maximum floods with respect to their maximum instantaneous discharges. To compare the extremity of floods on various rivers, they used the Francou index, which normalizes the common logarithm of maximum discharge by the common logarithm of the catchment area. Not surprisingly, maximum floods were located in the rainiest regions.

The standard approach to the evaluation of precipitation intensity is to search data series from individual gauges using commonly accepted indices (Zhang et al., 2011), mainly those defined by the Expert Team on Climate Change Detection and Indices (ETCCDI). According to ETCCDI, precipitation extremes can be defined as days with maximum 1-day (P_1) or 5-day (P_5) precipitation total in a period. Nevertheless, the duration of events can vary widely, and the precipitation intensity usually fluctuates during the event. Begueria et al. (2009) partly took account of this fact; they used declustering of daily precipitation totals to distinguish individual precipitation events and characterized them not only by magnitude and duration but also by peak intensity.

Even more important is the spatial aspect of precipitation events. They always affect a certain area; thus, precipitation extremes should be considered to be "regional events" (Ren et al., 2012). The latter approach is necessary if the intensity of precipitation and floods is to be compared, because the size of the affected area influences the hydrological response. In our previous paper (Kašpar and Müller, 2008), we used the concept of areal precipitation intensity and evaluated precipitation events based on the weighted average of daily areal precipitation totals on 3 consecutive days. Nevertheless, Konrad (2001) demonstrated that the extremity of an event depends on the size of the considered region. As a result, the areal average disadvantages events that were violent but affected only a part of the region over which the mean is taken (e.g., an administrative unit, a catchment).

Based on the concept of intensity, extreme events occur mainly in regions that are prone to heavy rains (in the Czech Republic, such regions are along the northern state border because of the orographic precipitation enhancement). In order to reflect regional climatic differences, the concept of rarity is applied; extreme precipitation and floods can thus be detected in the whole studied region. The concept is frequently used with regard to floods, and the intensity (magnitude of the peak flow) is usually compared with return levels. If a set of extreme floods is studied, they are defined as discharges with return periods exceeding a threshold. Nevertheless, Uhlemann et al. (2010) noted that flood events frequently affect several independent catchments and introduced the concept of trans-basin floods. We adopted and adapted this approach to our data because we compared flood extremity with precipitation, which also affects more than one catchment at a given time.

Table 1. Acronyms for proposed indices and studied hydrometeorological extremes.

WEI	Weather extremity index
WAI	Weather abnormality index
FEI	Flood extremity index
EPE	Extreme precipitation event
APE	(Seasonally) abnormal precipitation event
EFE	Extreme flood event

To enable this comparison, we propose indices that are based on the point estimates of return periods of precipitation totals and peak discharges and on spatial averaging of the values (Sects. 2.1, 2.3). The method is further enriched by the aspect of precipitation abnormality with respect to the season (Sect. 2.2). We demonstrate the method using data from the Czech Republic and present three sets of events: precipitation extremes regardless of and regarding the season and extreme floods (Sect. 3.1). These sets are further compared with regard to their inter-annual (Sect. 3.2) and seasonal (Sect. 3.3) distribution. The results obtained are discussed in Sect. 4.

2 Proposed methods

We proposed three extremity indices that enable one to compare the temporal distribution of precipitation extremes and floods. The indices are based on point return period estimates of precipitation totals and peak flows, respectively, spatial averaging of their values, and optimizing the areal extent and the duration of individual events. Table 1 summarizes acronyms for proposed indices and studied hydrometeorological extremes.

2.1 Evaluation of precipitation extremity

The weather extremity index (WEI) presented in detail by Müller and Kašpar (2014) is employed in searching for extreme precipitation events (EPEs). The WEI is based on return periods of 1-day to several-day precipitation totals at individual sites. In the presented study, we used data from 711 rain gauges with data series at least 20 years long between 1961 and 2010. The return periods were assessed using the generalized extreme value (GEV) distribution (Hosking and Wallis, 1997) because it was confirmed to be a suitable model for precipitation extremes in most regions of the Czech Republic (Kyselý and Picek, 2007). The GEV distribution was applied as the parametric model for annual maxima of the totals. Parameters of the GEV distribution were estimated by means of the L-moment algorithm (Hosking and Wallis, 1997) and the region-of-influence (ROI) method (Burn, 1990). The ROI method is based on "homogenous regions", in which all regional data, weighted by a dissimilarity measure, are used for estimating parameters of the distribution of extremes at the site of interest. Although the application

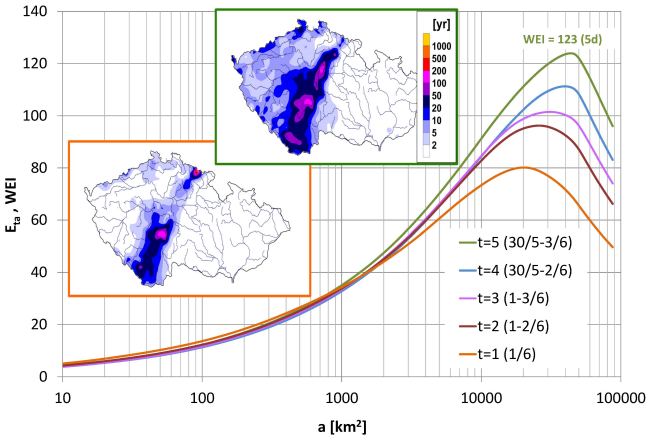

Figure 1. Determination of the WEI of the EPE in May–June 2013 by maximizing $E_{t\,a}$. The inset maps present interpolated return periods of 1-day totals on 1 June (left) and of 5-day totals from 30 May to 3 June (right).

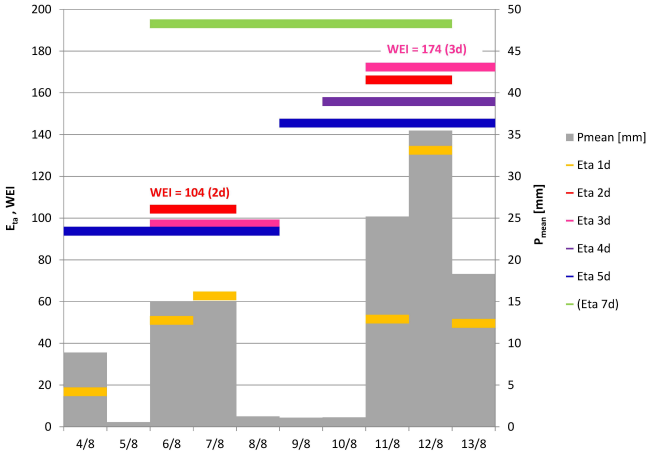

Figure 2. Mean daily precipitation totals P_{mean} in the Czech Republic (right axis) and respective maximum values of $E_{t\,a}$ on 4–13 August 2002 (color bars, left axis). Selected maximum $E_{t\,a}$ values for time windows with various lengths of t days are depicted including the hypothetical value of maximum $E_{t\,a}$ for the 7-day period of 6–12 August.

of the ROI method makes the estimations more robust than local analyses (Kyselý et al., 2011), we did not accept return periods longer than 1000 years. Instead, we set the return period to 1000 years.

The next step in the method is the interpolation of return periods from gauges in a regular grid. Experiments have demonstrated that the results are not affected by the resolution if it is constant across all studied events; we used a horizontal resolution of 2 km in the presented study. Because of the exponential nature of the GEV distribution from which the return periods are derived, common logarithms of the return period are interpolated instead of pure return period values. We chose linear kriging as the interpolation method. Using an inversion transformation, cell values of $N_{t\,i}$ are obtained; the value represents the return period of the precipitation total accumulated during t days in a cell i. The cells are then sorted in decreasing order with respect to $N_{t\,i}$ and considered within a stepwise increasing area a of n pixels (each representing 4 km^2 for the chosen horizontal resolution).

The WEI is calculated by maximizing the variable $E_{t\,a}$. This variable is defined as the common logarithm of the spatial geometric mean $G_{t\,a}$ of the return periods $N_{t\,i}$ multiplied by the radius R of a circle of the same area as the one over which the geometric mean is taken. This relationship can be expressed as

$$E_{t\,a} = \log\left(G_{t\,a}\right) R = \frac{\sum_{i=1}^{n} \log\left(N_{t\,i}\right)}{n} \frac{\sqrt{a}}{\sqrt{\pi}}. \quad (1)$$

The optimization of a is performed using a step-by-step enlarging of the area under consideration. The variable $E_{t\,a}$ initially increases as we accumulate cells with lengthy return periods; once the return periods are insufficiently long in the added cells, the value of $E_{t\,a}$ starts to decrease. When choosing a time window for which $E_{t\,a}$ reaches its maximum during the entire event, the respective maximum $E_{t\,a}$ equals the WEI. Then, it is also possible to determine the affected area a, the duration t, and the respective geometric mean of return periods $G_{t\,a}$ complying with the relationship $E_{t\,a} = \mathrm{WEI}$. The method is presented in Fig. 1, which shows the EPE from May–June 2013, which was subsequently added to the study because of catastrophic flooding observed during this time (Šercl et al., 2013). Although the maximum return period at a site belonged to the 1-day total on 1 June (Horní Maršov, 130.3 mm, > 1000 years), maximum $E_{t\,a}$ gradually increased with increasing t. The WEI corresponded to the 5-day period from 30 May to 3 June 2013.

Nevertheless, the time distribution of maximum $E_{t\,a}$ values can be more complex. Figure 2 presents such a case from August 2002, when a subsequent EPE followed the previous one after a break of only 3 days. In this case, two distinct maxima of $E_{t\,a}$ enabled us to recognize independent EPEs and determine the durations of both events (2 and 3 days, respectively). Adding an extra day would cause the $E_{t\,a}$ value to decrease. Therefore, we did not consider a longer time window (7 days); still the $E_{t\,a}$ would be even higher as the two EPEs would be aggregated. Moreover, we also decided to consider precipitation events of the length from 1 to 5 days only because the thresholds correspond with two main indices of precipitation extremes by ETCCDI (Zhang et al., 2011).

Figure 2 also shows that the extremity of precipitation with respect to the maximum $E_{t\,a}$ can substantially differ from the areal mean of daily precipitation totals. Although the mean was nearly twice as high on 11 August than on 6 August, the respective $E_{t\,a}$ maxima were the same. The advantage of the

concept of $E_{t\,a}$ is that the considered area and the time window are event-adjusted. Although comparably heavy rains were limited to southwestern Czech Republic on both days, weaker rains occurred only on the latter day throughout the whole country. These non-extreme precipitation totals generally increase the mean, whereas they are not included in the $E_{t\,a}$.

2.2 Precipitation abnormality with respect to the season

Both precipitation long-term means and extremes are not equally distributed among the seasons in most places on the Earth. In the Czech Republic, higher precipitation totals generally occur in summer (Tolasz et al., 2007). As a result, the WEI maxima are also concentrated in the summer.

However, even smaller precipitation totals can be considered to be extreme when they occur in a season when they are rare. If precipitation extremes are defined as events significantly different from seasonally normal conditions, then they can occur throughout the year. Precipitation extremes of this type will be referred to as abnormal precipitation events (APEs). They were evaluated using the weather abnormality index (WAI), which has the same design as the WEI, although it is calculated based on seasonally standardized precipitation totals.

The standardization of daily precipitation totals reflects their annual distribution. The mean, variance and skewness fluctuate significantly during the year (Fig. 3), and thus none of these parameters can be avoided in the process of standardization. The same is true for the kurtosis, which is very closely correlated with the skewness (not depicted). Furthermore, means and standard deviations are also closely correlated. Therefore, our standardization method consists of removing fluctuations of the mean μ_{d} and the skewness γ_{d} from the daily totals on individual calendar days d.

There are two types of fluctuations in the data. First, μ_{d} and γ_{d} change significantly from day to day depending on the presence or absence of heavy precipitation episodes on a given calendar day. These random fluctuations have to be smoothed using a proper time filter. Monthly means are sometimes used for these purposes, but we have excluded this method as it produces artificial edges in the data. Moving averages are only slightly better from this point of view. We used the Gaussian filter because it is considered the ideal time domain filter (Blinchikoff and Zverev, 2001). We tested several data series to identify the most appropriate length of the filter and chose Gaussian smoothing with a standard deviation σ of 30 days and a time window of 3σ. Time-smoothed values of the mean and skewness are hereinafter referred to as μ_{dG} and γ_{dG}, respectively.

Even the values of μ_{dG} and γ_{dG} fluctuate through the year because of seasonal changes in precipitation climatology. The actual daily totals P_1 are standardized using the relationship

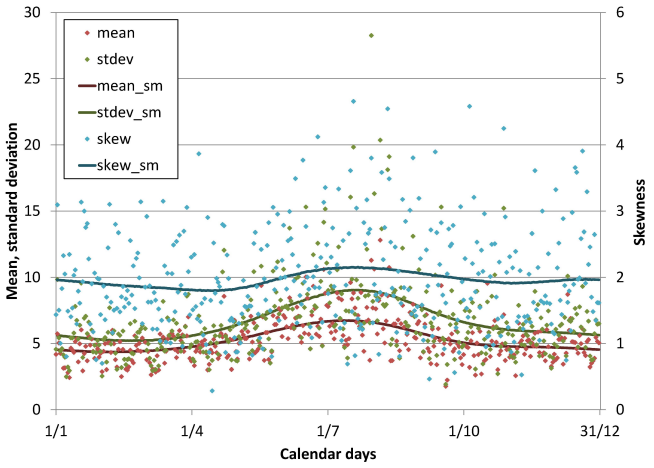

Figure 3. Annual cycle of the mean, standard deviation, and skewness of daily precipitation totals at Churáňov station. Individual points represent the values of the mean, standard deviation, and skewness calculated for each calendar day taking into account the period of 1961–2010; curves depict data smoothed using the Gaussian filter.

$$P_{\mathrm{ms}} = \overline{P}\left(\frac{P_1}{\mu_{\mathrm{dG}}}\right)^{\frac{\overline{\gamma}}{\gamma_{\mathrm{dG}}}}, \tag{2}$$

where P_{ms} is the seasonally standardized daily total, μ_{dG} is the time-smoothed mean, γ_{dG} is the time-smoothed skewness of the distribution of daily totals ≥ 0.1 mm for a calendar day d, and $\overline{P} = E(\mu_{\mathrm{dG}})$ and $\overline{\gamma} = E(\gamma_{\mathrm{dG}})$. The transformation (Eq. 2) directly standardizes the mean and skewness and indirectly standardizes the standard deviation and kurtosis of the daily data. The correction using $\overline{P}$ and $\overline{\gamma}$ induces an important feature of seasonally standardized daily totals: their mean annual sum equals the actual mean annual total. This process only redistributes precipitation amounts within the data series: seasonally standardized daily totals become higher and lower in seasons that are less and more exposed to high precipitation, respectively.

An example from the Czech mountain station Churáňov is presented in Figs. 3 and 4. The mean and skewness are at a maximum in the summer, whereas the winter is characterized by a minimum of smoothed means but a secondary maximum of the skewness. As a result, extreme totals were substantially reduced (approximately 30 %) by the dual standardization when they occurred in the summer. The winter totals were increased (20 %) due to the standardization of means; the increase in the totals due to the standardization of the skewness was present primarily in the spring (15 %). Figure 4 confirms that both moments need to be standardized to obtain a rather even annual distribution of extremes throughout the year.

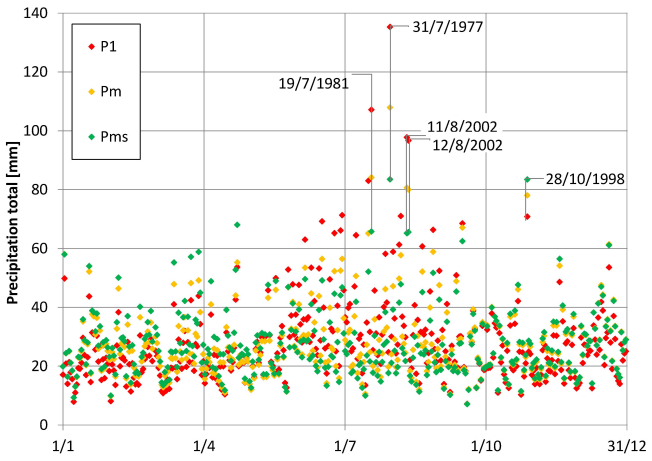

Figure 4. Daily precipitation maxima on individual calendar days at Churáňov station during the 1961–2010 period: non-standardized totals (P_1), totals standardized for the mean and variance only ($P_m = \overline{P}\,P_d/\mu_{dG}$) and fully standardized totals (P_{ms}). Dates of significant totals are indicated (day/month/yr).

2.3 Evaluation of flood extremity

To compare the precipitation and flood extremity, we also designed the flood extremity index (FEI), which is analogous to the WEI and enables us to recognize extreme flood events (EFEs). The FEI is based on return periods of peak discharges at individual sites. In the presented study, we used data from 198 Czech gauges beginning in 1961. However, only the approximate return period values of $N = 5$, 10, 20, 50, or 100 years were available. Each site represents a catchment with an area exceeding 100 km^2. If there are one or more considered sites upstream, the catchment area does not include the respective sub-catchments.

By analogy to the WEI, we combine the extremity at each site j expressed by the return period N_j with the area of the respective catchment a_j. The area of the basin indirectly represents the magnitude of the river. Return periods were considered without evaluating the possible human impact on peak discharge so the value of the FEI represents the actual course of the flood instead of the theoretical one. Nevertheless, the very high discharges that are crucial for the evaluation of an event are generally less affected by human activities (Langhammer, 2008).

The FEI is defined as the maximum of the variable F_a, which is given by the equation

$$F_a = \frac{\sum_{j=1}^{h} \left(\log\left(N_{t\,i}\right) a_j\right)}{a_a} \frac{\sqrt{a_a}}{\sqrt{\pi}}. \quad (3)$$

The aggregated area a_a consists of $h = 1, \ldots, 198$ considered catchments, which are ordered according to N_j in descending order. Return periods shorter than 5 years are assigned a value of $N_j = 1$, so that $\log(N_j) = 0$ and the respective catchments do not contribute to the resultant FEI value.

The method is demonstrated in Fig. 5, which compares flooding in the Czech territory due to the EPEs in August 1977 and in May–June 2013. The F_a curve representing the 2013 EFE increases more rapidly and starts to decrease later than in 1977; maxima of the curves depict values of the FEI. The reason is that return periods of peak discharges did not reach 50 years during the first event, whereas during the latter event, the total area of catchments corresponding to gauges with peak flows of $N_j \geq 100$ years exceeded 2000 km^2, and the value of a_a corresponding to the FEI was larger. Unlike in Fig. 1, the curves are not fluent because only discrete values of N_j were used (see above).

Because of similarities between Eqs. (1) and (3), the WEI and the FEI reach values of the same order. Nevertheless, values of the FEI were usually slightly smaller in the presented study for several reasons, primarily because all return periods between two values (20 and 50 years, for example) were assigned the lower value. Moreover, the maximum values were 100 and 1000 years when calculating the FEI and the WEI, respectively.

A serious problem is the separation of individual EFEs if additional peaks occur during a short period in the same catchments. We decided to separate EFEs with respect to EPEs. For example, we distinguished two EFEs in August 2002 because they were produced by two independent EPEs (Fig. 2). Naturally, the extremity of the latter EFE was affected not only by the latter EPE but also by the previous one in such a case; this fact can partly explain the discrepancies between the extremity of precipitation and of subsequent flooding.

Finally, we tried to assess how much the FEI can be influenced by human regulations. Therefore, a parallel calculation of the FEI was performed (hereinafter FEI_97) using only data from 97 Czech stations where no reservoir with flood protection function is present upstream. A linear dependence was detected between the FEI and the FEI_97 with Pearson correlation coefficient as high as 0.86. For example, four maximum EFEs were evaluated as the extremes regardless either the FEI or the FEI_97 is used. Only four outliers were detected when the FEI_97 was substantially reduced; it happened because flooding occurred almost only in catchments not involved in the FEI_97 calculation. Nevertheless, since the FEI_97 represents only rather small catchments, we prefer to use the FEI, which seems to be robust enough also from the viewpoint of human regulations.

2.4 Comparison of precipitation extremes and floods

Extremity of precipitation and of subsequent flooding can be compared using rankings of the events and, furthermore, by the normalized ratio of respective extremity indices:

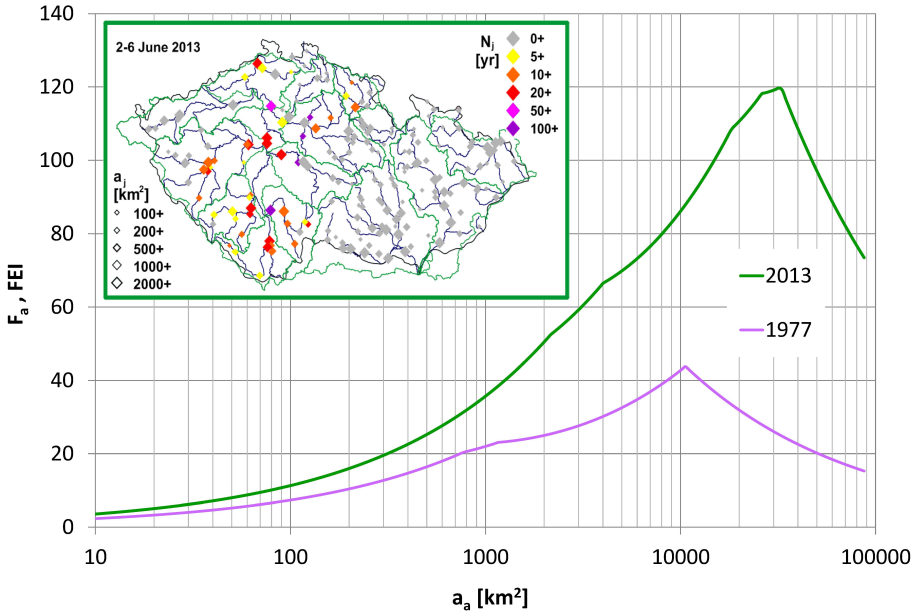

Figure 5. Evaluation of extremity of floods in May–June 2013 and in August 1977 using the FEI. The step-by-step aggregated catchments are ordered in descending order with respect to return periods recorded there. The inset map presents return periods N_j of peak discharges at gauges in 2013; blue and green curves correspond to the main rivers and watersheds, respectively.

$$C_\mathrm{e} = 100\,\frac{\mathrm{FEI}}{\mathrm{WEI}} \tag{4}$$

and

$$C_\mathrm{a} = 100\,\frac{\mathrm{FEI}}{\mathrm{WAI}}. \tag{5}$$

Values significantly above and below average resulting from Eqs. (4) and (5) indicate that the hydrological response to the precipitation event was most likely affected by factors other than only the extremity of precipitation. One of these factors may be antecedent saturation. This parameter can be expressed, e.g., using the antecedent precipitation index (Köhler and Linsley, 1951) spanning 30 days (API_{30}) before the first day of the EPE/APE, which is calculated using the relationship

$$\mathrm{API}_n = \sum_{i=1}^{n} P_i\, k^{n-i+1}, \tag{6}$$

where P_i is the daily total during the ith day of the period under consideration spanning $n = 30$ days, and the constant k represents evapotranspiration; the generally accepted value of k is 0.93 for the Czech Republic (Brázdil et al., 2005).

One of important climatological aspects of EPEs, APEs, and EFEs is their seasonal distribution. To analyze this distribution, we adopted the directional characteristics method (e.g., Black and Werritty, 1997), which was applied also to floods on selected Czech rivers by Čekal and Hladný (2008). Individual extreme events are depicted in a radial diagram where directions of vectors, which originate in the diagram's center and end in the signs representing individual events, account for calendar days. In contrast to the abovementioned papers, we modified the method so that signs representing individual events are not located on a unit circle but their distance from the diagram's center is proportional to the WEI, WAI, or FEI. The resultant diagram better represents the seasonality of extremes because strong events are assigned greater weighting.

3 Application to the Czech Republic

3.1 Precipitation extremes and floods

Although the WEI, the WAI, and the FEI itself are independent of thresholds, it was necessary to limit their values to constrain the sets of events that would be classified as EPEs, APEs, and EFEs. This step was performed because there are no natural limits dividing extreme from non-extreme events. In fact, the extremity of events gradually decreases with even smaller differences among the events as less-extreme events are considered. We selected the 50 events of each type so that one extreme event occurs per year on average. Sets of EPEs, APEs, and EFEs during the period of 1961–2010 in the Czech Republic are listed in Fig. 6.

The sets of EPEs, APEs, and EFEs partly overlap. We identified 22 precipitation extremes that were classified both as EPEs and APEs. More than a half of the EPEs and nearly 50 % of the APEs produced EFEs. If only the warm half of the year (MJJASO) is considered, the number of EFEs pro-

	EPEs					APEs					EFEs		
	EPEs + APEs												
						APEs + EFEs							
	EPEs + APEs + EFEs												
Rank-ings	First day [yyyy-mm-dd]	Duration [days]	WEI	Area [10^3 km^2]	C_e [%]	First day [yyyy-mm-dd]	Duration [days]	WAI	Area [10^3 km^2]	C_a [%]	First day [yyyy-mm-dd]	FEI	Area [10^3 km^2]
1	1997-07-04	4	**178.3**	38.2	70	1997-07-03	5	**133.6**	28.4	93	2002-08-12	**180.9**	35.8
2	1981-07-17	4	**177.3**	44.9	39	1981-07-18	3	**130.9**	31.0	53	2006-03-28	**139.4**	48.2
3	2002-08-11	3	**174.3**	55.1	104	2010-09-25	3	**126.4**	29.1	22	1997-07-07	**124.3**	20.2
4	1983-08-01	5	**148.3**	39.5	8	2002-08-11	3	**126.3**	43.0	143	1981-03-10	**77.5**	19.5
5	2006-08-03	5	**122.9**	38.6	15	1986-12-28	5	**109.0**	42.1	42	1981-07-20	**69.4**	16.7
6	2007-09-05	2	**115.8**	35.6	25	2007-09-05	3	**105.2**	27.0	28	2010-05-17	**65.9**	7.6
7	1977-07-31	3	**113.5**	44.1	35	1983-08-01	5	**101.2**	32.2	12	2002-12-30	**62.4**	18.5
8	1985-08-06	4	**109.2**	35.6	41	2010-01-08	3	**96.8**	33.5	0	2002-08-07	**60.8**	9.1
9	2002-08-06	2	**104.3**	20.7	58	2005-01-20	1	**86.1**	45.6	0	1988-03-26	**59.0**	16.9
10	1979-06-17	1	**102.5**	24.7	34	1970-02-20	4	**81.3**	47.6	23	2010-06-02	**48.2**	8.2
11	1979-09-21	4	**97.0**	37.9	0	1964-10-08	2	**79.9**	18.0	0	2000-03-09	**48.1**	6.7
12	2010-09-25	3	**91.5**	31.3	31	1978-05-07	1	**78.9**	17.9	49	2005-03-17	**47.3**	11.1
13	1978-08-07	2	**87.1**	25.5	32	1993-12-19	2	**78.5**	34.3	59	1982-01-06	**47.0**	9.9
14	2010-08-06	2	**81.7**	17.2	54	2002-08-06	2	**77.3**	14.3	79	1993-12-21	**46.0**	5.9
15	1964-08-08	3	**77.9**	18.3	21	1979-06-17	1	**76.8**	17.0	45	1986-12-30	**45.5**	10.4
16	2001-07-20	1	**73.7**	22.9	12	1974-12-05	4	**75.0**	19.0	40	1985-08-07	**44.7**	8.3
17	1986-05-27	4	**71.5**	26.3	37	1979-03-29	2	**72.1**	17.8	0	2010-08-07	**44.2**	4.9
18	2006-05-26	2	**70.1**	18.4	56	1985-08-06	4	**69.3**	27.6	64	1980-07-21	**43.9**	6.2
19	2006-06-29	1	**67.7**	15.3	64	2002-03-19	5	**68.9**	19.0	23	1977-08-22	**43.8**	10.6
20	1991-07-31	3	**67.1**	30.9	20	2004-03-23	3	**66.5**	28.4	0	2006-06-30	**43.3**	4.0
21	1997-07-17	5	**66.4**	45.7	29	1962-10-31	2	**66.5**	18.1	0	1985-05-20	**43.0**	5.9
22	1978-05-07	1	**64.0**	19.2	61	1977-07-31	3	**65.5**	30.9	60	1965-06-05	**41.3**	5.7
23	1985-05-17	5	**61.0**	10.5	70	2006-01-01	3	**65.0**	14.0	0	1962-05-14	**40.5**	7.4
24	1992-06-23	1	**57.1**	10.9	8	2004-01-11	3	**64.9**	40.1	10	1977-08-01	**39.6**	5.1
25	1968-06-08	3	**56.8**	15.6	28	1995-09-14	2	**62.6**	10.5	0	2006-05-27	**39.3**	5.8
26	1995-09-14	2	**55.9**	14.8	0	1970-11-21	2	**61.7**	21.6	15	1978-05-08	**39.0**	6.3
27	1995-08-28	2	**55.7**	34.7	0	2006-05-26	2	**61.5**	15.7	64	1962-03-31	**38.2**	7.8
28	1977-08-21	2	**55.5**	35.0	79	1961-10-17	4	**61.4**	14.5	0	2009-06-23	**37.7**	3.6
29	1965-07-17	1	**54.1**	13.8	59	1980-10-12	2	**60.9**	31.8	0	1996-05-13	**35.4**	4.7
30	1996-07-08	1	**51.6**	37.2	0	1990-02-26	3	**59.3**	34.5	0	1966-07-23	**35.0**	5.7
31	1986-12-28	5	**50.4**	19.0	90	1978-08-07	2	**57.3**	19.0	48	1979-06-17	**34.7**	4.9
32	1994-08-25	1	**49.8**	18.8	10	1996-02-19	1	**56.1**	10.7	0	1972-08-21	**34.2**	4.3
33	1977-08-10	1	**49.6**	10.4	0	2010-08-06	2	**55.7**	7.8	79	1987-03-28	**34.0**	6.3
34	1998-06-10	4	**49.4**	38.3	0	1986-05-27	4	**55.6**	22.1	48	1965-06-10	**33.3**	6.8
35	2009-06-22	3	**49.0**	13.9	77	1998-10-28	2	**55.3**	28.3	53	1970-07-19	**32.9**	3.3
36	1963-06-14	2	**48.3**	22.1	0	1968-01-14	1	**54.5**	31.7	18	1976-11-17	**32.0**	3.2
37	1970-08-02	1	**48.1**	6.1	9	1983-05-01	1	**54.3**	9.9	25	1965-07-16	**31.9**	3.5
38	1970-07-16	3	**47.9**	13.2	69	1979-11-16	5	**53.1**	19.5	0	1987-04-04	**30.9**	3.4
39	1972-08-20	2	**47.1**	5.4	73	2010-05-16	2	**51.9**	4.3	127	1996-09-07	**30.8**	2.8
40	1964-10-08	2	**46.9**	19.3	0	1967-09-07	5	**51.7**	29.6	24	1974-12-08	**30.2**	4.8
41	1998-10-28	5	**46.2**	21.7	63	2009-04-17	1	**51.5**	10.0	0	1998-10-29	**29.2**	4.9
42	1967-09-08	4	**45.9**	24.7	27	1982-03-18	2	**50.0**	26.0	21	2007-09-06	**29.1**	2.2
43	2007-06-21	2	**42.5**	5.1	0	2000-03-08	2	**48.7**	10.3	99	2010-09-28	**28.4**	3.3
44	1976-09-15	3	**42.4**	13.6	0	1995-01-25	1	**48.5**	11.8	39	1978-08-09	**27.8**	2.0
45	1988-09-02	1	**42.0**	20.7	0	1964-08-08	3	**48.3**	7.7	34	1977-02-23	**27.2**	3.3
46	2010-05-16	2	**41.7**	4.2	158	1976-09-16	2	**48.1**	13.3	0	1986-05-30	**26.8**	3.9
47	1966-07-22	4	**41.4**	13.4	85	1969-11-24	3	**48.1**	22.4	0	1982-01-31	**26.5**	3.1
48	2004-09-22	2	**41.2**	19.5	0	2004-09-22	2	**47.9**	20.1	0	1969-03-13	**26.3**	2.3
49	1998-07-22	1	**41.0**	2.0	60	1991-11-16	1	**46.9**	24.6	0	1986-06-05	**26.2**	3.3
50	1962-05-13	2	**40.9**	16.9	99	1987-12-18	1	**46.6**	25.4	15	1998-07-23	**24.6**	0.7
	2013-05-30	5	**123.2**	43.3	97						2013-06-02	**119.6**	33.3

Figure 6. EPEs, APEs, and EFEs in the Czech Republic, 1961–2010. Colors denote the assignment of events to one or more types of extremes; the ratios of the FEI to the WEI and to the WAI are designated the C_e and C_a, respectively. For comparison, an extra event from May–June 2013 is represented by values of the WEI and the FEI.

duced by EPEs increases to 75 %. This fact suggests that the magnitude of causal precipitation is the main factor conditioning most of floods in the Czech Republic. Nevertheless, we also identified cases in which the hydrological response to an EPE was too small or too big. These events confirm that flooding is also significantly influenced by other factors, which are further discussed in Sect. 4.2.

3.2 Inter-annual variability of extremes

The temporal distribution of extreme events during the period of 1961–2010 is shown in Fig. 7. Regardless of the type of extremes (EPEs, APEs, and EFEs), there are certain common features of their variations in time. One such feature is the below-normal frequency and magnitude of all types of extremes during the first 16 years of this time period. The situation dramatically changed in 1977, when three EPEs occurred in the span of less than 1 month; two of them produced EFEs (Fig. 6). Similar conditions occurred during the following 2 years. Moreover, the second and the fourth highest values of the WEI were recorded in July 1981 and August 1983, respectively. The wet years of 1985–1986 ended a decade of all types of extremes with above-normal frequency and magnitude.

In contrast, the following decade of 1987–1996 was lacking in hydrometeorological extremes. EFEs were completely absent from the warm half of the year (MJJASO) and did

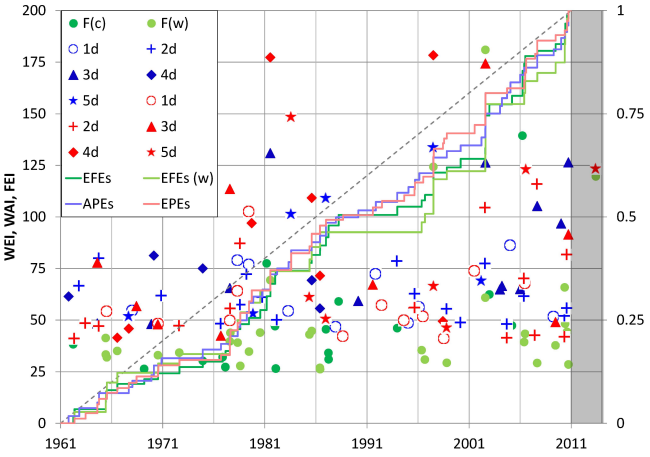

Figure 7. Temporal variability of extreme events, 1961–2010, in the Czech Republic. The red, blue, dark green, and light green symbols denote EPEs, APEs, EFEs during colder half of the year (NDJFMA), and EFEs during warmer half of the year (MJJASO), respectively. The symbol shapes denote the duration (no. of days) of EPEs and APEs. The curves express relative cumulative values (right axis) of the WEI, the WAI, and the FEI (dark green denotes all seasons, light green denotes warmer half-years only).

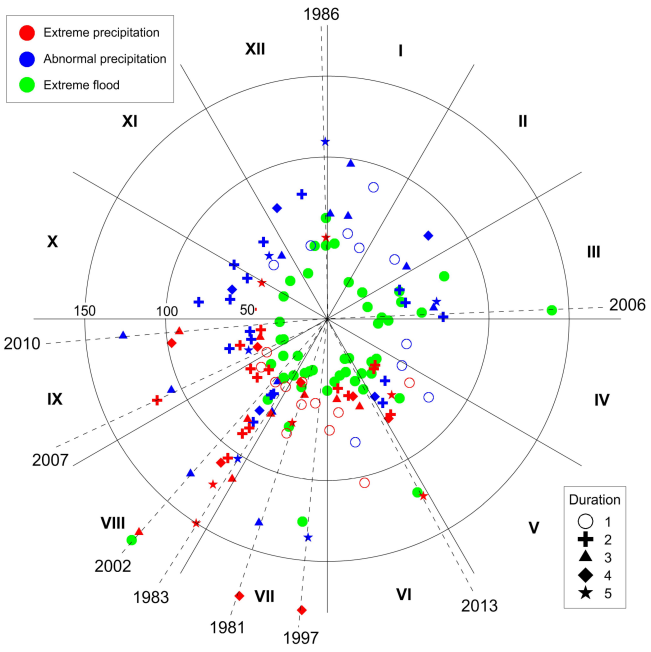

Figure 8. Seasonal distribution of extreme events in the Czech Republic, 1961–2010. EPEs were evaluated using the WEI (red), APEs using the WAI (blue), and EFEs using the FEI (green). Values of the indices are depicted by the distance of symbols from the center of the diagram. The shape of symbols depicts how many days the precipitation event lasted.

not occur again until 1996. The rest of the 1990s would also be considered to be below normal if July 1997 were not included. The first of two EPEs in this month exhibited maximum values of both the WEI and WAI. Similar values were also observed 5 years later, in August 2002. Compared to similarly strong precipitation events in the early 1980s, these two events produced much greater flooding. The last 5 years of the study period were characterized by an abnormally high number of extremes, which were concentrated primarily in 2006 and 2010. If the 2013 flood were considered, four maximum EFEs occurred recently approximately every 5 years.

3.3 Seasonal distribution of extremes

The seasonal distribution of EPEs was significantly unequal during the period of 1961–2010 (Fig. 8). Based on the selected threshold, these events occurred from May to December. Nevertheless, only three such events occurred since October, all rather weak. The months of greatest activity were clearly July and August, when the five highest values of WEI were noted. The level of activity during the first half of August was particularly pronounced: this time period was the seasonal peak in EPEs during the period of 1961–2010.

Naturally, APEs were distributed more equally from season to season during the 1961–2010 period than were the EPEs (Fig. 8). We noted at least one event in every calendar month. From October to March, the distribution of APEs was very uniform in terms of both the number of events and the magnitude. The values of the WAI were less than 100 with only one exception, which occurred during the 5 days from 28 December 1986 to 1 January 1987. This event was so exceptional that it also qualified as an EPE (see above). In contrast, only one APE was noted in April. This event and two others in the first half of May lasted only 1 day each.

The seasonal distribution of EFEs partly correlates with the seasonality of precipitation extremes, but it is also significantly affected by snow accumulation during the winter and by changes in the saturation of basins. As a result, we identified three main periods when the frequency of EFEs is increased: (i) the period from May to August, when most of the EPEs occur; (ii) the second half of December and early January, when the values of the WAI are slightly increased in comparison with the months before and after; and (iii) March and very early April, when the values of the WAI are not very high. Mainly the last period is affected by thawing. The rest of April is characterized by a distinct break both in precipitation and flood events. As in the winter apart from December, only weak EFEs occurred during the fall, when, in contrast, APEs were frequently noted. September appears to be the month with maximum differences between precipitation and flood extremity; nevertheless, the EFEs remained small although several high EPEs were noted then.

4 Discussion of results

4.1 Comparison with standard indices

In this section, the presented evaluation of precipitation and flood events is compared with standard methods mentioned in Sect. 1.

Regarding precipitation extremes, they are usually detected by maximum daily totals P_1 at any individual rain gauge (Ustrnul et al., 2015) or by areal precipitation means A_d during d days, for example, for $d = 2$ days (Konrad, 2001). The first approach is commonly used in the Czech Republic: Štekl et al. (2001) analyzed days during the period of 1876–2000 when a daily total reached at least 150 mm anywhere in the Czech Republic. The Czech maximum occurred on 29 July 1897 when a P_1 of 345.1 mm was measured at the Nová Louka gauge in the Jizerské Hory Mts. Indeed, this event was the maximum P_1 ever recorded in central Europe (Munzar et al., 2011).

Figure 9 compares 50 maximum WEI values with maximum P_1 and areal 1-, 2-, and 3-day means during the EPEs. It demonstrates that areal precipitation means generally decrease with decreasing WEI values, but it is not fully true for point daily totals. As a result, the ranking of precipitation events significantly depends on the evaluation criterion. For example, daily point maxima were above 200 mm on 20 August 1972 and 22 July 1998 but the 1-day areal means were only 5.2 and 7.3 mm, respectively. The affected area was very small in both cases (see Fig. 6). In 1972, strong precipitation affected a large area but mainly outside the Czech state border (Müller et al., 2009), whereas the 1998 case was due to a strong convective storm within a limited area (Řezáčová and Sokol, 2003). Thus, the WEI seems to be a good compromise between the two standard approaches.

In contrast, there were many significant EPEs with high areal totals but without any point daily total exceeding 150 mm. For example, the second largest EPE in July 1981 was characterized by P_1 of only 122.0 mm but extra high areal totals (absolute maximum of A_1) produced the third largest EFE during MJJASO (Fig. 6). A still lower daily maximum (only 97.6 mm) was recorded during the historical case on 2 September 1890 when the 3-day areal precipitation total (1–3 September) was nearly as high as in August 2002 and subsequent flooding was only slightly less catastrophic (Řezáčová et al., 2005a). The WEI reached very high value in July 1981 because the index reflects the size of the affected area and the fact that heavy rains occurred not only in mountains but also in lowlands where they are rare.

Moreover, some precipitation events lasted virtually only 1 day (e.g., 23 June 1992) but others lasted 3 or even more days (e.g., 4–7 July 1997). The first case is not properly evaluated by the areal 3-day mean total and the latter by the areal 1-day mean while the WEI accommodates to the real duration of the events. All abovementioned examples demonstrate the advantage of the WEI, which combines the intensity of precipitation with its spatial extent and reflects also duration of precipitation events.

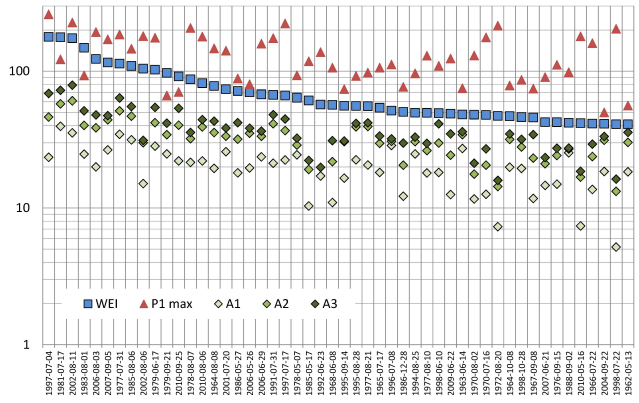

Figure 9. EPEs characterized by the WEI, maximum daily precipitation total [mm] at a site (P_1), and areal mean precipitation total [mm] in the Czech Republic recorded during 1 day (A_1), 2 days (A_2), and 3 days (A_3).

Precipitation extremes are usually evaluated regardless the season when they occurred. Recently, Ramos et al. (2014) suggested an index ranking daily precipitation extremes, which employs 1-day precipitation totals normalized by their climatology on the given calendar day. The index can be hardly compared with the WAI because Ramos et al. (2014) do not reflect duration of precipitation events. Nevertheless, we decided to accumulate daily values of their index on individual days of the APEs and compare the sums (hereinafter called RI) with the WAI values (Fig. 10).

Naturally, the WAI is more closely related to the WEI than the RI. Values of the WAI are higher than the WEI from September to the middle of May and lower in the rest of the year. Values of the RI seem to be a bit more equally distributed through the calendar year but they correspond less to the precipitation extremity. It can be demonstrated by the comparison of two July events: the maximum EPE from the beginning of July 1997 is represented by only the 16th highest RI value but significantly less extreme event from 1977 reached the 6th highest value of the RI though the turn of July and August is the top season of heavy rains in the Czech Republic. A possible reason can be the fact that daily precipitation totals are not normally distributed but the RI standardizes them only by the mean and the variance.

Finally, the FEI was compared with the Francou index (FI) and the index by Uhlemann et al. (2010) (hereinafter UI); see Sect. 1. Data from only eight large Czech catchments were at our disposal: Labe in Brandýs, Otava in Písek, Berounka in Beroun, Vltava in Prague, Labe in Děčín, Odra in Bohumín, Morava in Strážnice, and Dyje in Doní Věstonice/Nové Mlýny. We considered the maximum FI value from the eight catchments and the UI representing all these catchments together. To enable the comparison, the FEI was recalculated again using data from only the eight gauges (here-

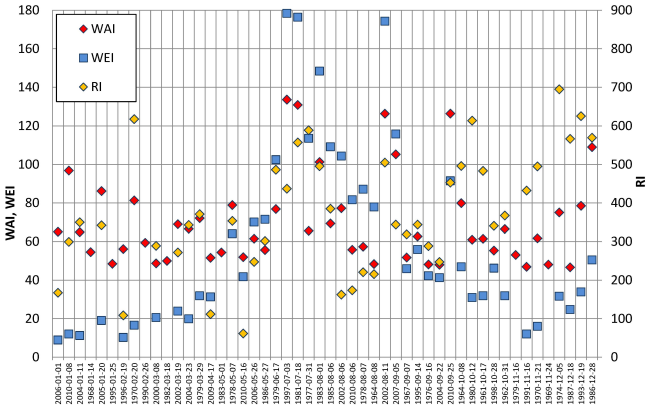

Figure 10. APEs characterized by the WAI, the WEI, and values of the index RI according to Ramos et al. (2014). The 50 APEs are ordered with respect to the calendar day in the increasing order.

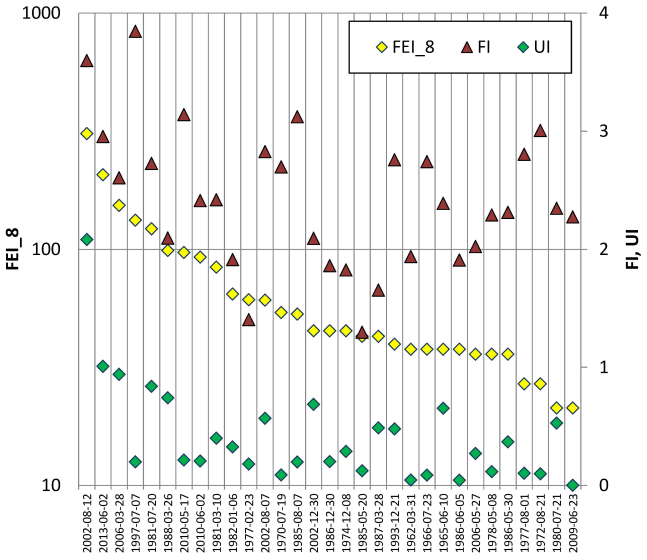

Figure 11. EFEs characterized by the FEI, the index by Uhlemann et al. (2010) (UI), and by the maximum Francou index (FI) calculated within eight selected large Czech catchments.

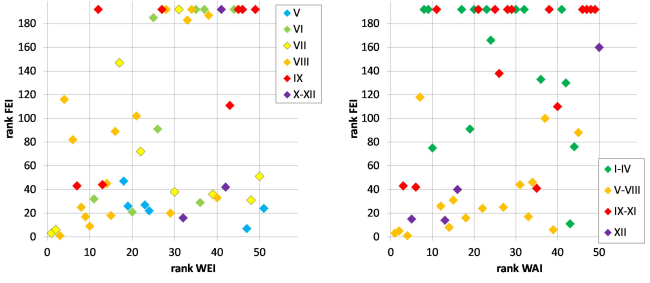

Figure 12. Relationship between rankings of 50 maximum EPEs (left)/APEs (right) and rankings of subsequent floods in various months (distinguished by colors). Precipitation events, whose hydrological response was too small (no peak flow with return period at least 5 years), are depicted at the top of the diagram.

inafter FEI_8). Only 31 of EFEs reached the FEI_8 values above zero (Fig. 11). Even such a rough comparison of the indices shows that the FEI is a compromise between the FI representing the most affected catchment and the UI, which emphasizes the size of the affected area even more than the FEI. The difference between the FI and the UI was mainly evident in July 1997 when the floods were extreme in the eastern part of the Czech Republic but no flood occurred in the western part.

4.2 Relationship between precipitation extremes and floods

Though many precipitation extremes correspond with EFEs, there are still discrepancies between the WEI and the FEI and even greater discrepancies between the WAI and the FEI values. For example, the fourth largest EPE did not produce an EFE in August 1983; in fact, this EPE resulted in very limited flooding ($C_e = 8\,\%$; see Fig. 6). Several factors affected the hydrological response of this event. These include unusually low antecedent saturation (mean API_{30} only 9.3 mm) and a moderately even distribution of rainfall over 5 days, whose maximum occurred on the second day of the event. Regulation processes by the dams could also play a role; nevertheless, Brázdil et al. (2005) confirm that no even unaffected peak flow with the return period of 2 or more years occurred at Vltava River in Prague even though the catchment belonged to the most affected by heavy rains.

All these factors will be studied in the future together with spatial patterns of precipitation to elucidate the discrepancies between individual precipitation and flood events. One of the factors to be considered should be the season when an EPE occurred, as discussed in Sect. 3.3. The important role of this factor is confirmed by Fig. 12. It is clear that the hydrological effect of an EPE is typically strong in May, more ambiguous in summer, and considerably weaker in September. The very last event from the turn of May and June 2013 also supports this conclusion ($C_e = 97\,\%$; see Fig. 6). If an EPE occurs in the last month of the year, it can also produce rather big flooding, although such events are very rare.

The hydrological effect of APEs (Fig. 12) is substantially reduced in the winter, early spring (most likely due to precipitation in the form of snow), and autumn. In contrast, if precipitation events are sufficiently high to qualify as APEs in the late spring and summer, they are usually flood producing; surprisingly, this was also the case with all APEs in December. A subsequent detailed study of intra-annual variations in precipitation patterns is necessary to explain these findings.

However, seasonality can hardly explain the difference in flood activity between two periods with unusually high EPEs (1977–1986 and 1997–2010). The FEI exceeded 50 in association with only two EFEs during the first period, whereas

this has occurred six times since 1997 (Fig. 7). Several factors most likely explain the difference: (i) if two or more EPEs appeared during one year in the first period, they were separated by a much longer interval than in the latter period (the shortest interval between two EPEs was 8 days in 1977 but only 3 days in 2002); (ii) in cases of EPEs following one after another, the magnitude decreased in the first period (WEI decreasing from 113.5 to 49.6 in July/August 1977) but increased in the second period (WEI increasing from 104.3 to 174.3 in August 2002); (iii) just before the main EPEs, the mean antecedent saturation was much lower on 17 July 1981 (24.6 mm) and on 1 August 1983 (9.3 mm) than on 4 July 1997 (34.5 mm) and on 11 August 2002 (50.1 mm because of the above-mentioned preceding EPE); and (iv) the EPEs in 1981 and 1983 lasted 1 day longer than those in 1997 and 2002. It demonstrates that changes in a flood regime can also occur without significant changes in only the magnitude of precipitation events.

5 Conclusions

The paper presents three indices for evaluation of hydrometeorological extremes. In contrast to common indices, the presented indices reflect not only maxima of precipitation amounts and peak discharges at individual gauges but also the rarity of values, the size of the affected area, and the duration of precipitation. Besides that, the aspect of precipitation seasonality was considered, which enables the detection of precipitation extremes throughout the year. A unified design of the presented indices enables one to easily compare interannual and seasonal distributions of precipitation extremes and large floods.

The application of the indices to the Czech territory demonstrates that this approach enables one to compare the extremity of precipitation and consequent floods rather than when precipitation events are evaluated only by the maximum precipitation total at one station. Extreme floods correspond to precipitation extremes; nevertheless, not only the magnitude of precipitation extremes influences the hydrological response but also the season, the antecedent saturation and other factors. The study confirms that variations in the frequency and/or magnitude of floods can be due to not only variations in the magnitude of precipitation events but also variations in these factors.

Additional detailed studies are necessary for elucidating the way in which seasonality influences the hydrological effect of precipitation extremes. This effect could be due to seasonal differences in evapotranspiration or to possible seasonal variations in the attributes of the precipitation itself. The events can differ, e.g., in the spatial distribution of precipitation within the affected area or in the temporal concentration of precipitation during the event (intensity can increase, remain the same or decrease). In addition, various circulation conditions could explain the differences among the extremes (Kašpar and Müller, 2010). In a next step, we plan to explore the dependences on the circulation extremity index (Kašpar and Müller, 2014), which completes the set of tools for studying the pathway of causation from circulation to precipitation and runoff.

Acknowledgements. The research presented in this study is supported by the Czech Science Foundation under the GACR P209/11/1990 project. Precipitation and runoff data were provided by the Czech Hydrometeorological Institute. We would also like to thank J. Kyselý and L. Gaál from the Institute of Atmospheric Physics in Prague for implementing the ROI method.

Edited by: U. Ehret

References

Alexander, L. V., Zhang, X., Peterson, T. C., Caesar, J., Gleason, B., Klein Tank, A. M. G., Haylock, M., Collins, D., Trewin, B., Rahimzadeh, F., Tagipour, A., Rupa Kumar, K., Revadekar, J., Griffiths, G., Vincent, L., Stephenson, D. B., Burn, J., Aguilar, E., Brunet, M., Taylor, M., New, M., Zhai, P., Rusticucci, M., and Vazquez-Aguirre, J. L.: Global observed changes in daily climate extremes of temperature and precipitation, J. Geophys. Res., 111, D05109, doi:10.1029/2005JD006290, 2006.

Barredo, J. I.: Major flood disasters in Europe: 1950–2005, Nat. Hazards, 42, 125–148, 2007.

Begueria, S., Vicente-Serrano, S. M., Lopez-Moreno, J. I., and Garcia-Ruiz, J. M.: Annual and seasonal mapping of peak intensity, magnitude and duration of extreme precipitation events across a climatic gradient, northeast Spain, Int. J. Climatol., 29, 1759–1779, 2009.

Black, A. R. and Werritty, A.: Seasonality of flooding: a case study of North Britain, J. Hydrol., 195, 1–25, 1997.

Blinchikoff, H. J. and Zverev, A. I.: Filtering in the time and frequency domain, Scitech Publishing, Raleigh, USA, 2001.

Brázdil, R., Dobrovolný, P., Elleder, L., Kakos, V., Kotyza, O., Květoň, V., Macková, J., Müller, M., Štekl, J., Tolasz, R., and Valášek, H.: Historical and recent floods in the Czech Republic, in: History of weather and climate in the Czech lands, vol. 7, Masaryk University, Brno, Czech Republic, 370 pp., 2005.

Burn, D. H.: Evaluation of regional flood frequency analysis with a region of influence approach, Water Resour. Res., 26, 2257–2265, 1990.

Čekal, R. and Hladný, J.: Analysis of flood occurrence seasonality on the Czech Republic territory with directional characteristics method, AUC Geographica, 43, 3–14, 2008.

Herschy, R. W. (Ed.): World catalogue of maximum observed floods, IAHS Press, Wallingford, IAHS-AISH Publ. 284, 285 pp. + supplement, 2003.

Hosking, J. R. M. and Wallis, J. R.: Regional Frequency Analysis: An Approach Based on L-Moments, Cambridge University Press, New York, 1997.

Kašpar, M. and Müller, M.: Selection of historic heavy large-scale rainfall events in the Czech Republic, Nat. Hazards Earth Syst. Sci., 8, 1359–1367, doi:10.5194/nhess-8-1359-2008, 2008.

Kašpar, M. and Müller, M.: Variants of synoptic patterns inducing heavy rains in the Czech Republic, Phys. Chem. Earth, 35, 477–483, 2010.

Kašpar, M. and Müller, M.: Combinations of large-scale circulation anomalies conducive to precipitation extremes in the Czech Republic, Atmos. Res., 138, 205–212, 2014.

Köhler, M. A. and Linsley, R. K.: Predicting the runoff from storm rainfall, US Weather Bureau Research Paper no. 34., Washington, 9 pp., 1951.

Konrad, C. E.: The most extreme precipitation events over the Eastern United States from 1950 to 1996: Considerations of scale, J. Hydrometeorol., 2, 309–325, 2001.

Kyselý, J. and Picek, J.: Regional growth curves and improved design value estimates of extreme precipitation events in the Czech Republic, Clim. Res., 33, 243–255, 2007.

Kyselý, J., Gaál, L., and Picek, J.: Comparison of regional and at-site approaches to modelling probabilities of heavy precipitation, Int. J. Climatol., 31, 1457–1472, 2011.

Langhammer, J.: Modelling the impact of anthropogenic modifications to river channels on the course of extreme floods. Case study: August 2002 flood, Blanice River basin, Czechia, Geografie, 113, 237–252, 2008.

Müller, M. and Kašpar, M.: Event-adjusted evaluation of weather and climate extremes, Nat. Hazards Earth Syst. Sci., 14, 473–483, doi:10.5194/nhess-14-473-2014, 2014.

Müller, M., Kašpar, M., and Matschullat, J.: Heavy rains and extreme rainfall-runoff events in Central Europe from 1951 to 2002, Nat. Hazards Earth Syst. Sci., 9, 441–450, doi:10.5194/nhess-9-441-2009, 2009.

Munzar, J., Ondráček, S., and Auer, I.: Central European one-day precipitation records, Moravian Geographical Reports, 19, 32–40, 2011.

Ramos, A. M., Trigo, R. M., and Liberato, M. L. R.: A ranking of high-resolution daily precipitation extreme events for the Iberian Peninsula, Atmos. Sci. Let., 15, 328–334, 2014.

Ren, F. M., Cui, D. L., Gong, Z. Q., Wang, Y. J., Zou, X. K., Li, Y. P., Wang, S. G., and Wang, X. L.: An objective identification technique for regional extreme events, J. Climate, 25, 7015–7027, 2012.

Řezáčová, D. and Sokol, Z.: A diagnostic study of a summer convective precipitation event in the Czech Republic using a nonhydrostatic NWP model, Atmos. Res., 67–68, 559–572, 2003

Řezáčová, D., Kašpar, M., Müller, M., Sokol, Z., Kakos, V., Hanslian, H., and Pešice, P.: A comparison of flood precipitation in August 2002 with historical extreme precipitation events from the Czech territory, Atmos. Res., 77, 354–366, 2005a.

Řezáčová, D., Pešice, P., and Sokol, Z.: An estimation of the probable maximum precipitation for river basins in the Czech Republic, Atmos. Res., 77, 407–421, 2005b.

Rodier, J. A. and Roche, M. (Eds.): World catalogue of maximum observed floods, IAHS Press, Wallingford, IAHS Publ. 143, 1984.

Šercl, P., Tyl, R., and Pecha, M.: The course and the extremity of the June 2013 floods, Meteorologické zprávy, 66, 197–202, 2013.

Štekl, J., Brázdil, R., Kakos, V., Jež, J., Tolasz, R., and Sokol, Z.: Extreme daily precipitation totals during 1879–2000 in the Czech territory a their synoptic causes, Národní klimatický program České republiky 31, Prague, Czech Republic, 140 pp., 2001.

Stephenson, D. B.: Definition, diagnosis, and origin of extreme weather and climate events, in: Climate Extremes and Society, edited by: Diaz, H. F. and Murnane, R. J., Cambridge University Press, New York, 11–23, doi:10.1017/CBO9780511535840.004, 2008.

Tolasz, R., Míková, T., Valeriánová, A., and Voženílek, V. (Eds.): Climate atlas of Czechia, Czech Hydrometeorological Institute, Prague, Czech Republic, 256 pp., 2007.

Uhlemann, S., Thieken, A. H., and Merz, B.: A consistent set of trans-basin floods in Germany between 1952–2002, Hydrol. Earth Syst. Sci., 14, 1277–1295, doi:10.5194/hess-14-1277-2010, 2010.

Ustrnul, Z., Wypych, A., Henek, E., Maciejewski, M., and Bochenek, B.: Climatologically based warning system against meteorological hazards and weather extremes: the example for Poland, Nat. Hazards, 77, 1711–1729, 2015.

Zhang, X. B., Alexander, L., Hegerl, G. C., Jones, P., Klein Tank, A., Peterson, T. C., Trewin, B., and Zwiers, F. W.: Indices for monitoring changes in extremes based on daily temperature and precipitation data, WIREs Clim. Change, 2, 851–870, 2011.

2.3.3 Evaluation of moisture flux anomalies

As heavy precipitation is mainly a result of ascending low-level moist air (Doswell et al., 1998), information about vertical velocity and zonal and meridional moisture fluxes was used together for the evaluation of circulation conditions during large-scale precipitation events. To each of the reference events, a variant of moisture flux conditions was assigned with regard to four directional sectors of moisture flux: west, east, south and north.

The evaluation of moisture flux anomalies is described in detail in the data and methods section in Chapter 5. To summarize briefly, the process can be divided into several steps: (i) Transformation of the daily absolute values of zonal and meridional moisture fluxes into relative values with respect to their climatology; (ii) Finding grid points with extra high upward vertical velocity on each day of reference events; (iii) Calculation of a geometric mean of relative values of zonal and meridional moisture fluxes over all such grid points for each event; (iv) Assignment of the most significant anomaly of the moisture flux from a given direction to each event.

2.3.4 Predictability assessment

Although the geometric means calculated for the evaluation of moisture flux anomalies represented the rarity of moisture flux values, they did not reflect the real total amount of transported water vapour during the event over a certain area. Such a parameter was needed to compare precipitation and moisture flux extremes and in case of the reasonable connection between them, it was possible to use the parameter as support for predicting precipitation extremes.

The accumulated ascending moisture flux, as referred in Chapter 6, reflected moisture flux accumulations over areas of extra high upward vertical velocity and was calculated by the vector sum of the accumulated zonal flux (the larger of the western and eastern fluxes) and the meridional flux (the larger of the southern and northern fluxes). It was calculated for both reanalysis and forecast when the results were compared day by day based on exceeding a certain threshold. The four possible combinations of forecasts (yes/no) and reanalysis (yes/no) then specified the elements of a 2×2 contingency table (hits, false alarms, misses and correct negatives), which can be used to calculate a large variety of categorical statistics (Wilks, 2011).

For the assessment of the predictability of vertical velocity and moisture fluxes separately, the Pearson correlation coefficient between the grid points of a single pair of reanalysis/forecast fields was computed. However, the method operates rather on anomalies of values, after which it is called anomaly correlation. Since it allows the predictability of different variables to be compared, the results for vertical velocity and moisture fluxes could also be compared with the predictability of precipitation.

3 Extensive floods

Paper II: Gvoždíková, B., Müller, M., 2017. Evaluation of extensive floods in western/central Europe. Hydrology and Earth System Sciences, 21, 3715–3725. https://doi.org/10.5194/hess-21-3715-2017.

Hydrol. Earth Syst. Sci., 21, 3715–3725, 2017
https://doi.org/10.5194/hess-21-3715-2017
© Author(s) 2017. This work is distributed under
the Creative Commons Attribution 3.0 License.

Hydrology and Earth System Sciences
Open Access
EGU

Evaluation of extensive floods in western/central Europe

Blanka Gvoždíková[1] **and Miloslav Müller**[1,2]

[1]Faculty of Science, Charles University, Prague, Czech Republic
[2]Institute of Atmospheric Physics AS CR, Prague, Czech Republic

Correspondence to: Blanka Gvoždíková (gvozdikb@natur.cuni.cz)

Received: 22 September 2016 – Discussion started: 27 October 2016
Revised: 23 April 2017 – Accepted: 6 June 2017 – Published: 21 July 2017

Abstract. This paper addresses the identification and evaluation of extreme flood events in the transitional area between western and central Europe in the period 1951–2013. Floods are evaluated in terms of three variants on an extremity index that combines discharge values with the spatial extent of flooding. The indices differ in the threshold of the considered maximum discharges; the flood extent is expressed by a length of affected river network. This study demonstrates that using the index with a higher flood discharge limit changes the floods' rankings significantly. It also highlights the high severity events.

In general, we detected an increase in the proportion of warm half-year floods when using a higher discharge limit. Nevertheless, cold half-year floods still predominate in the lists because they generally affect large areas. This study demonstrates the increasing representation of warm half-year floods from the northwest to the southeast.

1 Introduction

Hydrological events, especially floods, are serious natural hazards in western and central Europe (Kundzewicz et al., 2005; Munich Re, 2015). Several extreme floods occurred in western and central Europe, e.g., in August 2002, January 2003, March/April 2006, and June 2013. The last was one of the largest in some river basins over the last 2 centuries (Blöschl et al., 2013).

In addition to river floods, flash floods affect this part of Europe, although these are mostly local events that usually produce less damage (Barredo, 2007). Therefore, we are interested in extensive floods affecting several river basins. Uhlemann et al. (2010) call these floods trans-basin. They are usually triggered by persistent heavy rainfall and/or snowmelt. Differences in the causes of river floods can be detected between the western and central parts of Europe. Western Europe experiences flooding primarily during the cold half of the year due to zonal westerly circulation systems (Caspary, 1995; Jacobeit et al., 2003). Towards the east, warm half-year floods become more frequent. This is largely due to cyclones moving along the Vb pathway described by van Bebber (1891). These cyclones move from the Adriatic in a northeasterly direction (e.g., Nissen et al., 2014), and the "overturning" moisture flux brings warm and moist air into the central part of Europe (Müller and Kašpar, 2010). However, it is not possible to delineate the borders of western and central Europe precisely with respect to differences in their flood events because of a broad transitional zone where both types of flooding occur.

An extremity index is useful for comparing individual flood events and determining their overall extremity. Various indicators and indices are used for the assessment of extreme events (including floods) and in their quantitative comparison. Different approaches are applied because the definition of event extremity is not uniform (Beniston et al., 2007), so various sets of extreme floods have been compiled in individual papers. The assessment of extreme floods is based on the quantification of human and material losses (severity), high discharge values (intensity), peak discharge return periods (rarity), or a combination of these indicators. The ranking of the largest floods can differ depending on which aspect of extremity was evaluated.

An assessment based on flood severity may be a simple way to evaluate a flood's extremity. Barredo (2007) identified major flood events in the European Union between 1950 and 2005 to create a catalog and map of the events. He utilized two simple selection criteria: damage amounting to at least

0.005 % of EU GDP and a number of casualties higher than 70.

Other authors prefer evaluations based on the intensity or rarity of flooding because these aspects better reflect causal natural processes. Some authors classified floods into extremity classes based on the observed water levels (Brázdil et al., 1999; Mudelsee et al., 2003), which is most suitable for long-term pre-instrumental flood records. Water level values for individual flood events are at our disposal due to high water marks, chronicle records or other documents. This type of flood extremity evaluation was applied to the long-term flood records of the Basel gauge station on the Rhine River (Brázdil et al., 1999) and in the Elbe and Oder River basins (Mudelsee et al., 2003).

Additionally, Rodda (2005) used maximum discharges to express flood extremity in the Czech Republic. He considered the ratio of the maximum mean daily discharge to the median annual flood. This was completed for each station and flood event to study the spatial correlations among flood intensities in various basins.

Rarity can be used to compare extreme floods at different locations, when extremity is defined not by absolute thresholds (e.g., discharge values), but by relative ones (e.g., nth quintile of the dataset). Keef et al. (2009) focused on the spatial dependence of extreme rainfall and discharges in the UK and used return periods to define extreme values. Their work confirms that it is possible to compare the event extremities at different locations, even when the actual discharge values vary considerably.

Comprehensive indicators of flood extremity typically combine some aspect of extremity or consider other factors, such as the areal extent or duration of events. When creating these indicators, researchers attempt to add information about flooding from all locations where it was observed. The Francou index k (Francou and Rodier, 1967; Rodier and Roche, 1984; Herschy, 2003) is one of the older indices that assess flood extremity only at a particular station. In the Francou index, the common logarithm of maximum discharge is divided by the common logarithm of the catchment area (Rodier and Roche, 1984; Herschy, 2003). Among others, it was used to evaluate the largest floods in the World Catalogue of Maximum Observed Floods (Herschy, 2003).

Müller et al. (2015) designed a more complicated extremity index using return periods of peak discharges. They present 50 maximum floods in the Czech Republic for the period 1961–2010, which are identified based on the so-called flood extremity index (FEI) (Müller et al., 2015). In addition to the peak discharge return periods, the size of the relevant basin is considered for each location. The authors also suggested extremity indices other than the FEI that are applicable to precipitation events: the weather extremity index (Müller and Kašpar, 2014) and the weather abnormality index. Comparison of these indices with the FEI may aid in examining the relationship between precipitation and flood extremity (Müller et al., 2015).

To analyze the spatial and temporal distribution of floods in Germany, Uhlemann et al. (2010) developed a comprehensive method for the identification and evaluation of major flooding affecting several river basins. They used a time series of mean daily discharges and searched for simultaneously occurring significant discharge peaks comprising individual flood events. Their index accounts for the spatial extent of flooding (expressed by the length of the affected rivers) and discharge peak values exceeding the 2-year return value. The authors present 80 major flood events in Germany from 1952 to 2002.

Subsequently, Schröter et al. (2015) adopted the approach of Uhlemann et al. (2010) and compared several major floods in Germany. Their modified index compiled only those maximum discharges that exceeded the 5-year return value; the discharges were normalized by the respective 5-year return values and weighted by the portion of the affected river length. The final index equals the sum of these values from affected stations. Thus, the indices by Uhlemann et al. (2010) and Schröter et al. (2015) differ only in the threshold of the discharge values entered into the index calculation (2- and 5-year return values, respectively). However, Schröter et al. (2015) presented only the June 2013 flood extremity in comparison with two other major floods in August 2002 and July 1954. Because other major flood events were not presented for comparison, it is not possible to precisely identify the influence of this methodological change on their results.

The main aim of this paper is to present lists of extreme flood events from the period 1951–2013 and describe their spatial and temporal distribution. The flood events are selected on the basis of extremity indices with different thresholds of the considered maximum discharges. The discussion of the role of discharge thresholds in the floods' rankings is a part of the paper. The presented indices are based primarily upon the approach of Uhlemann et al. (2010). Each of the indices combine the flood discharge magnitude with the spatial extent of flooding.

The area of interest might be called "Midwestern" Europe and is basically a transitional area between western and central Europe. It has natural boundaries: the Alps to the south, the Carpathian Mountains and Lesser Poland Upland to the east and the coasts of the North and Baltic seas to the northwest and the north. The area is defined by six main river basins: Rhine, Elbe, Oder, Weser, Ems, and Danube up to Bratislava. As mentioned above, this area is interesting because of a noticeable shift in the seasonality of floods in a west-to-east direction. Due to its heterogeneity and vastness, the area is also convenient for index design assessment when evaluating the extremity of floods affecting several river basins.

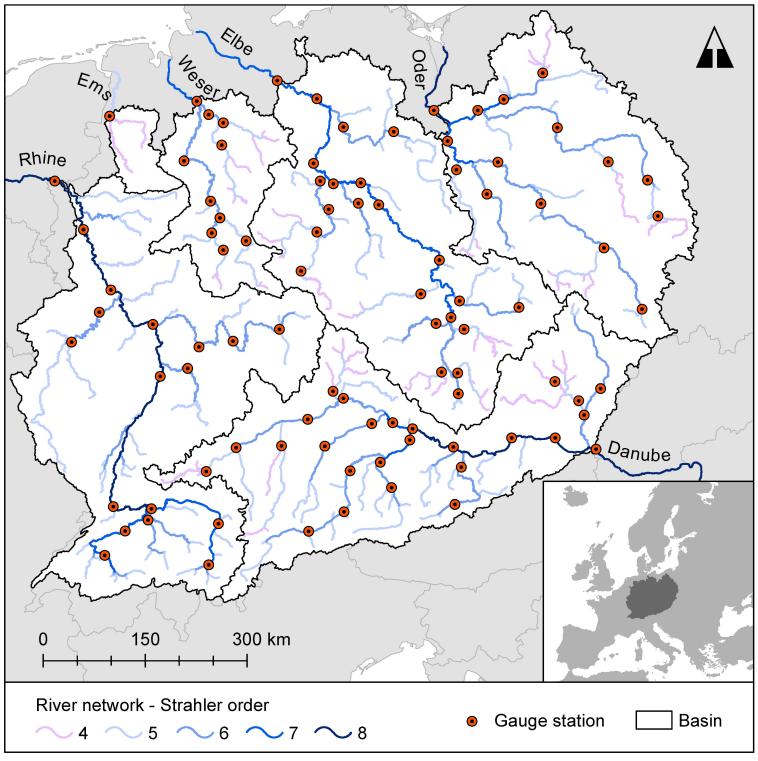

Figure 1. Gauge stations in the area of interest. Strahler stream order is distinguished by color.

2 Data and methods

2.1 Data

We used mean daily discharge values at selected stations (for each day during the period 1951–2013) as a basis when searching for floods that occurred simultaneously within the study area. Only data from stations enclosing at least 2500 km^2 of the relevant river basin were used due to poor data availability for smaller catchments and to exclude minor floods. This work is based primarily on data that were obtained from the database of the Global Runoff Data Centre (GRDC, 2017), an international archive of monthly and daily discharges. The time series was incomplete in some cases, so we used additional data from national hydrological yearbooks, the Czech Hydrometeorological Institute, the Austrian server eHYD (2016) and the Polish Institute of Meteorology and Water Management – National Research Institute (IMGW-PIB, 2017). When necessary, missing values were obtained using linear regression.

As a result, 93 gauging stations from seven countries (the Czech Republic, Slovakia, Poland, Austria, Switzerland, Germany and the Netherlands) were selected to analyze the time series of mean daily discharges between 1951 and 2013. The study area is approximately 579 000 km^2, with the length of the river network reaching almost 17 700 km. The total river length is given by the summation of river segments of a certain Strahler order upstream from each station. The selected stations and stream orders are depicted in Fig. 1. The length of river segments ranges from 55 to 522 km, with a mean length of 190 km.

2.2 Methods

The methodology is primarily based upon the approach of Uhlemann et al. (2010). Here, we briefly describe the used methods and we focus mainly on the differences arising from the larger size of the study area.

2.2.1 Identification of flood peak discharges

The first step in this study is the selection of flood peaks at individual stations. The local maxima within the time series of mean daily discharges (Q_d) must be identified. Local maxima are Q_d values that are higher than values on both the previous and following days. If several consecutive days have exactly the same value of Q_d, the first day is used.

For each gauging station, most sets of local maxima are due to minor flow fluctuations. To select real flood peak discharges, the local maxima are compared with the 2-year return periods of mean daily discharges at a station (Q_2). Peak discharges that are equal to or greater than the 2-year return level are denoted as Q_p. Nevertheless, we assume that a serious flood must be characterized by even higher discharges at least in a part of the affected area. Therefore, we also search

for peak discharges that are equal to or greater than the 10-year return level of mean daily discharge (Q_{10}). The values of Q_2 and Q_{10} are estimated from the series of annual maxima of Q_d at a station. Each annual maxima series is approximated by the generalized extreme value distribution (GEV) using the maximum likelihood estimation method (Wilks, 2006).

2.2.2 Determination of flood events

A flood event is defined here as a group of time-related Q_p at various stations where at least one Q_p value equals or exceeds Q_{10}. However, Q_p values often do not occur exactly on the same day due to, e.g., the extent of the study area, the propagation of flood waves downstream, or the movement of the precipitation field. Therefore, a time window when Q_p values seem to belong to the same event is defined. After analyzing all of the data series, we chose a time window that includes 12 days before and 12 days after the occurrence of the first value of $Q_p \geq Q_{10}$. If there are other values of $Q_p \geq Q_{10}$ within that time span, the time window is further extended with respect to the date of this peak discharge. This time span is slightly longer than that used by Uhlemann et al. (2010), but this difference is reasonable because a larger area is studied here. Moreover, the values of Q_p systematically lag behind at hydrometric profiles on the Havel River and its largest tributary the Spree. This may be due to the lowland character of these basins permitting extensive spilling of water. However, the chosen time window may be too long in some cases because another atmospherically unrelated event may begin.

Therefore, we introduce an additional rule for dividing flood peaks that were identified as time-related but are in fact associated with different atmospheric causes. If more Q_{10} values are identified in some time series within an individual flood event and the time span between those peaks is at least 5 days long, we divide the peaks into two floods; otherwise, only one flood event is considered. Finally, only the highest Q_p in a time series is considered.

2.2.3 Extremity indices design

Over 150 flood events are identified in the period 1951–2013. Each event can be described by its extent expressed as a length of affected river network:

$$L = \sum_{i=1}^{k} l_i, \tag{1}$$

where l_i denotes the length of the river segment belonging to one of k stations where Q_2 is detected. The considered part of the river network upstream from station i consists of individual river segments of a certain order. Strahler's stream ordering method is used (Strahler, 1957) when the first order is assigned to a headstream. Stream orders increase when two river segments of the same order meet. This method is dependent on the chosen layer of the river network. In this study, we use the European catchments and Rivers network system of the European Environment Agency (EEA, 2017). However, only rivers of certain orders are included in the river length l_i. If a station is located on a stream of the fourth order, we consider only this particular river segment upstream from the station. In the case of the fifth and sixth orders, also river segments of one lower order are counted. Two lower orders are considered when the station is located on the stream of the seventh and eighth orders.

Both the spatial extent of floods and the aspect of the discharge magnitudes must be incorporated into an extremity index for evaluating extreme flood events. To demonstrate the role of the threshold of the considered maximum discharges, we defined three index variants with differences in discharge limits and applied them to the identified flood events.

Generally, the index is derived from L by multiplying l_i by normalized peak discharges. The basic variant considers all of the Q_p values normalized by the respective exact value of the 2-year return period Q_2:

$$E_2 = \sum_{i=1}^{k} \left(\frac{Q_{pi}}{Q_{2i}} l_i \right). \tag{2}$$

The modification of the extremity index involves changing the threshold of considered discharge values. Although all Q_p values are used in the basic variant calculation, two other variants labeled E_5 and E_{10} consider Q_p values that are equal to or greater than 5-year (Q_5) or 10-year return periods (Q_{10}). As in Eq. (2), the new Q_p values are normalized by the respective value of Q_5 or Q_{10}.

Finally, we select 30 major floods according to each of the three extremity index variants. As the total study period covers 63 years, we select approximately one flood per 2 years. This enables a comparison of the rankings of flood events with respect to the individual index variants. This comparison opens the discussion of the role of extremity index design.

The floods are sorted based on whether they occurred in the colder or warmer half of the year; the decisive day for classification is the mean point of the event. The mean day is found using the method of directional statistics, which was originally designed for the analysis of flood seasonality (Black and Werritty, 1997). However, it is applicable to the determination of the mean day of the flood event. The method transforms the day of Q_p occurrence into directional vectors in a circle representing 1 year and the mean vector is translated into the mean day of the event. The colder half-year is set from November to April; the events with a mean day between May and October are classified as warm half-year floods.

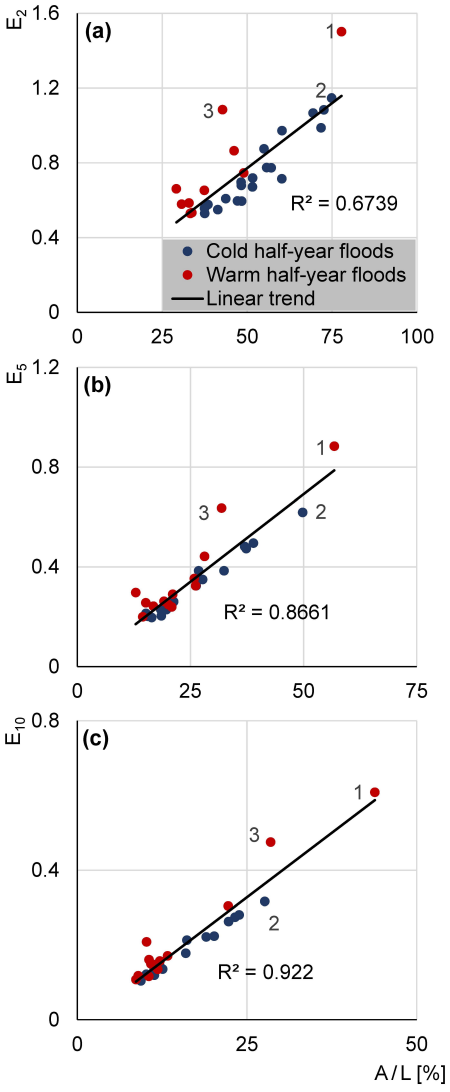

Figure 2. Relationship between the proportion of the affected river length (x axis) and the flood extremity E (y axis) according to E_2 **(a)**, E_5 **(b)** and E_{10} **(c)**. R^2 indicates the value of the coefficient of determination.

3 Results

The identified floods have various natures, from 1- or 2-day flood events caused mainly by localized convective precipitation to long-lasting and extensive cold half-year floods. Although the cold half-year events hit mostly larger areas than warm half-year floods, the flood of June 2013 was the largest one with respect to the affected river network. Flows higher than a 2-year return period occurred at about 13 700 km of the river network, which is 78 % of the total considered river length.

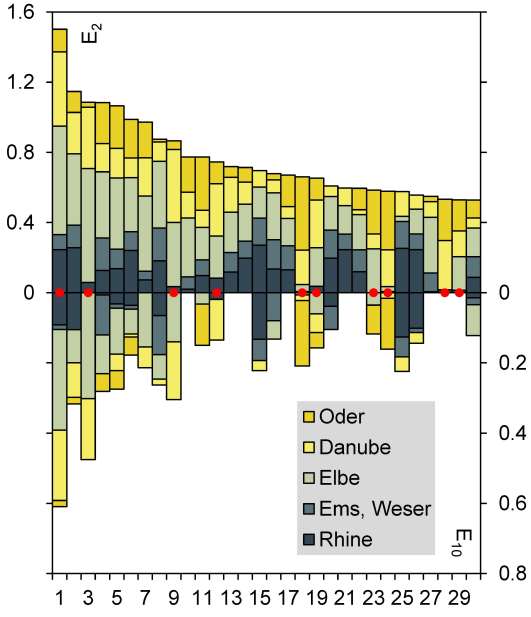

Figure 3. The 30 largest flood events in the study area from 1951 to 2013 according to E_2 and the corresponding events according to E_{10}. Missing bars indicate events which are not included in the set of 30 largest floods compiled by E_{10}. Contributions of individual river basins to the index value are distinguished by color. Red dots indicate warm half-year floods.

3.1 Comparison of the extremity index variants

As we mainly focus on extensive floods affecting more river basins at the same time, three lists of 30 major floods are created according to values of the index variants (Table 1). The events are listed with respect to the E_2. Floods selected by E_2 are primarily extensive events as small flood discharges are also considered. The flood of June 2013 is the first of the major floods, followed by the March flood of 1988 and the flood of August 2002. Overall, there are 10 events in the warm half-year among 30 maxima. By contrast, the lists of floods according to the E_5 and E_{10} are more balanced from this point of view. They contain several events that are not present among the maxima according to E_2; most of these extra floods belong to the warm half-year. These floods replaced some cold half-year floods with relatively low values of Q_p. More floods with lesser extent are present in the lists according to the E_5 and E_{10}. Mainly the latter list contains relatively shorter and spatially limited May floods, which are associated with spring convection causing higher discharges. Nevertheless, three floods were evaluated as being at the maximum, regardless of the index variant, with only different ranking among them; the June flood of 2013 is the biggest according to each index variant.

Figure 2 depicts differences among the extremity index variants in terms of their dependence on the proportion of the affected river length A/L. Each chart in Fig. 2 represents

Table 1. List of 30 major floods according to the E_2, E_5 and E_{10} indices. The date is displayed in the YYYY/MM/DD format. The A/L column refers to the proportion of the affected river length to the total length of the river network. Warm half-year floods are in bold.

Ranking	Flood duration	E_2	A/L (%)	E_5	Ranking	A/L (%)	E_{10}	Ranking	A/L (%)
1	**2013/05/30–2013/06/17**	**1.50**	**78**	**0.88**	**1**	**57**	**0.61**	**1**	**44**
2	1988/03/25–1988/04/08	1.15	75	0.62	3	50	0.32	3	28
3	**2002/08/12–2002/08/23**	**1.09**	**43**	**0.64**	**2**	**32**	**0.48**	**2**	**28**
4	1981/03/11–1981/03/30	1.08	73	0.48	5	37	0.28	5	24
5	2011/01/14–2011/01/29	1.07	69	0.50	4	39	0.27	6	23
6	1982/01/01–1982/01/17	0.99	72	0.38	9	32	0.18	12	16
7	2006/03/29–2006/04/12	0.97	60	0.38	8	27	0.21	10	16
8	2003/01/03–2003/01/19	0.88	55	0.47	6	37	0.26	7	22
9	**1954/07/02–1954/07/21**	**0.87**	**46**	**0.44**	**7**	**28**	**0.30**	**4**	**22**
10	1974/12/08–1974/12/26	0.77	56	0.20	28	16	–	–	–
11	1979/03/06–1979/03/30	0.77	57	0.21	26	15	0.15	18	12
12	**1965/06/10–1965/06/20**	**0.75**	**49**	**0.32**	**13**	**26**	**0.14**	**22**	**12**
13	1956/03/04–1956/03/14	0.72	52	0.23	24	20	–	–	–
14	1999/02/21–1999/03/07	0.71	60	–	–	–	–	–	–
15	1995/01/25–1995/02/12	0.70	48	0.35	11	28	0.22	9	19
16	1986/12/31–1987/01/10	0.68	48	0.26	18	21	0.13	23	11
17	1968/01/16–1968/01/28	0.67	52	–	–	–	–	–	–
18	**1997/07/06–1997/07/24**	**0.66**	**29**	**0.30**	**14**	**13**	**0.21**	**11**	**10**
19	**1981/07/19–1981/07/30**	**0.65**	**37**	**0.35**	**10**	**26**	**0.16**	**15**	**12**
20	1998/10/30–1998/11/13	0.61	44	0.24	22	20	0.10	30	9
21	1980/02/05–1980/02/18	0.60	47	0.20	27	19	–	–	–
22	2002/02/27–2002/03/12	0.59	48	–	–	–	–	–	–
23	**1958/06/29–1958/07/16**	**0.58**	**33**	**0.29**	**15**	**21**	**0.12**	**27**	**9**
24	**1997/07/19–1997/08/02**	**0.58**	**31**	**0.26**	**19**	**15**	**0.16**	**14**	**11**
25	1970/02/23–1970/02/28	0.58	38	0.32	12	26	0.22	8	20
26	1993/12/21–1993/12/30	0.56	37	0.26	16	21	0.14	19	12
27	1987/03/26–1987/04/11	0.55	41	–	–	–	–	–	–
28	**1985/08/06–1985/08/28**	**0.53**	**34**	**0.25**	**20**	**20**	–	–	–
29	**1965/05/30–1965/06/10**	**0.53**	**33**	–	–	–	–	–	–
30	1994/04/13–1994/04/27	0.53	37	0.23	25	18	0.12	25	10
34	**2010/06/03–2010/06/14**	–	–	**0.24**	**23**	**21**	–	–	–
35	2011/01/04–2011/01/14	–	–	0.20	30	16	0.12	24	11
39	**1977/08/24–1977/09/13**	–	–	**0.20**	**29**	**14**	–	–	–
40	**1977/08/01–1977/08/16**	–	–	–	–	–	**0.11**	**29**	**9**
44	**2005/08/22–2005/08/26**	–	–	**0.24**	**21**	**17**	**0.15**	**17**	**11**
47	**1999/05/20–1999/05/27**	–	–	**0.26**	**17**	**19**	**0.17**	**13**	**13**
60	**2010/05/18–2010/06/01**	–	–	–	–	–	**0.15**	**16**	**11**
65	**1999/05/13–1999/05/19**	–	–	–	–	–	**0.14**	**20**	**12**
66	1955/01/14–1955/01/21	–	–	–	–	–	0.14	21	13
72	1983/04/10–1983/04/21	–	–	–	–	–	0.12	26	11
87	**1983/05/25–1983/05/31**	–	–	–	–	–	**0.12**	**28**	**11**

one variant of the extremity index. The correlation between A/L and the index values is much higher when the discharge threshold is set to a 10-year return period. If we only consider such high discharges, the summation of the affected river length will approach the index values. The correlation is not so close in the case of Fig. 2a. The placement of cold and warm half-year events has a specific character in Fig. 2. The cold half-year floods are more extensive and have lower index values compared to the floods of the warm half-year, which applies to each chart. The rankings of the three highlighted flood events remain close, regardless of the variant. However, relatively smaller discharges of the March 1988 flood cause the decrease in its E_5 and E_{10} values. By contrast, the extremity of the June 2013 flood is even more highlighted in Fig. 2c as it significantly departs from other events. This is also shown in Fig. 3 representing the differences between E_2 and E_{10} values for 30 individual events. In the case of E_{10} both the June 2013 and August 2002 floods reach much higher index values than the rest of the events. Floods are ranked as in Table 1.

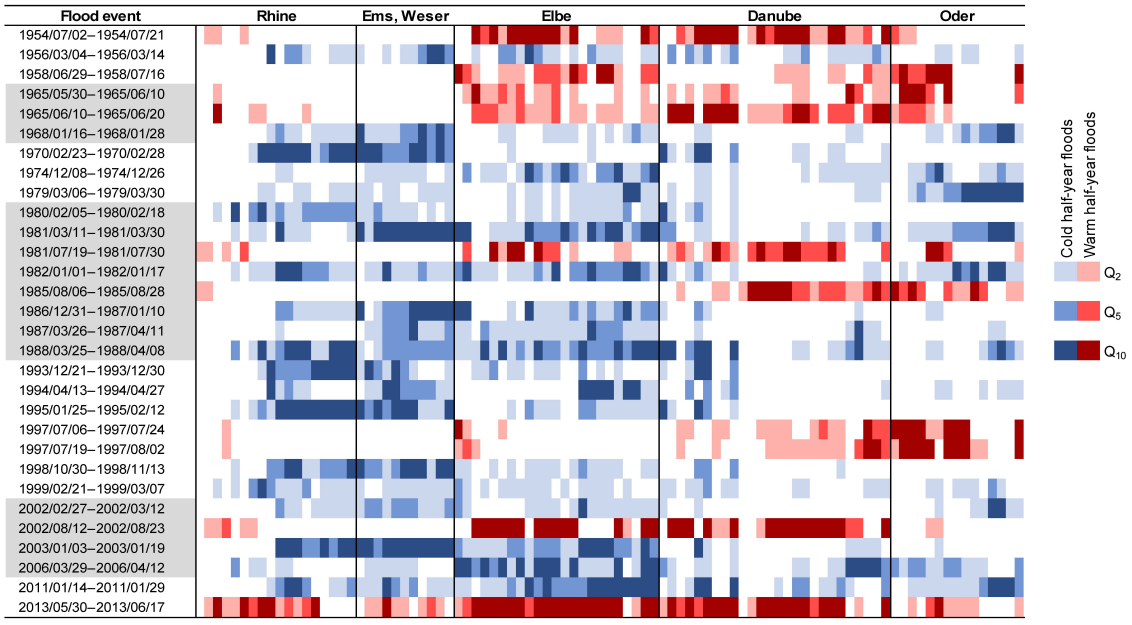

Figure 4. The occurrence of discharges equal to or greater than 2-, 5- and 10-year flood at individual stations during each of the 30 maximum floods according to the E_2 index. The basins are indicated at the top of the chart; the stations are arranged according to their position downstream.

3.2 Major flood characteristics

Figure 3 indicates large spatial differences among the flood events. It is clear that the warm half-year floods relate more to the Oder, Danube and Elbe River basins. The Rhine River basin is less represented and, in the Weser and Ems River basins, the warm half-year floods rarely occur. A more comprehensive insight into this issue is provided in Fig. 4. The occurrence of flood discharges in the basins is demonstrated on 30 maximum floods according to E_2. The differences are evident within the individual basins. There is a shift from warm to cold half-year floods when we move from the upper Rhine or Oder downstream. The Warta, a main tributary of the Oder, is affected mainly by cold half-year events. However, the last displayed station is located on the Oder River. Within the Danube basin, a gap in the occurrence of cold half-year floods is visible in the middle part of the basin. Some consecutive flood events are similar to each other, which is due to the fact that they both occur in a relatively short time. The first event has an effect on the initiation of the second one, which is the case for a pair of floods in June 1965 and July 1997. The flood of June 2013 is unique as it is the only event which largely affected the Weser and Rhine basins.

3.2.1 Seasonal distribution

Floods of the cold half-year are generally better represented among the major flood events. The seasonal distribution is quite similar for E_2 and E_{10}, with a frequency maximum in winter and a secondary maximum in summer (Fig. 5). According to E_2, major events are concentrated in January and March, but the March floods are not so pronounced in the case of E_{10}. The secondary frequency maximum occurs in July and for both indices has a similar character. Surprisingly, a great difference arose in the number of extreme floods in

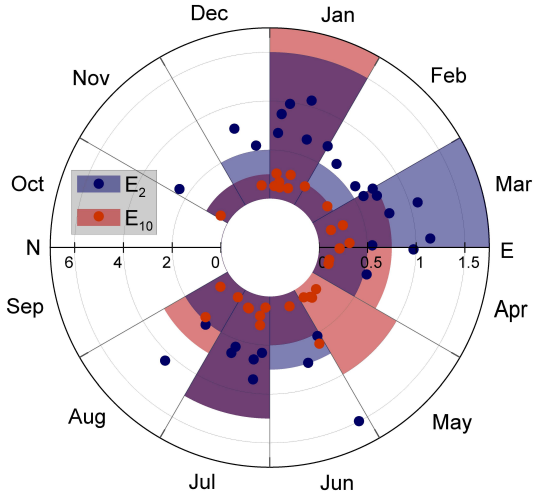

Figure 5. Seasonal distribution of 30 maximum floods according to E_2 and E_{10} indices. The number of extreme floods in individual months N is depicted by shading; the mixed color indicates overlapping data. The signs represent mean calendar days of the events; the distance of the sign from the center of the diagram reflects the flood extremity given by the values of E_2 and E_{10}.

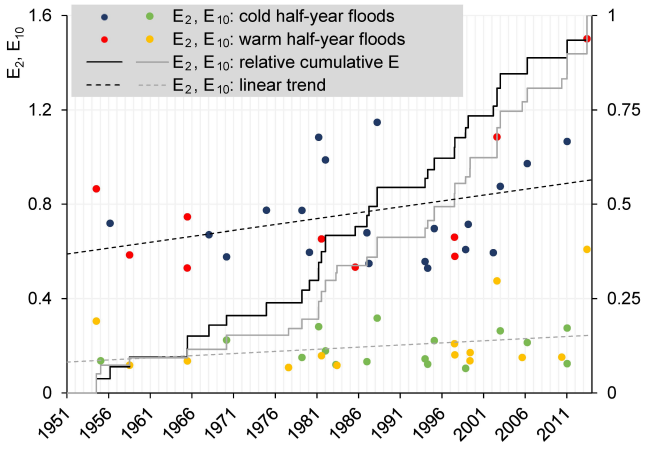

Figure 6. Interannual variability of 30 major floods according to E_2 and E_{10}. The symbols represent the extremity of cold and warm half-year floods with respect to E_2 and E_{10}; lines depict linear trends and relative cumulative values of the flood extremity.

May. These are spatially limited events, which moved up in ranking due to higher discharges. The rest of the year is characterized by a low frequency of major floods. Only a single major flood occurred from late August to the beginning of December. It began at the end of October 1998, but the mean day of the event lies in November. Its extremeness was surprisingly high, mainly according to the E_2 variant of the extremity index.

3.2.2 Interannual variability

Major floods do not occur regularly over time. Some clusters of flood events are apparent in Fig. 6, which presents the distribution of major floods between 1951 and 2013. The July flood of 1954 is the first recorded flood in the period examined. A significant accumulation of flooding is apparent in the 1980s and from 1993 to 2006. By contrast, a long period without major floods occurred at the beginning of the 1960s. The first 15 years have only one flood of the cold half-year.

Generally, there are more major floods in the second half of the period, which applies to both index variants. It seems that the number of events increases mainly from the 1980s, as is their extremity. However, the extremity according to E_2 increases more rapidly.

3.2.3 Spatial distribution

Regarding the spatial distribution of floods, Fig. 3 demonstrates that floods during the warm half-year relate more to the Oder, Danube and Elbe River basins. Warm half-year floods are less frequent in the Rhine River basin, and they occur very rarely in the Weser and Ems River basins, where cold half-year floods dominate. This is confirmed by Fig. 7, which depicts the frequency of 30 major floods in both half-years within individual gauge stations.

In general, the number of cold half-year floods decreases towards the southeast, whereas the number of warm half-year floods increases in the same direction. Regardless of the variant of the extremity index, there are regions affected by extreme floods only in one part of the year. This is true for the Weser, Ems, and the lower part of the Rhine River basin including the Main (cold half-year) and most of the Alpine rivers (warm half-year). By contrast, other regions are prone to extreme floods in both the cold and warm halves of the year: the Oder, Elbe and Danube River basins, apart from the Alpine tributaries. However, a low number of identified floods does not exclude their occurrence at individual stations. It means that floods in a given location are not part of large-scale cold or warm half-year floods, which were evaluated in this study.

4 Discussion and conclusions

This paper addresses the evaluation of major flood events in the transitional area between western and central Europe in the period 1951–2013. Major floods are defined according to the value of a flood extremity index. We created three variants of the index with differences in terms of discharge thresholds. We were motivated by Uhlemann et al. (2010) and Schröter et al. (2015), who used similar flood extremity indices, with only a difference in the threshold of the discharge values entered into the calculation. Uhlemann et al. (2010) used a 2-year flow threshold, while Schröter et al. (2015) chose a higher limit of a 5-year flow, thus making these studies incomparable. In this paper, we introduce the differences that arise in the resulting lists of major floods when we use indices with different discharge thresholds. We selected the value of Q_2 as a basic threshold and two additional threshold values: Q_5 and Q_{10}. We found that the value of this threshold is crucial for the ranking of major floods. The number of warm half-year floods slightly increases in the lists of major floods when using the higher discharge thresholds. Two sets of 30 major floods are presented according to E_2 and E_{10} indices, and the respective lists are compared in terms of seasonality, interannual variability and spatial distribution.

Generally, the lists of major floods are quite similar to the list of German trans-basin floods presented by Uhlemann et al. (2010) because Germany covers more than half of the area studied in this work. The duration of "identical" floods is slightly different, as is their ranking. This is mainly due to the different size of the area of interest. Schröter et al. (2015) used an index similar to Uhlemann et al. (2010), but the authors only offered a comparison of the extremity of three summer flood events: the floods of 1954, 2002 and 2013. The flood event of 2013 is reported as the largest, followed by the flood of 1954. In this paper, the flood of August 2002 is always more extreme than the flood of 1954, regardless of the index variant used, because of the differences in the extent

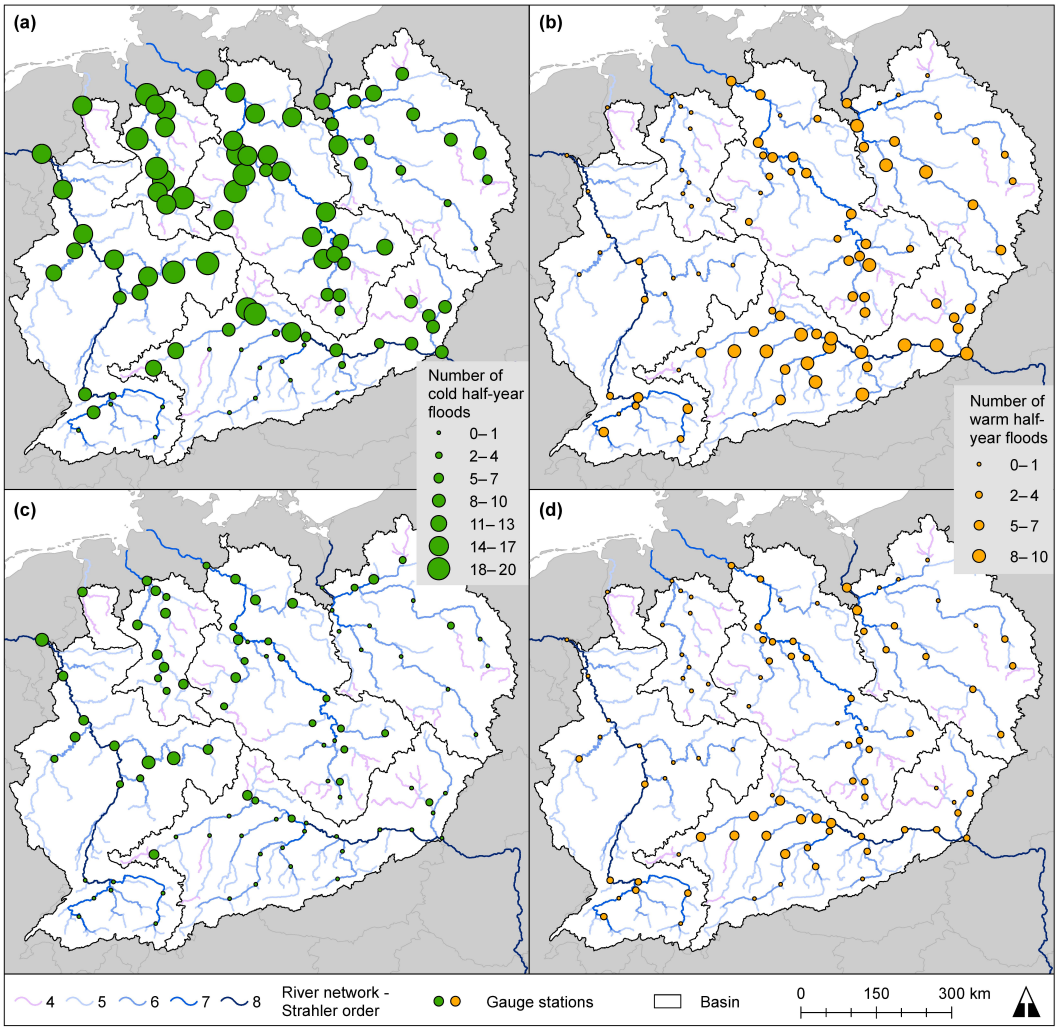

Figure 7. Spatial distribution of 30 maximum floods according to E_2 **(a, b)** and E_{10} **(c, d)**. The numbers of cold **(a, c)** and warm **(b, d)** half-year floods identified in individual gauge stations during 1951–2013 are depicted by circle size.

of the area of interest. Nevertheless, the flood of June 2013 remains on top of the lists.

We can also compare our results with those of Barredo (2007), who provided a set of 21 large European river floods compiled according to the amount of damage caused. Six of these floods affected our area of interest; all are included in the set of major floods according to E_{10}, but only four belong to the 30 major events with respect to E_2. Obviously, floods that caused major damage are better represented by the variant of the extremity index, with a higher threshold of considered discharge values. From this point of view, the E_{10} index might be better able to identify major floods, which however noticeably depart from other events.

Regarding the seasonal distribution of major flood events, the predominance of cold half-year floods is apparent in both lists. Uhlemann et al. (2010) showed the same result. By contrast, floods during the warm half of the year dominate the list of the 30 major floods in the Czech Republic by Müller et al. (2015). This may be due to the fact that the occurrence of warm half-year floods is increasing from the northwest to the southeast in the studied area.

The temporal distribution of major flood events during the period between 1951 and 2013 is rather uneven. There are certain clusters in terms of the occurrence of major floods. Some periods of reduced or increased frequencies of major flooding are identical to the results of other papers (Uhlemann et al., 2010; Müller et al., 2015). For example, we found these identical trends: a higher frequency of major floods in the 1980s and a decline in the number of identified floods in the 1990s. The 5-year period between 2006 and 2010 is different, however, because it is a period with a higher frequency of major flooding in Müller et al. (2015). The increase in major flooding in the second half of the period is again consistent with the findings of Uhlemann et al. (2010). However, it remains unclear whether this is a trend or just a part of a cycle. In recent years, there has been a discussion

about increasing flood risk due to ongoing climate change and anthropogenic modifications of the landscape and especially floodplains. On a local level, the runoff is influenced by the changes in land use, riverbeds or the surface drainage, which often lead to runoff acceleration and steeper flood waves (Langhammer and Vilímek, 2008). By contrast, the construction of water reservoirs can reduce a flood. The Slapy Dam at the Vltava River was only partially filled before the flood of July 1954. Unaffected discharge of 2920 $m^3 s^{-1}$ would be the second largest in Prague in the 20th century after the flood of March 1940; the actual discharge was only 2240 $m^3 s^{-1}$ (Brázdil et al., 2005). However, the effect of local landscape changes can be less significant for extensive events, as it depends on the flood extremity (Langhammer and Vilímek, 2008).

The temporal characteristics of major flood events are also connected with the opposite extreme. The historical records show that an extreme flood was followed by a great drought in same cases (Brázdil et al., 2005). Lloyd-Hughes and Saunders (2002) conclude that the greater pan-European droughts occurred in the early 1950s and the 1990s; lesser drought incidence is apparent in the 1980s. For the analysis, they used the Palmer drought severity index and standardized precipitation indices calculated at different timescales.

At a shorter timescale, the wetness conditions are crucial for flood initiation; antecedent soil moisture can highly influence the flood extremity. The June 2013 flood was the case when great precipitation amounts coincided with high antecedent soil moisture and produced an exceptional flood (Blöschl et al., 2013). The effect of antecedent wetness conditions depends on the season and a type or an extremity of flood. High antecedent soil moisture relates in particular to cold half-year floods, while the signal varies in warm half-year cases (Nied et al., 2013).

Further research on the topic of extreme floods will examine the related meteorological conditions. A comprehensive evaluation of antecedent wetness conditions, causal atmospheric circulation, the consequent precipitation and the flow response is needed. A comparison of major floods with precipitation and circulation extremes would be useful for a better understanding of the causes of extensive floods, which affect several river basins.

Data availability. Mean daily discharge data were mainly provided by the Global Runoff Data Centre (GRDC, 2017). Some data are accessible via the Austrian server eHYD (2016) at http://ehyd.gv.at/ and the Polish Institute of Meteorology and Water Management – National Research Institute (IMGW-PIB, 2017) at https://dane.imgw.pl/. Data of the Czech Hydrometeorological Institute were purchased for research purposes. The European catchment and river network system (EEA, 2017) was used to determine the lengths of affected river networks.

Competing interests. The authors declare that they have no conflict of interest.

Acknowledgements. This work was supported by the Czech Science Foundation (grant number 17-23773S). Acknowledgements also belong to the Global Runoff Data Centre and the Czech Hydrometeorological Institute for providing runoff data.

Edited by: Vazken Andréassian
Reviewed by: two anonymous referees

References

Barredo, J. I.: Major flood disasters in Europe: 1950–2005, Nat. Hazards, 42, 125–148, https://doi.org/10.1007/s11069-006-9065-2, 2007.

Bebber van, W. J.: Die Zugstrassen der barometrischen Minima nach den Bahnenkarten der Deutschen Seewarte für den Zeitraum 1875–1890, Meteorol. Z., 8, 361–366, 1891.

Beniston, M., Stephenson, D. B., Christensen, O. B., Ferro, C. A. T., Frei, C., Goyette, S., Halsnaes, K., Holt, T., Jylhä, K., Koffi, B., Palutikof, J., Schöll, R., Semmler, T., and Woth, K.: Future extreme events in European climate: an exploration of regional climate model projections, Climatic Change, 81, 71–95, https://doi.org/10.1007/s10584-006-9226-z, 2007.

Black, A. R. and Werritty, A.: Seasonality of flooding: a case study of North Britain, J. Hydrol., 195, 1–25, 1997.

Blöschl, G., Nester, T., Komma, J., Parajka, J., and Perdigão, R. A. P.: The June 2013 flood in the Upper Danube Basin, and comparisons with the 2002, 1954 and 1899 floods, Hydrol. Earth Syst. Sci., 17, 5197–5212, https://doi.org/10.5194/hess-17-5197-2013, 2013.

Brázdil, R., Glaser, R., Pfister, C., Dobrovolný, P., Antoine, J.-M., Barriendos, M., Camuffo, D., Deutsch, M., Enzi, S., Guidoboni, E., Kotyza, O., and Rodrigo, F. S.: Floods events of selected European rivers in the sixteenth century, Climatic Change, 43, 239–285, 1999.

Brázdil, R., Dobrovolný, P., Elleder, L., Kakos, V., Kotyza, O., Květoň, V., Macková, J., Müller, M., Štekl, J., Tolasz, R., and Valášek, H.: Historical and Recent Floods in the Czech Republic, Masaryk University and Czech Hydrometeorological Institute, Brno, Prague, Czech Republic, 2005.

Caspary, H. J.: Recent winter floods in Germany caused by changes in the atmospheric circulation across Europe, Phys. Chem. Earth, 20, 459–462, 1995.

EEA: European catchments and Rivers network system, https://www.eea.europa.eu/data-and-maps/data/european-catchments-and-rivers-network, last access: 13 March 2017.

eHYD: Hydrographic data of Austria, http://ehyd.gv.at/, last access: 9 May 2016.

Francou, J. and Rodier, J.-A.: Essai de classification des crues maximales observées dans le monde, Cah. Orstrom Hydrol., IV, 19–46, 1967.

GRDC: River discharge data, http://www.bafg.de/GRDC/, last access: 23 February 2017.

Herschy, R. W. (Ed.): World Catalogue of Maximum Observed Floods, IAHS Press, Wallingford, IAHS-AISH Publ. 284, 2003.

IMGW-PIB: Central database, https://dane.imgw.pl/, last access: 26 February 2017.

Jacobeit, J., Glaser, R., Luterbacher, J., and Wanner, H.: Links between flood events in central Europe since AD 1500 and large-scale atmospheric circulation modes, Geophys. Res. Lett., 30, 1172–1175, https://doi.org/10.1029/2002GL016433, 2003.

Keef, C., Svensson, C., and Tawn, J. A.: Spatial dependence in extreme river flows and precipitation for Great Britain, J. Hydrol., 378, 240–252, 2009.

Kundzewicz, Z. W., Ulbrich, U., Brucher, T., Graczyk, D., Kruger, A., Leckebusch, G. C., Menzel, L., Pinskwar, I., Radziejewski, M., and Szwed, M.: Summer floods in Central Europe – climate change track?, Nat. Hazards, 36, 165–189, 2005.

Langhammer, J. and Vilímek, V.: Landscape changes as a factor affecting the course and consequences of extreme floods in the Otava river basin, Czech Republic, Environ. Monit. Assess., 144, 53–66, https://doi.org/10.1007/s10661-007-9941-6, 2008.

Lloyd-Hughes, B. and Saunders, M. A.: A drought climatology for Europe, Int. J. Climatol., 22, 1571–1592, https://doi.org/10.1002/joc.846, 2002.

Mudelsee, M., Börngen, M., Tetzlaff, G., and Grünewald, U.: No upward trends in the occurrence of extreme floods in central Europe, Nature, 425, 166–169, 2003.

Müller, M. and Kašpar, M.: Quantitative aspect in circulation type classifications – an example based on evaluation of moisture flux anomalies, Phys. Chem. Earth, 35, 484–490, https://doi.org/10.1016/j.pce.2009.09.004, 2010.

Müller, M. and Kaspar, M.: Event-adjusted evaluation of weather and climate extremes, Nat. Hazards Earth Syst. Sci., 14, 473–483, https://doi.org/10.5194/nhess-14-473-2014, 2014.

Müller, M., Kašpar, M., Valeriánová, A., Crhová, L., Holtanová, E., and Gvoždíková, B.: Novel indices for the comparison of precipitation extremes and floods: an example from the Czech territory, Hydrol. Earth Syst. Sci., 19, 4641–4652, https://doi.org/10.5194/hess-19-4641-2015, 2015.

Munich Re: Topics Geo Natural Catastrophes 2014: Analyses, Assessments, Positions, Munich Reinsurance Company, Munich, Germany, 2015.

Nied, M., Hundecha, Y., and Merz, B.: Flood-initiating catchment conditions: a spatio-temporal analysis of large-scale soil moisture patterns in the Elbe River basin, Hydrol. Earth Syst. Sci., 17, 1401–1414, https://doi.org/10.5194/hess-17-1401-2013, 2013.

Nissen, K. M., Ulbrich, U., and Leckebusch, G.: Vb cyclones and associated rainfall extremes over Central Europe under present day and climate change conditions, Meteorol. Z., 22, 649–660, https://doi.org/10.1127/0941-2948/2013/0514, 2014.

Rodda, H. J. E.: The Development and application of a flood risk model for the Czech Republic, Nat. Hazards, 36, 207–220, 2005.

Rodier, J. A. and Roche, M. (Eds.): World Catalogue of Maximum Observed Floods, IAHS Press, Wallingford, IAHS Publ. 143, 1984.

Schröter, K., Kunz, M., Elmer, F., Mühr, B., and Merz, B.: What made the June 2013 flood in Germany an exceptional event? A hydro-meteorological evaluation, Hydrol. Earth Syst. Sci., 19, 309–327, https://doi.org/10.5194/hess-19-309-2015, 2015.

Strahler, A. N.: Quantitative analysis of watershed geomorphology, EOS T. Am. Geophys. Un., 38, 913–920, 1957.

Uhlemann, S., Thieken, A. H., and Merz, B.: A consistent set of trans-basin floods in Germany between 1952–2002, Hydrol. Earth Syst. Sci., 14, 1277–1295, https://doi.org/10.5194/hess-14-1277-2010, 2010.

Wilks, D. S.: Statistical Methods in the Atmospheric Sciences, 2nd Edn., Academic Press, Burlington, USA, 2006.

4 Extreme precipitation events

Paper III: Gvoždíková, B., Müller, M., Kašpar, M., 2019. Spatial patterns and time distribution of central European extreme precipitation events between 1961 and 2013. International Journal of Climatology, 39, 3282−3297. https://doi.org/10.1002/joc.6019.

Received: 11 July 2018 | Revised: 20 January 2019 | Accepted: 21 January 2019

DOI: 10.1002/joc.6019

International Journal of Climatology RMetS

RESEARCH ARTICLE

Spatial patterns and time distribution of central European extreme precipitation events between 1961 and 2013

Blanka Gvoždíková[1] | Miloslav Müller[1,2] | Marek Kašpar[2]

[1]Faculty of Science, Charles University, Prague, Czech Republic

[2]Department of Meteorology, Institute of Atmospheric Physics AS CR, Prague, Czech Republic

Correspondence
Blanka Gvoždíková, Faculty of Science, Charles University, Prague, Czech Republic.
Email: blanka.gvozdikova@natur.cuni.cz

Funding information
Czech Science Foundation, Grant/Award Number: 17-23773S

Precipitation extremes always have an area-related effect, emphasizing the need for a spatial assessment of extreme precipitation events that sometimes show similar behaviour in precipitation patterns due to recurring synoptic features. Our study investigates spatial patterns in the extreme precipitation events (EPEs) that occurred in central Europe between 1961 and 2013. As many as 53 maximum events were selected by the weather extremity index (WEI), reflecting simultaneously the spatial extent and the return periods of *t* day precipitation totals within an event-adjusted study area. The extremity of the EPEs is further evaluated at two lower spatial levels, the main river basins (the Rhine, Weser/Ems, Elbe, Danube, and Oder) and 20 smaller subcatchments, which enables a more detailed study of the events' spatial structure and similarity. A correlation analysis demonstrated that heavy precipitation occurs simultaneously not only in neighbouring subcatchments but also in rather distant regions with similar orientations of mountain ranges (e.g., in the Elbe-a and Danube-b subcatchments). In contrast, strong negative correlations appeared between several subcatchments in the Oder and Rhine River basins, which exclude heavy precipitation from occurring simultaneously in both basins. Similar spatial patterns are obvious among precipitation extremes; using the relative WEI values as the similarity measure, agglomerative hierarchical clustering detected two well-separated groups of events, namely, W-CE and E-CE, affecting mainly the western and eastern parts of central Europe, respectively. A finer division of the EPEs distinguished five clusters of events with different spatio-temporal characteristics. Only two clusters, ED (Elbe-Danube) and O (Oder), were represented among the top 10 central European EPEs, which occurred exclusively from the end of May to the beginning of September. Three other clusters consisted of generally lower extreme events rather equally distributed throughout the year.

KEYWORDS

agglomerative hierarchical clustering, central Europe, extreme precipitation, seasonality, spatial patterns, weather extremity index

1 | INTRODUCTION

Rather than long-term averages of meteorological variables, it is usually hourly, daily, or multi-day extremes that are responsible for damage to society and ecosystems (Zhang *et al.*, 2011). Extreme precipitation can have a large impact itself or it often induces floods or landslides, which can cause additional damage or even loss of lives. According to Munich Re's NatCatSERVICE (http://natcatservice.munichre.com/), the results of extreme precipitation events (EPEs) with a connection to subsequent floods are among the costliest natural losses in Europe, with the costs still increasing. It is partly a matter of the higher exposure of humans to extreme weather events (IPCC, 2014). However, it has also been reported that the frequency and intensity of EPEs have likely increased in Europe in the last decades (IPCC, 2014), although a trend

 © 2019 Royal Meteorological Society

analysis can be uncertain due to the rarity of the events and the short lengths of the available time series of daily data (Zhang *et al*., 2011). Climate projections suggest further increases in EPEs over most mid-latitudes (IPCC, 2014), including central Europe (Munich Re, 2011).

Precipitation extremes are generally less frequent events, which go far into the tail of the probability distribution of daily data (Zhang *et al*., 2011). They can result from large-scale circulation patterns as well as locally restricted convection, which differ in their temporal scales but can result in similar rainfall amounts. It is possible to evaluate their extremity on the basis of point measurements at individual sites (Zhang *et al*., 2011); one can use indices with a fixed threshold, for example, daily precipitation totals exceeding 30 mm (Ustrnul *et al*., 2014), or a percentile threshold that is generally more suitable for the spatial comparison of extremes (Zhang *et al*., 2011). However, apart from the magnitude and the event duration, the extremity of an event has an important aspect of the spatial extent of the precipitation (Müller and Kašpar, 2014), which should be taken into account. The involvement of the affected area in the evaluation of the event extremity is common even in the case of other meteorological phenomena, for example, heat waves (Lhotka and Kyselý, 2014; Valeriánová *et al*., 2017) or windstorms (Roberts *et al*., 2014; Kašpar *et al*., 2017). On the other hand, a regional evaluation technique is often prone to the choice of the study area and its extent (Konrad, 2001). That is why Müller and Kašpar (2014) presented an event-adjusted evaluation of precipitation extremes. Their method does not depend on a certain area extent, but it optimizes the considered area, as well as the event duration.

According to them, most of the EPEs in Czechia occur in the summer months when the extremity of events is also the highest (Müller *et al*., 2015). The EPEs identified between 1961 and 2010 affected up to 70% of the Czech territory (55,100 km^2 in the case of the most extensive event of August 2002), but the majority of EPEs did not reach 50% (Müller *et al*., 2015). It seems that the events always affect either Bohemia (the western part of Czechia) together with the Austrian Alps and Saxony or Moravia and Silesia (the eastern part of Czechia) together with western Slovakia (Müller *et al*., 2009). This implies that the extent and the overall extremity of the Czech EPEs may be even larger than that reported by Müller *et al*. (2015).

A pronounced summer peak is evident in the case of EPEs in Poland (Ustrnul *et al*., 2014) and in the Alpine region (Seibert *et al*., 2007), although the latter may experience some winter cases, especially in the north of Switzerland and the northwest of Austria (Seibert *et al*., 2007; Stucki *et al*., 2012). The southern side of the Alps (from southwestern Switzerland to southeastern Austria) and the east of Austria show another autumn maximum of heavy precipitation days (Seibert *et al*., 2007; Stucki *et al*., 2012). The shift from summer to autumn events becomes more visible when moving further south (e.g., to Slovenia) (Müller and Kašpar, 2011).

The situation is changing towards the Atlantic, as the western part of Germany has experienced heavier winter rainfall situations during westerly circulation patterns (Beurton and Thieken, 2009; Hofstätter *et al*., 2017). Otherwise, cyclones moving along the Vb track (van Bebber, 1891) are the most relevant for summer extreme precipitation over large parts of central Europe (Messmer *et al*., 2015; Hofstätter *et al*., 2017) and especially the Elbe, Oder, and parts of the Danube basin (Kyselý, 2009; Nissen *et al*., 2014). Towards western central Europe, the frequency of Vb cyclones decreases, although strongly deviated Vb tracks were reported with EPEs arising, for example, in the Vosges Mountains (Minářová *et al*., 2018).

A clear change is therefore evident in central Europe when moving from the northwest to the southeast. Spatial differences result from specific circulation conditions conducive to precipitation extremes. Nevertheless, it is possible that a single precipitation event affects a large part of the territory, as was the case in May and June of 2013 (Grams *et al*., 2014; Nissen *et al*., 2014).

Despite a high diversity of central European EPEs, we want to compare the levels of their extremity. Therefore, there is a need to unify the methodology for the identification of EPEs as well as to evaluate events within a larger territory crossing national borders to get a comprehensive view of a whole event.

In our previous study (Gvoždíková and Müller, 2017), extreme floods were objectively evaluated within a study area covering the Rhine, Weser, Ems, Elbe, and Oder River basins and the Danube up to Bratislava. To be able to analyse the genesis of floods, we present the following study of extreme precipitation events that occurred in this area between 1961 and 2013. The EPEs are chosen based on the event-adjusted weather extremity index (Müller *et al*., 2015), which determines itself both the size of the affected area and the duration of events. We mainly aim to analyse the EPEs hierarchically, on three different spatial levels, with respect to the areal precipitation extremity. This allows us to identify specific spatial patterns in the central European EPEs and investigate the relationships among individual parts of the study area during an EPE occurrence.

2 | METHODS

A set of EPEs is compiled based on the weather extremity index (WEI), which was proposed by Müller and Kašpar (2014) and used for the evaluation of EPEs in Czechia (Müller *et al*., 2015). The index reflects return periods N of the precipitation totals and the event duration t and the extent a, which are optimized for each event. The return periods are estimated from the daily precipitation totals at 341 rain gauges within the study area (Figure 1) of approximately 578,200 km^2, which is

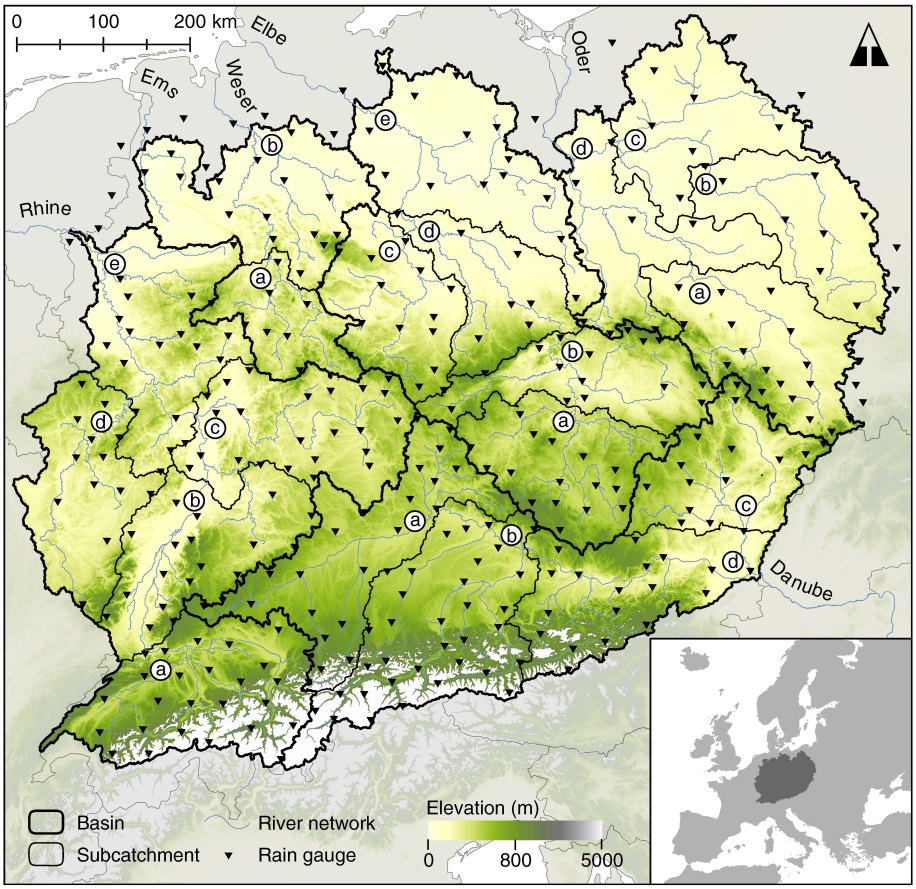

FIGURE 1 Rain gauges and the study area divided into basins and subcatchments (compare with Table 1). The letters indicating subcatchments correspond with Figures 4, 7, and 9 [Colour figure can be viewed at wileyonlinelibrary.com]

the same as the area used for the extreme flood assessment in our previous study (Gvoždíková and Müller, 2017). The data series cover at least 30 years in the study period between 1961 and 2013; generally, they are even longer, with 80% of all series longer than 50 years.

In the methodology chapter, we briefly introduce the search process of events, which has been described in more detail by Müller and Kašpar (2014) and Müller *et al.* (2015). The evaluation of EPEs is carried out on three spatial levels: the whole study area of central Europe, five basic river basins, and 20 individual subcatchments (Figure 1 and Table 1), which areas were adjusted to a certain hydrometric profile to be easily comparable with flood extremes in future research. The subcatchment WEI values form the basis for finding analogous EPEs via an agglomerative hierarchical clustering method, which is described in section 2.3.

2.1 | Searching for extreme precipitation events

Unlike the precipitation totals, the return periods are suitable for the comparison of regions with different precipitation climatologies. We estimate the return periods from series of 1–10-day precipitation totals; the evaluation of multi-day precipitation totals allows us to optimize the duration t of the

TABLE 1 Areas of the river basins and their subcatchments within central Europe

Basin		River Rhine	A (10^3 km^2) 159.2	River Weser/Ems	A (10^3 km^2) 46.8	River Elbe	A (10^3 km^2) 130.8	River Danube	A (10^3 km^2) 132.0	River Oder	A (10^3 km^2) 109.4
Subcatchment	a	Upper Rhine+Aare	35.6	Werra+Fulda	15.1	Vltava	26.0	Upper Danube+Lech	35.6	Upper Oder	29.7
	b	Middle Rhine+Neckar	30.3	Weser+ Aller+Ems	31.7	Upper Elbe	24.8	Isar+Inn	40.7	Upper Warta	25.8
	c	Main	32.6			Saale	23.3	Morava+Thaya	24.4	Middle Warta	27.9
	d	Mosel	26.8			Middle Elbe+Mulde	20.9	Middle Danube+Enns	31.3	Lower Oder	26.0
	e	Lower Rhine	33.9			Lower Elbe+Havel	35.8				

event. The generalized extreme value (GEV) distribution is fitted to the annual maxima of the totals and the return periods are calculated from that distribution. We set the maximum considered return period to a value of 1,000 years. The GEV distribution is frequently used in climatological or hydrological applications (Wilks, 2006), and it was found to be the most suitable distribution for the modelling of precipitation extremes in many regions of Czechia (Kyselý and Picek, 2007) and elsewhere in Europe (Fowler and Kilsby, 2003). We can estimate the GEV parameters by the methods of *L*-moments or maximum likelihood, which was applied in this study. The point return periods have to be interpolated, as the WEI works with a regular grid instead of station data. Using linear kriging, we interpolated rather the common logarithms of the return periods due to the exponential nature of the GEV (Müller and Kašpar, 2014). The resulting grid has a horizontal resolution of 10 km.

The calculation of the WEI is made by maximizing the variable E_{ta}. According to Müller and Kašpar (2014), E_{ta} is the product of the common logarithm of the spatial geometric mean G_{ta} of the return periods N_{ti} and the radius R of a circle whose area a is equal to the area summed up according to the number i of cells included in the geometric mean,

$$E_{ta} = \log(G_{ta})R = \frac{\sum_{i=1}^{n} \log(N_{ti})}{n} \frac{\sqrt{a}}{\sqrt{\pi}}. \quad (1)$$

The cells enter Equation 1 sequentially in descending order (from the highest to the lowest return period). The variable E_{ta} increases when accumulating cells of high return periods, but it starts to decrease when the continuously expanding area does not compensate for the mean return period decrease (Figure 2). The inflexion point corresponds to the value of the WEI and relates to a certain size of the affected area *a*. Equation 1 can be applied to the return periods of each day. However, we did not calculate E_{ta} for days with return periods shorter than 2 years, due to the elimination of rarer precipitation episodes and to save the processing time.

Within a single event, the WEI changes when separately considering return periods of 1–10-day precipitation totals (t increasing from 1 to 10 in Equation 1). If the WEI continuously increases upon extending the event duration, the maximum value will be considered as the final absolute WEI (WEI_{abs}) describing the EPE with the affected area a and duration t. An example is shown for the May/June 2013 event in Figure 2, where E_{ta} curves are displayed up to 4-day durations of the event. In this case, the WEI_{abs} was reached in the fourth day, with an affected area of approximately 177,100 km^2. We again exclude multi-day values of

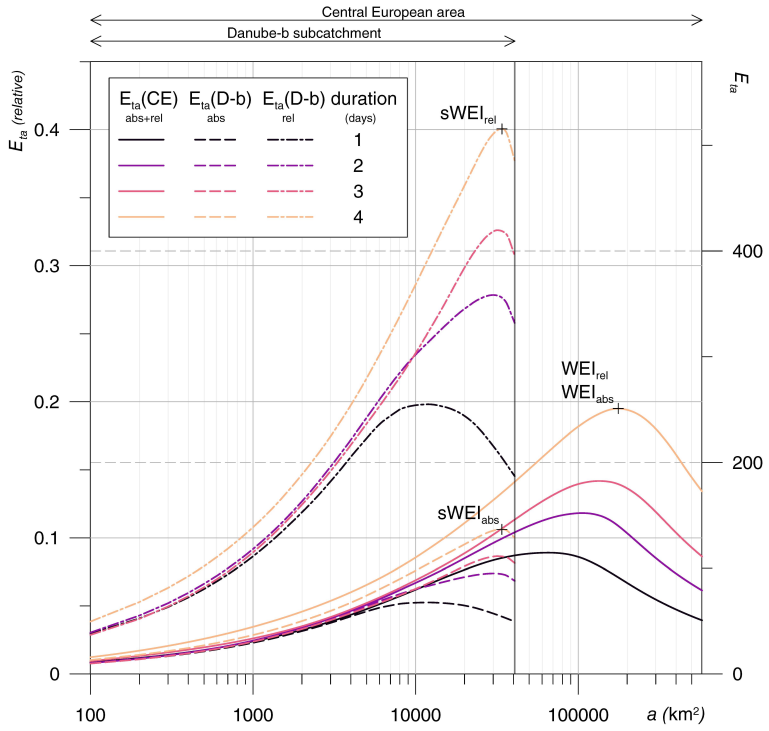

FIGURE 2 Values of E_{ta} with the increasing extent of the considered area and extending duration for the case of the May/June 2013 event. E_{ta} and WEI (both absolute and relative) are displayed for the spatial level of central Europe and one subcatchment (abbreviation "s") [Colour figure can be viewed at wileyonlinelibrary.com]

the WEI when the single-day WEI is missing due to low return periods of the precipitation totals. The events are labelled according to their first day, which is also crucial for a seasonal classification of the events.

2.2 | Comparing the events

In this study, the WEI is calculated on 3 different spatial levels: the study area as a whole, 5 basins, and 20 subcatchments (Figure 1). However, the values are hard to compare even on a single sublevel due to the various extents of the basins and the subcatchments. The standardization of the WEI is needed with respect to the highest theoretically possible WEI in the given area (WEI_{max}). The potential value of the WEI_{max} counts with t-day return periods of 1,000 years over all cells within the basin or the subcatchment of the surface area a. After basic operations transforming Equation 1, WEI_{max} is expressed as 3 times the radius R as follows:

$$WEI_{max} = 3\frac{\sqrt{a}}{\sqrt{\pi}}. \quad (2)$$

The standardized value of the WEI (the relative WEI, WEI_{rel}) corresponds to the ratio of the absolute and maximum WEIs of the same event,

$$WEI_{rel} = \frac{WEI_{abs}}{WEI_{max}}. \quad (3)$$

The difference between WEI_{abs} and WEI_{max} is demonstrated for three precipitation events by diagrams in Figure 3, where one can compare how the WEI_{rel} was derived for central Europe and the individual basins. A specific difference between the values of WEI_{rel} and WEI_{abs} can be found in the example of Figure 2, with E_{ta} and WEI (both absolute and relative) displayed on the spatial levels of central Europe and one subcatchment. To unify the results, we use only WEI_{rel} for all spatial levels. We primarily select 53 maximum central European events detected at the first spatial level—one event per year on average. They are analysed with respect to the areal precipitation extremity when we mainly focus on comparing the temporal and spatial distributions of the events. The method of directional statistics (Black and Werritty, 1997) is used for displaying the events' seasonality in a circle representing 1 year. The method transforms the day of the EPE occurrence into directional vectors in that circle.

2.3 | Spatial similarity of events

The EPEs seems to repeat over time in accordance with recurring atmospheric circulation conditions (Hofstätter *et al*., 2017; Jacobeit *et al*., 2017). We expect a similarity in the spatial distribution of the precipitation and employ a clustering method to check the similarity and to find groups of analogous EPEs within the 53 maximum events.

As we do not know the number of the groups and their initial membership in advance, we use an agglomerative hierarchical clustering procedure, which merges the closest single- or multiple-member groups hierarchically according to a chosen measure of distance. Finally, only one group remains to contain all members (Wilks, 2006). The method seems useful for finding regional spatial patterns of weather and climate extremes (Gibson *et al*., 2017). Differences appear in defining an intergroup dissimilarity, which is commonly based on the Euclidean distances between points or clusters (Wilks, 2006). Among the various approaches for hierarchical clustering, Ward's method seems to be the most accurate (Gong and Richman, 1995), as it minimizes the within-group sum of the squared distances over all created groups.

Using Ward's method, we want to cluster the EPEs with respect to the spatial distribution of the precipitation extremity. The aim is to minimize the sum of the squared distances between the merging EPEs and the centroids of the resulting groups. The degree of similarity is assessed based on the subcatchment WEI_{rel} ($sWEI_{rel}$) during the 53 maximum events. For each subcatchment s, the value of the $sWEI_{rel}$ is standardized and expressed as a proportion ($pWEI_{rel}$) of all $sWEI_{rel}$ values summed for an individual event e as follows:

$$pWEI_{rel\ e} = \frac{sWEI_{rel}}{\sum_{s=1}^{20} sWEI_{rel}}. \quad (4)$$

The standardization of the $sWEI_{rel}$ seems to be appropriate due to differences in the variable means and variances

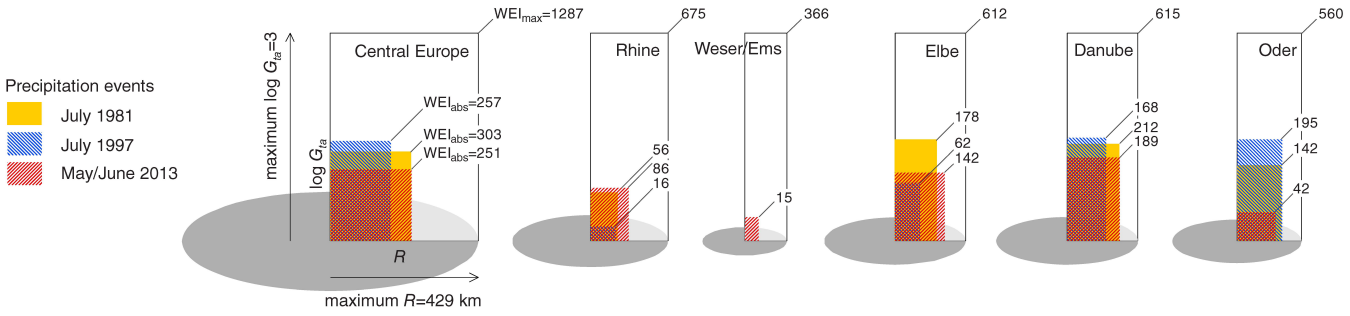

FIGURE 3 Demonstration of the relationship between WEI_{abs} and WEI_{max} when multiplying the common logarithm of the spatial geometric mean G_{ta} by the radius R (or their maximum possible values) in the case of precipitation events in July 1981 and 1997 and May/June 2013. The relationship is determined at the spatial level of central Europe and the individual basins [Colour figure can be viewed at wileyonlinelibrary.com]

(Gong and Richman, 1995). The final distances are determined from a numeric matrix with rows representing individual EPEs and columns indicating dimensions, that is, values of the $p\mathrm{WEI}_{\mathrm{rel}}$ during the 53 maximum events. This means that the closest events form clusters in 20-dimensional space (as the number of the subcatchments). A final number of five groups is then set in to keep a reasonable quantity of events in each cluster. At the previous hierarchical level, one group would remain with only a single event.

3 | EXTREME PRECIPITATION EVENTS AND THEIR SPATIAL PATTERNS

3.1 | Extreme precipitation events between 1961 and 2013

The calculation of the $\mathrm{WEI}_{\mathrm{rel}}$ for the whole study area determines a ranking of the EPEs; the 53 maximum central European events are presented in Table 2. The methodology allows us to detect EPEs lasting up to 10 days, but in fact, the events are much shorter, usually between 2 and 4 days. Events longer than 5 days are very rare, with a maximum detected duration of 8 days. Generally, the duration of the EPEs slightly increases with the increasing $\mathrm{WEI}_{\mathrm{rel}}$, but the seven most highly ranked EPEs still last only up to 5 days. Moreover, there are two time-concentrated precipitation events among them (August 2002 and 1978), with only 2-day durations. In 1978, the event was associated with a high precipitation intensity (24-hr precipitation over 100 mm) mainly in northern Bohemia and the eastern part of Germany (Marx, 1980). The 2002 EPE was accompanied by even heavier precipitation, with a maximum of 312 mm within 24 hr measured at Zinnwald (Germany) on 12 August (Ulbrich *et al*., 2003).

To demonstrate the spatial patterns of the precipitation during the events, Table 2 also presents the 10 maximum values of the $\mathrm{WEI}_{\mathrm{rel}}$ within the five river basins constituting the study area (Figure 1). Apart from only one Weser/Ems event, all other basin-related maximum events belong to the 53 central European EPEs. Eight of the top 10 central European EPEs are at the same time among the 10 maximum events in two or even three river basins (the latter case corresponds to the No. 1 EPE in July 1981). However, the representation of the basin-related maxima among the central European EPEs is very unequal. While the maximum events of the Elbe, Danube, and Oder basins are almost always highly ranked according to the total $\mathrm{WEI}_{\mathrm{rel}}$, the top 10 events of the Rhine and Weser/Ems basins do not appear very often among the highly ranked events. This particularly applies to the rather small Weser/Ems basin, whose precipitation extremes are isolated from the others, apart from three events, which coincide with the Rhine events. Nevertheless, the maximum events from July 2002 in the Weser/Ems basin and October 1986 in the Rhine basin did not have large responses in the other basin. Both events affected quite large areas of their own basins (82% in the Weser/Ems and 66% in Rhine basin), while the mean return periods were just 4 and 7 years, respectively. On the other hand, the Elbe, Danube, and Oder maximum events had mean return periods between 25 and 28 years, with the maximum in the Oder basin during the August 1985 event. The affected area reached 55% of the basin extent, as did the maximum Danube event in July 1981. In the case of the Elbe maximum event in August 2002, the affected area was slightly smaller, with 51% of the Elbe basin covered (see Figure 3 for a comparison of the 1981 and 2002 events in individual basins). Although the percentages are lower than for the Weser/Ems and Rhine basins, the maximum events of the Danube, Elbe, and Oder basins are always highly ranked in the other basins (Table 2). These facts suggest a significant difference in the nature of the maximum events between the Rhine and Weser/Ems EPEs on one hand and the EPEs of the other three river basins on the other hand.

The final division of the basins into the smaller subcatchments (Figure 1) enables the analysis of even detailed spatial patterns of the events, presented in Figure 4b. It reveals a large variability of the $\mathrm{sWEI}_{\mathrm{rel}}$ for the individual EPEs. Nevertheless, some EPEs seem to be very similar from the viewpoint of their spatial patterns. To study these relations objectively, a cluster analysis (section 2.3) was performed using the $\mathrm{sWEI}_{\mathrm{rel}}$ values as the criteria.

3.2 | Clusters of events with respect to their spatial patterns

Figure 4a presents the results of the clustering process. Sharp differences are evident between the two main groups of events, which were generated at the next to last stage of the agglomerative clustering. The "Western" (W-CE) and "Eastern" (E-CE) groups of the central European events roughly refer to a border of the main drainage basins. The upper (Alpine) Rhine catchment (Rhine-a subcatchment) is an exception, as it belongs more frequently to the E-CE group otherwise limited to the Elbe, Danube and Oder events. On the other hand, the Saale catchment (Elbe-c) often stays with the W-CE group, which may also apply to the upper non-alpine Danube catchment (Danube-a) in some cases. However, the spatial variability of the precipitation extremes is still high within each of these groups (Figure 4b). Therefore, a finer division of the EPEs was employed with respect to the clustering dendrogram.

The W-CE events can be clearly divided into two groups: (a) EPEs affecting mainly the northwestern part of the study area (NW cluster)—the Weser, Ems, lower Rhine, and middle and lower Elbe and (b) EPEs of the non-alpine Rhine (R cluster), with only a small contribution of the upper Danube catchment. The group of the E-CE events consists of three distinct groups: (c) the Danube (without the Morava catchment) and upper Rhine events (RD), (d) Elbe-

TABLE 2 List of 53 maximum central European EPEs according to the total WEI_{rel} in contrast to 10 maximum EPEs within individual river basins. Each precipitation event is represented by its first day; the date is displayed in yyyy-mm-dd format. The clusters refer to Figure 4a

				WEI_{rel} ranking					
Ranking	**Precipitation event**	**Duration (days)**	**Cluster**	**Central Europe**	**Rhine**	**Weser/Ems**	**Elbe**	**Danube**	**Oder**
1	Jul 17, 1981	4	ED	0.235			0.292^{4}	0.345^{1}	0.254^{7}
2	Jul 4, 1997	5	O	0.200				0.273^{3}	0.348^{2}
3	May 30, 2013	4	ED	0.195			0.232^{6}	0.307^{2}	
4	Aug 11, 2002	2	ED	0.194			0.339^{1}	0.228^{6}	
5	Aug 7, 1978	2	ED	0.187	0.189^{6}		0.333^{2}		
6	Aug 6, 1985	4	O	0.176				0.195^{10}	0.360^{1}
7	Aug 1, 1983	5	ED	0.165			0.321^{3}		
8	Aug 3, 2006	6	O	0.153				0.197^{9}	0.257^{6}
9	Aug 9, 1964	5	O	0.148			0.195^{9}		0.266^{5}
10	Sep 5, 2007	2	ED	0.144				0.254^{4}	
11	Sep 25, 2010	3	ED	0.140			0.279^{5}		
12	Oct 20, 1986	3	R	0.140	0.227^{1}				
13	Jul 20, 2011	3	O	0.138					0.289^{3}
14	Jul 31, 1977	3	ED	0.137					0.225^{10}
15	Jul 15, 1997	7	O	0.137			0.224^{7}		0.232^{8}
16	Aug 6, 2002	2	ED	0.137				0.237^{5}	
17	Jul 16, 2002	2	NW	0.128		0.386^{1}			
18	Jul 8, 1996	1	O	0.123					0.276^{4}
19	Dec 19, 1993	2	R	0.121	0.210^{3}				
20	Mar 19, 2002	4	RD	0.119				0.219^{8}	
21	May 10, 1970	3	R	0.118	0.225^{2}				
22	Jul 31, 1991	3	ED	0.117				0.226^{7}	
23	Aug 7, 1981	4	R	0.115	0.170^{9}	0.214^{8}			
24	May 22, 1978	2	R	0.112	0.206^{4}				
25	Jun 17, 1979	1	ED	0.110					
26	Oct 27, 1998	2	R	0.107	0.193^{5}	0.222^{7}			
27	Sep 4, 1984	8	R	0.106	0.168^{10}	0.214^{9}			
28	Jul 22, 2010	3	O	0.106			0.165^{10}		
29	Sep 27, 2007	3	NW	0.103		0.264^{3}			
30	Jun 28, 1981	2	NW	0.102		0.307^{2}			
31	Jun 16, 1991	2	RD	0.102					
32	Jun 11, 1993	2	O	0.101			0.212^{8}		
33	Jun 24, 2013	2	O	0.101					
34	Feb 13, 1990	3	RD	0.100					
35	Jul 31, 1961	1	O	0.099					0.228^{9}
36	Jun 1, 1961	2	R	0.098	0.186^{7}				
37	Oct 6, 1982	2	R	0.095	0.173^{8}				
38	Apr 12, 1994	2	NW	0.094					
39	Dec 21, 1991	2	RD	0.089					
40	May 23, 1983	3	R	0.089					
41	May 27, 2007	3	NW	0.089					
42	Sep 12, 1998	4	R	0.088					
43	Aug 7, 2007	3	R	0.087					
44	Aug 21, 2005	2	RD	0.087					
45	Dec 28, 1986	3	NW	0.085		0.235^{5}			
46	May 7, 1978	2	ED	0.085					
47	Aug 21, 2007	1	NW	0.085		0.206^{10}			
48	Aug 20, 1970	3	NW	0.085					
49	Jul 3, 1981	1	NW	0.084		0.225^{6}			

(*Continues*)

TABLE 2 (Continued)

				$WEI_{rel}^{ranking}$					
Ranking	**Precipitation event**	**Duration (days)**	**Cluster**	**Central Europe**	**Rhine**	**Weser/Ems**	**Elbe**	**Danube**	**Oder**
50	May 16, 2010	3	O	0.084					
51	Jul 8, 1990	3	O	0.083					
52	Feb 25, 1997	1	R	0.082					
53	Aug 8, 1970	2	RD	0.082					
67	Aug 26, 2010	1		0.076		0.262[4]			

Danube events (ED), in which the Elbe is represented mainly by its Czech and Saxon parts, and (e) Oder events (O), when adjacent parts of the Elbe basin and the Morava catchment can also be hit. These five clusters were further considered. In Figure 5, each cluster is represented by the maximum EPE, when both the return periods and *t*-day precipitation totals are depicted and compared with the median return periods derived from all events merged in the respective cluster. It demonstrates the fact that the maximum events were often anomalous in rarity and extent, too.

Within the ED cluster, there are 6 of the top 10 central European EPEs, including the absolute maximum EPE of July 1981 and the more recent events of August 2002 and May 2013 (Table 2). The core area of the cluster is spread from the Alpine tributaries of the Danube (Inn, Enns, etc.) over Bohemia (the western part of Czechia) into Saxony, but individual events also affected parts of the Oder and Upper Rhine basins, as it was, for example, in July 1981 (Figure 5b). As a result, the cluster contains 6 of the 10 maximum events in both the Elbe and Danube basins, but only 2 events and 1 event of the 10 maxima in the Oder and Rhine basins, respectively (Table 2).

The other four central European EPEs of the top 10 belong to the O cluster. Three of these events were very

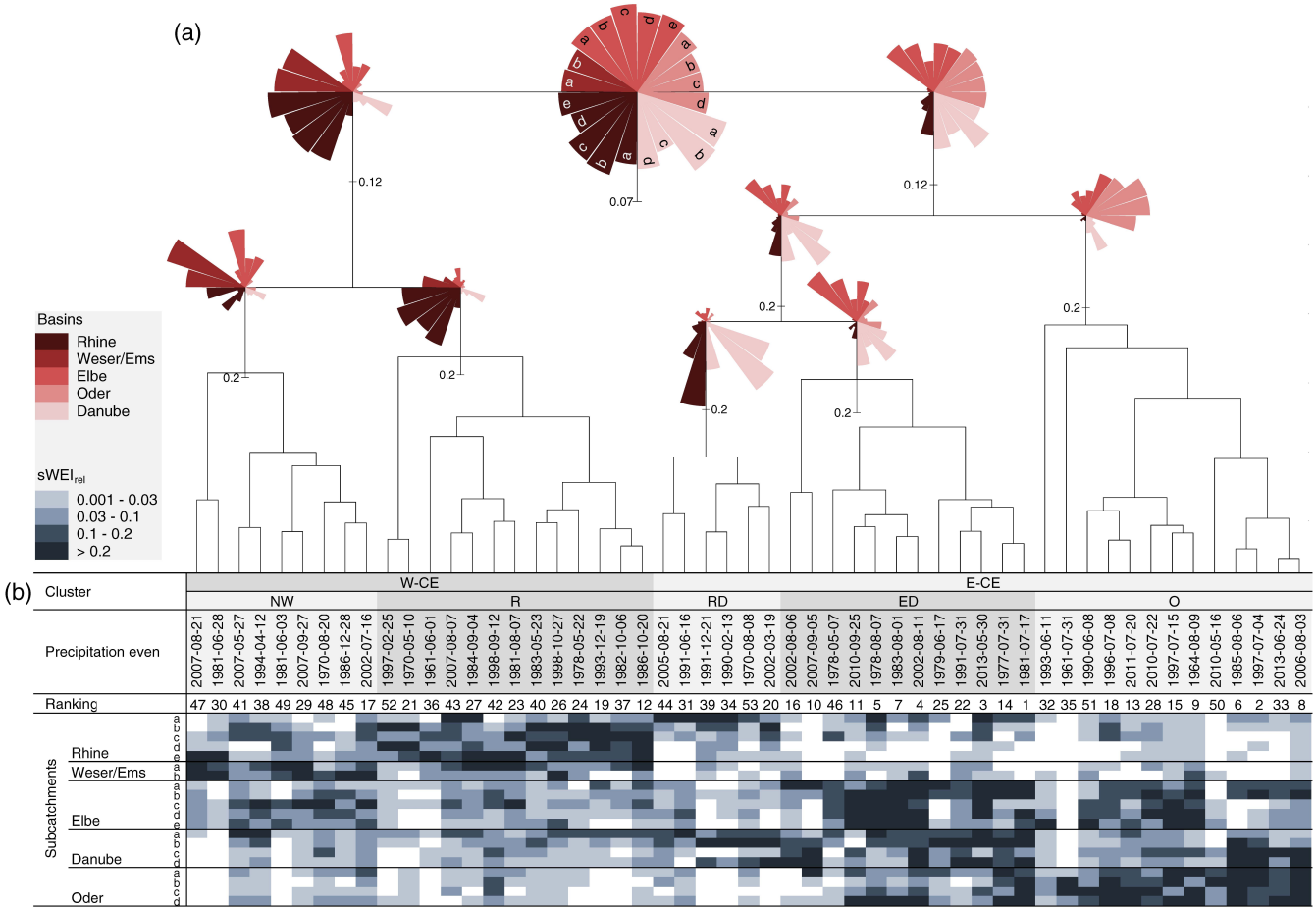

FIGURE 4 Hierarchical clustering of EPEs. (a) Dendrogram plot with polar bar charts showing the average values of $pWEI_{rel}$ in the whole set of events and in the selected clusters. (b) $sWEI_{rel}$ during the 53 maximum precipitation events. Each precipitation event is represented by its first day; the date is displayed in the yyyy-mm-dd format [Colour figure can be viewed at wileyonlinelibrary.com]

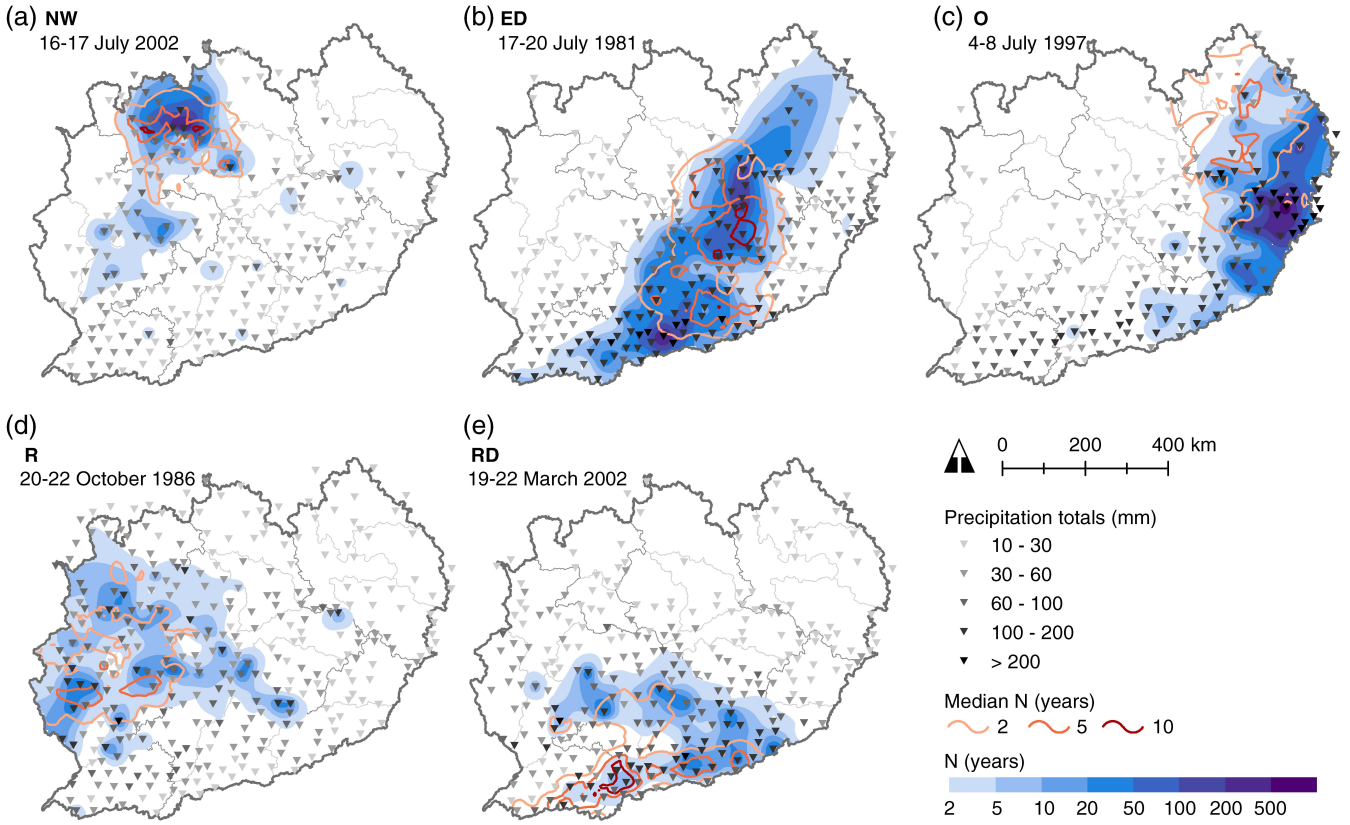

FIGURE 5 The return periods of *t*-day precipitation totals during the maximum EPE within each of the five distinguished clusters (NW, R, RD, ED, O). The contour lines depict the median position of the return periods during a set of events belonging to the cluster [Colour figure can be viewed at wileyonlinelibrary.com]

similar with respect to the spatial pattern of precipitation when they also affected the lower part of the Danube and the Czech part of the Elbe River basins (Figure 4b), as it was, for example, at the beginning of July 1997. Nevertheless, the core area of the cluster shifts to the northwest (Figure 5c). Apart from 8 of the 10 maximum events in the Oder River basin, the cluster also contains four and three of such maxima in the Elbe and Danube River basins, respectively (Table 2).

The remaining three clusters contain fewer highly ranked EPEs. The RD cluster, the third one complementing the E-CE group of events, is rather small with only six EPEs. The core area of the cluster is limited to the Alps in both the Rhine and Danube River basins. Only its maximum event from March 2002, which substantially exceeded the core area (Figure 5e), was large enough that it belongs to the 10 maximum Danube events (Table 2). In contrast, the R cluster contains as many as 9 of the 10 maximum Rhine events (Table 2), when the core area of the cluster lies in the middle part of the Rhine basin (Figure 5d). However, the EPEs of the R cluster also often affected the Weser/Ems River basin (Figure 4b). As a result, the cluster contains 3 of the 10 maximum events there. The rest of them belong to the NW cluster (Table 2), with a rather small core area covering mainly the Weser and the adjacent parts of the Elbe River basin (Figure 5a).

3.3 | Spatial extent of extreme precipitation events

The NW cluster generally includes less extensive events; the largest one did not exceed 100,000 km^2 (Figure 6a). It is comparable with the RD events; on the contrary, the extent of the events varies a lot for the other clusters. Especially in the case of the ED and O clusters, the events are distributed unevenly within Figure 6a, but they often have a larger extent and longer return periods of precipitation totals. This suggests the exceptional character of the highly ranked EPEs, which only arise from an interaction of high return periods and large extents of events. Within the top 10 EPEs, at least 15% of the areas were hit by precipitation of the 9-year average return periods. During the No. 1 case of July 1981, the average precipitation return period of 19 years affected approximately 30% of the study area. It resulted in a much higher WEI than for the No. 2 event in July 1997, which was characterized by a very high average return period (28 years) and the affected area reaching 17%. Finally, the No. 3 (May 2013) event was the most extensive, with 31% of the area hit, but the average return period was only approximately 11 years (see also Figure 3 for the comparison of the three maximum events). The remaining clusters contain events with lower WEI_{rel} values, which often result from a combination of high/low return periods and a local/large extent of the event (Figure 6a).

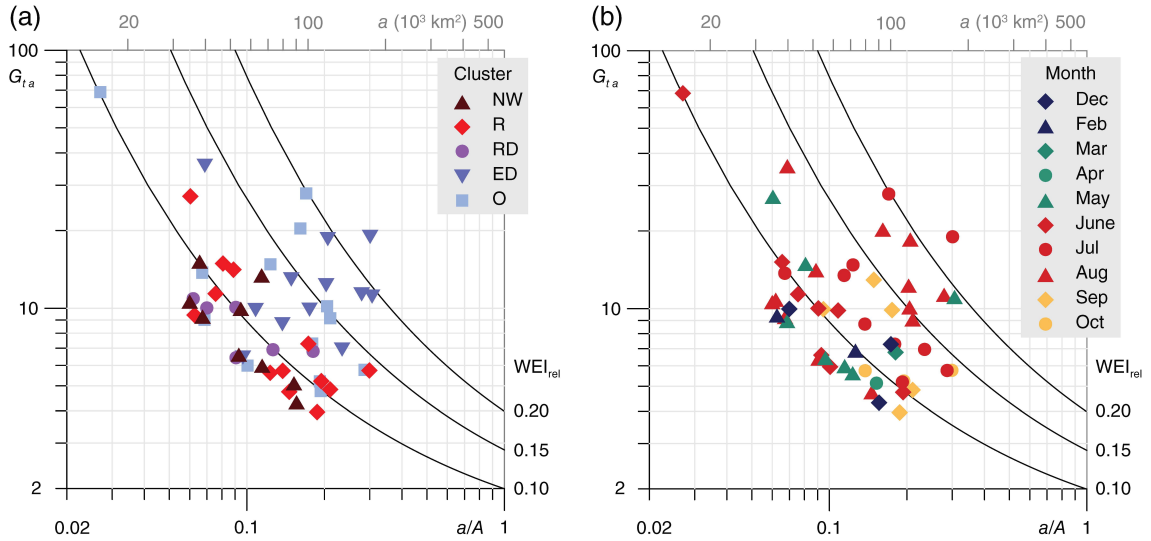

FIGURE 6 WEI$_{rel}$ values as a function of the affected area a and the geometric mean of the return periods of the precipitation totals G_{ta} during the 53 maximum precipitation events differentiated by (a) the clustering (compare with Figure 4) and (b) the month of the occurrence. The affected area a is expressed as a proportion of the total area considered (A)

Although the affected area of the individual EPEs reaches up to 31% (Figure 6a) of the total area of central Europe (as defined in Figure 1), it is not always continuous, but pronounced relations in precipitation are evident between distant areas due to similar orientations of mountain ranges, which enhance precipitation on their windward side. As a result, precipitation often occurs simultaneously in the Elbe-a and Danube-b subcatchments (Figure 7), which are both located north of mountain ranges (the Bohemian Forest and the Alps, respectively) but are otherwise adjacent only marginally (Figure 1). However, the orography not only connects distant subcatchments but also divides the neighbouring ones—as it does, for example, in the case of the Elbe-b and Elbe-d subcatchments, which, despite their proximity, have a relatively low value of Spearman's correlation coefficient between the values of the sWEI$_{rel}$ (Figure 7). The Ore Mountains between subcatchments acts as a barrier to airflow, causing the Elbe-b to lie in the rain shadow. The disparity is even greater between the Elbe-b and Elbe-c subcatchments (with a correlation coefficient close to 0). On the other hand, the low correlation between the Danube-c and Elbe-a is rather related to the narrower precipitation zone during the events caused by Vb cyclones (Müller *et al.*, 2009).

High positive correlation values occur especially among the Rhine (except for the Rhine-a) and Weser/Ems or the Oder and Danube-c subcatchments (Figure 7), when they do not necessarily need to be adjacent. However, there are some other highly correlated neighbouring subcatchments within the Elbe (Elbe-a and Elbe-b; Elbe-c and Elbe-d), Danube (Danube-a and Danube-b; Danube-b and Danube-d) or two adjacent river basins (Danube-a and Rhine-a), etc.

Surprisingly, we also noticed many negative correlations, which means that the occurrence of precipitation in

		Rhine					Weser/Ems		Elbe					Danube				Oder			
		a	b	c	d	e	a	b	a	b	c	d	e	a	b	c	d	a	b	c	d
Rhine	a	1.0																			
	b	0.5	1.0																		
	c	0.1	0.7	1.0																	
	d	0.2	0.6	0.6	1.0																
	e	0.1	0.5	0.6	0.8	1.0															
Weser/Ems	a	-0.2	0.4	0.7	0.6	0.8	1.0														
	b	-0.3	0.0	0.3	0.3	0.6	0.7	1.0													
Elbe	a	0.1	-0.3	-0.4	-0.4	-0.5	-0.6	-0.6	1.0												
	b	-0.2	-0.6	-0.5	-0.5	-0.4	-0.4	-0.3	0.6	1.0											
	c	-0.2	0.0	0.3	-0.1	0.1	0.4	0.5	-0.3	-0.1	1.0										
	d	-0.1	-0.5	-0.3	-0.6	-0.4	-0.2	0.1	0.2	0.3	0.6	1.0									
	e	-0.4	-0.4	-0.2	-0.4	-0.4	-0.1	0.3	-0.1	0.0	0.4	0.5	1.0								
Danube	a	0.5	0.4	0.3	0.1	0.0	-0.1	-0.2	0.3	-0.1	-0.1	-0.2	-0.3	1.0							
	b	0.4	0.0	-0.2	-0.1	-0.3	-0.4	-0.5	0.5	0.1	-0.4	-0.2	-0.4	0.5	1.0						
	c	-0.3	-0.6	-0.7	-0.4	-0.4	-0.5	-0.2	0.2	0.4	-0.4	-0.1	0.0	-0.4	0.1	1.0					
	d	0.1	-0.2	-0.4	-0.3	-0.2	-0.4	-0.3	0.4	0.2	-0.4	-0.1	-0.4	0.1	0.5	0.5	1.0				
Oder	a	-0.2	-0.6	-0.6	-0.6	-0.6	-0.6	-0.3	0.1	0.3	-0.4	0.1	0.3	-0.4	0.0	0.7	0.1	1.0			
	b	-0.2	-0.4	-0.6	-0.4	-0.5	-0.6	-0.5	0.1	0.1	-0.5	-0.1	0.1	-0.4	-0.1	0.5	0.1	0.8	1.0		
	c	-0.3	-0.5	-0.5	-0.5	-0.5	-0.5	-0.4	0.1	0.2	-0.3	0.1	0.3	-0.5	-0.2	0.4	-0.1	0.6	0.8	1.0	
	d	-0.4	-0.6	-0.7	-0.7	-0.7	-0.6	-0.4	0.3	0.4	-0.2	0.3	0.5	-0.4	-0.1	0.5	0.0	0.7	0.7	0.8	1.0

neighboring subcatchments

FIGURE 7 Matrix of Spearman's correlation coefficients between values of sWEI$_{rel}$ in individual subcatchments during the 53 maximum central European precipitation events [Colour figure can be viewed at wileyonlinelibrary.com]

two subcatchments is often mutually exclusive. In this context, we can separate two groups of subcatchments, which have mostly negative correlations with the members of the other group. It roughly corresponds to the division of the EPEs into the two main clusters, W-CE and E-CE (Figure 4a). The strongest negative correlations appear between the Oder, Danube-c, Elbe-a, and the non-alpine Rhine and Weser/Ems subcatchments (Figure 7), although there exist negative correlations within individual basins, too: e.g., the Elbe-a and Elbe-c or the Danube-a and Danube-c, which is apparently connected to the rather narrow precipitation zone producing the EPE.

3.4 | Spatial patterns in the seasonal distribution of events

Central European EPEs are distributed through the whole year but with higher concentrations in the warm half-year (from May to October) and mainly in July and the first half of August (Figure 8a). This is especially true in the case of highly ranked EPEs: all of the top 10 EPEs occurred in the warm half-year, 7 of them in the second half of July or the first half of August (Table 2). In contrast, only seven cold half-year events (from November to April) were detected at all.

The cold half-year events are only limited to the NW, R and RD clusters (Figure 8a), when they have typically lower return periods, and at the same time, the affected area is comparable to others or even smaller (Figure 6b). That is why the resulting values of the WEI_{rel} are quite small for these events. The situation is mostly similar to that of events occurring in May with few exceptions. The May 2013 event had an abnormal spatial extent; it occurred at the end of May, but it remains exceptional when comparing it to June events (Figure 6b). In contrast, two other May EPEs (1970 and 1978) with WEI_{rel} values above 0.1 had limited spatial extents, but they deviated from the average due to high return periods; both were concentrated mainly in the Rhine basin (Figure 4b) and classified into the R cluster.

The summer EPEs (JJA) are quite varied; the combination of relatively long return periods and large spatial extents often results in high values of the WEI_{rel}. However, it applies mainly to July and August EPEs (Figure 6b), while June events have rather lower WEI_{rel} values, including also the June 1993 event, which is located in the upper left corner of Figure 6b, indicating its local character and very high average return periods. The summer EPEs form the majority of the ED and O events, which both have clear seasonal patterns—occurring from May to September and the beginning of August, respectively (Figure 8a). Generally, the affected area is roughly the same for the summer and the rest of the year, but the return periods of the precipitation totals during the summer events overtop the others (Figure 6b).

In the autumn (SON), lower return periods are evident, especially within October events, when the affected area is approximately equal to or greater than that in the winter and spring. The autumn EPEs almost exclusively belong to the R cluster except for three September EPEs (Figure 8a).

Among the top 10 EPEs in individual subcatchments, the number of autumn events decreases towards the east, when it is the highest in the lower Rhine River basin (Figure 8c). In contrast, the upper and middle Rhine is the only area with two or more winter EPEs among the top 10 in subcatchments. The event seasonality is quite various in the Rhine River basin as well as in the Danube basin (Figure 8c). This feature is not very obvious in the Elbe or Oder River basins, where the seasonal distribution of the top 10 EPEs is similar across all subcatchments and their respective basins, too (Figure 8b). In the case of the Oder basin, a high concentration of events in the summer months is more or less apparent at both spatial levels.

3.5 | Spatial patterns in the inter-annual distribution of events

During the period between 1961 and 2013, the 53 maximum central European EPEs tend to occur in accumulations, whether lasting years or just a few weeks (Figure 9). The first 16 years of the study period (1961–1976) are characterized by a relatively low number of EPEs. Only six events were recognized, and all of them occurred in the warm half-year. These years are completely without greater events in the Danube and Weser/Ems basins, where EPEs first appeared in summer 1981. This year, we have recorded four central European events, including the absolute maximum event, over a relatively short period of 2 months (Figure 9b). Approximately a decade of wetter conditions ranges from 1977 to 1986, when we identified a large number of events with a high overall WEI_{rel} as well as the basins WEI_{rel} (Figure 9a).

This is in contrast with the 1990s, when many events occurred, but their WEI_{rel} values were much smaller; the two exceptions both appeared in July 1997 (Figure 9b). The period around the 1990s is, however, unique in the occurrence of cold half-year events, which only occurred between 1986 and 2002. This applies to the central European area and the individual basins, too. The period is somewhat longer in the case of the EPEs in the Rhine subcatchments (Figure 9a), but still, the cold half-year events occurred only from 1978 to 2003. The last period from 2002 to 2013 has, again, a large number of events with higher overall and basin WEI_{rel} although without any greater Rhine basin event. Many smaller accumulations of events occurred in this period: e.g., July/August 2002, August/September 2007 (Figure 9b) and May/June 2013.

An interesting shift in the seasonality is evident when looking at the top 10 EPEs in certain subcatchments. Only summer events occurred in the subcatchments (except for the Rhine-a to Rhine-d) until the mid-1980s (Figure 9a). In contrast, there has been no summer EPE in the Weser/Ems-a subcatchment since 1984 and in the Danube-a and Danube-b subcatchments since 1992.

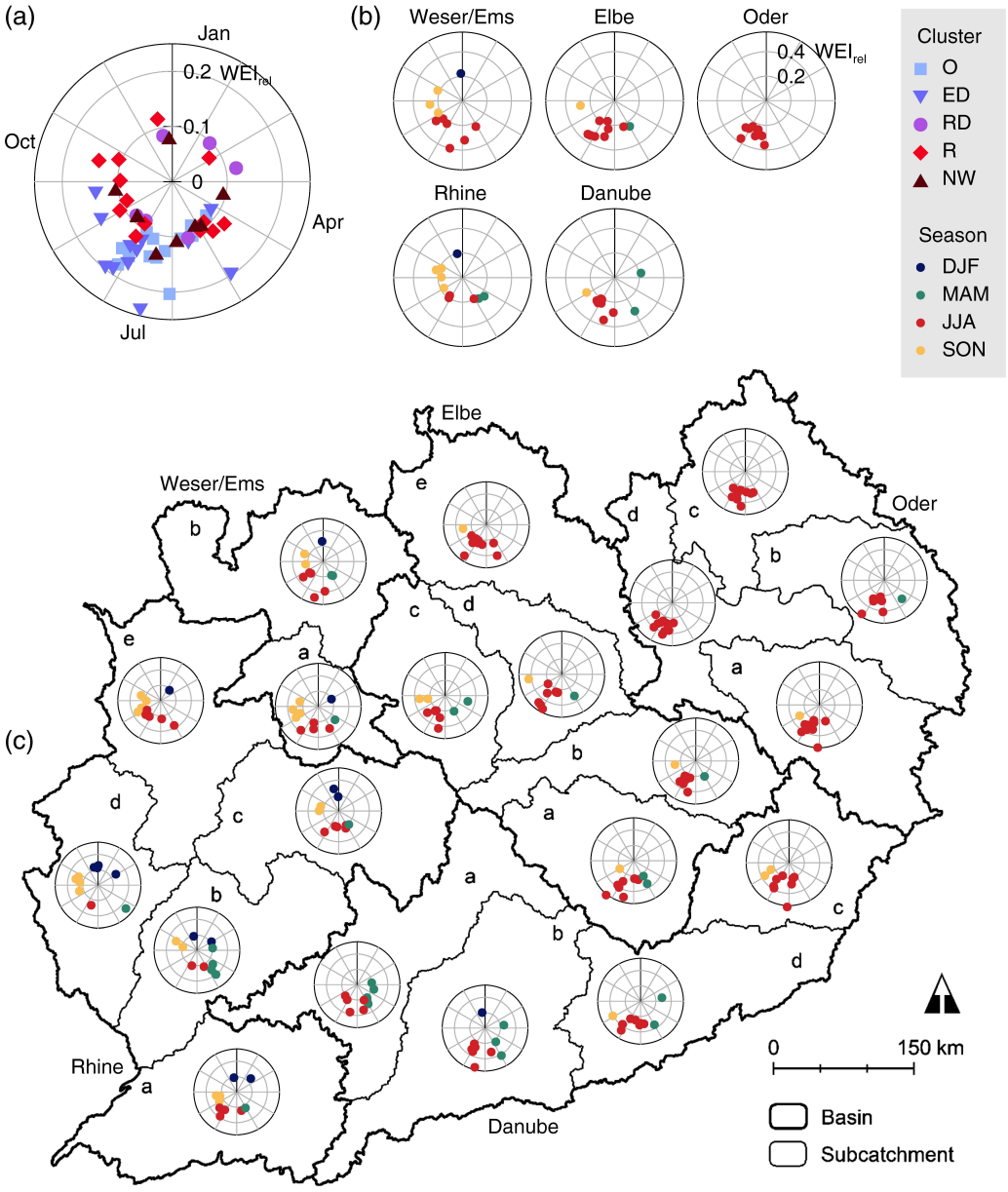

FIGURE 8 Seasonal distribution of precipitation extremes according to the WEI_{rel}. (a) The 53 maximum central European EPEs differentiated by the clustering (compare with Figure 4). (b) The 10 maximum events in each basin. (c) The 10 maximum events in each subcatchment. The values of WEI_{rel} are expressed by the distance from the diagram centre; all diagrams in (b) and (c) have the same scale [Colour figure can be viewed at wileyonlinelibrary.com]

4 | DISCUSSION

A point evaluation of precipitation totals is a frequent way of detecting extreme precipitation events. However, as already mentioned, for example, by Ren *et al.* (2012), precipitation extremes are rather regional phenomena with a specific duration and extent, which also applies to other weather and climate extremes. The WEI represent a set of regional evaluation techniques together with some other methods proposed for different regions (Ren *et al.*, 2012; Ramos *et al.*, 2017). Although the regional evaluation of weather extremes often depends on a selection of a study area, the WEI adjusts events to their actual extent and thus it is not subject to this problem. It seems that the WEI is a good compromise when comparing it with some standard methods including maximum precipitation totals or areal means (Müller *et al.*, 2015). It has an advantage of using return periods instead of precipitation totals, thus enabling the comparison of the extremity of events at different locations (Keef *et al.*, 2009). However, the uncertainty rises with the increasing estimated return periods. Therefore, we had to use a subjective threshold and limit their values to 1,000 years. The number seems realistic in the context of the hydrometeorological extremes of the last decades, when high return periods of several hundreds of years have been recorded in August 2002 (Ulbrich *et al.*, 2003) and July 1997 (Kundzewicz *et al.*, 1999).

Based on the WEI, we present the 53 maximum central European EPEs between 1961 and 2013; they mostly occurred during the warm half-year. In the period after 2013,

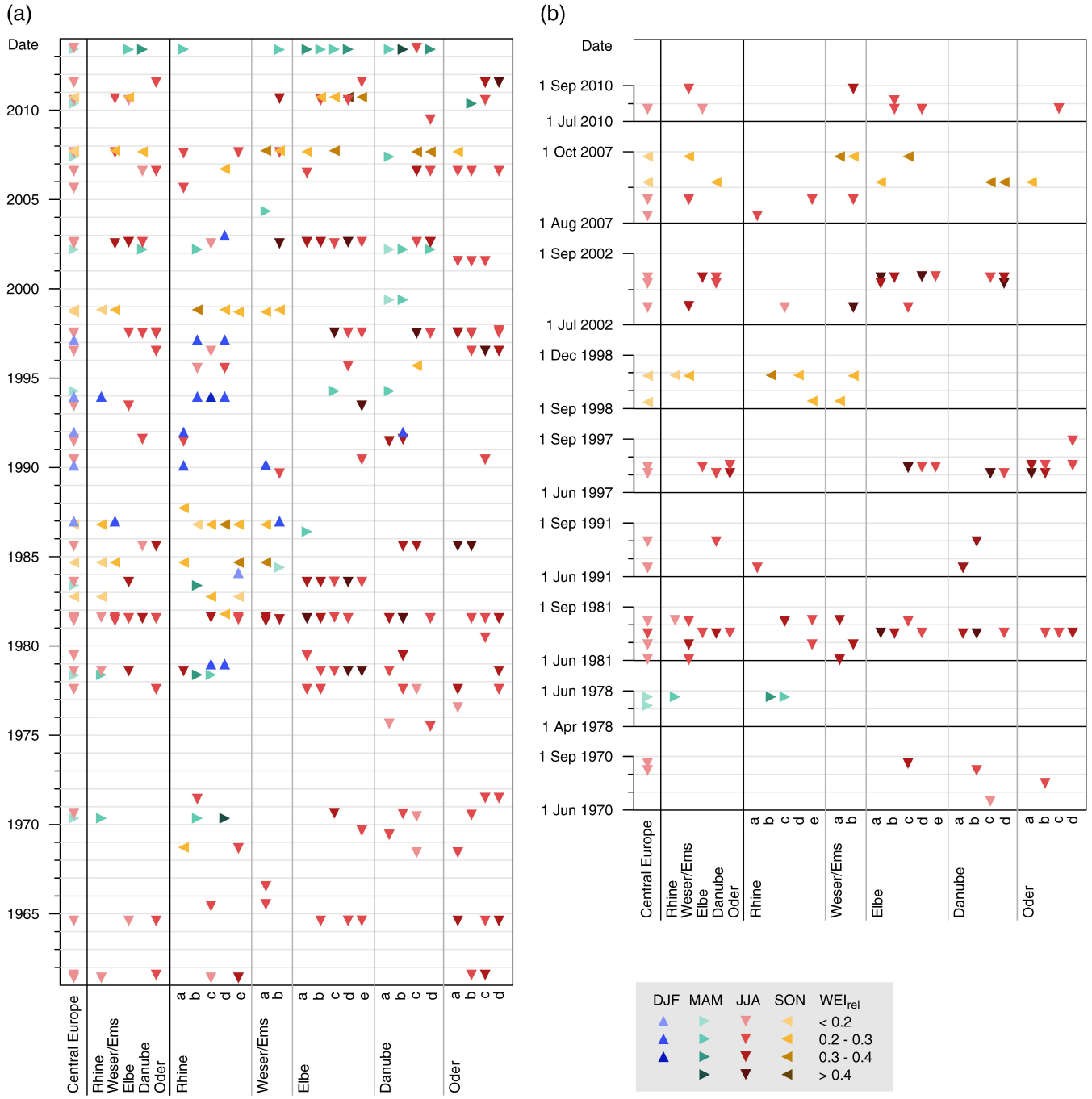

FIGURE 9 Timeline of the extreme precipitation events in central Europe. (a) The 53 maximum events in the whole study area (left column) and the 10 maximum events in each basin and subcatchment. (b) Segments of the timeline presenting selected periods with higher accumulations of events. Symbols represent the seasons; the darker shades indicate higher WEI_{rel} values [Colour figure can be viewed at wileyonlinelibrary.com]

there is no evidence of precipitation events with an extremity at the level of the five maximum central European EPEs, although three 24-hr precipitation extremes were reported by Hofstätter *et al.* (2017) during the years 2014 and 2015 in two smaller central European regions. The authors highlighted the period between 2006 and 2011 for the occurrence of heavy precipitation around Czechia. In contrast, the last years were mainly discussed in terms of extensive droughts in central Europe (Piniewski *et al.*, 2017).

The identified EPEs had various durations from 1 to 8 days. Depending on the size of the territory, it was appropriate to limit the possible duration. Müller *et al.* (2015) used a 5-day limit for Czechia, which we needed to extend. Although we considered up to 10-day precipitation extremes, only three events lasted longer than 5 days, but this does not apply to the five maximum events. In contrast, some of the five maximum EPEs lasted only 2 days (e.g., the August 2002 event). Nevertheless, they often resulted in rapid runoff increases in the affected rivers (Müller *et al.*, 2009) and severe floods (Müller *et al.*, 2015; Gvoždíková and Müller, 2017). They are generally well-documented, especially the most recent events of 2013 and

2002 (e.g., Ulbrich *et al*., 2003; Blöschl *et al*., 2013). The top 10 EPEs within central Europe are also significant in Czechia alone; however, not all EPEs are included in the list of extreme precipitation presented by Müller *et al*. (2015), which points to the spatial heterogeneity of the study area.

The events substantially differ in terms of the spatial distribution of the precipitation extremity (Figure 4b). Nevertheless, many similar events were coupled together by agglomerative hierarchical clustering, when the individual groups may later be connected to specific circulation conditions producing extremes (Seibert *et al*., 2007). We decided for a final number of five groups, which seems reasonable, given the number of events in each group. According to Wilks (2006), the choice is often subjective, and the final number of groups is adapted to a given problem, although some supporting methods have been proposed. According to, for example, Tibshirani *et al*. (2001) and their method of gap statistics, we should only consider two groups of events—it agrees with the aforementioned sharp contrast between the W-CE and E-CE events. On the other hand, the spatial variability of the precipitation extremes is still high within each of these groups (Figure 4b), which discourages us from this choice.

The five proposed clusters suggest the core areas of the precipitation events (Figure 5) and some clear seasonal patterns (Figure 8a), which basically agrees with other findings (e.g., Stucki *et al*., 2012; Ustrnul *et al*., 2014; Müller *et al*., 2015). Western Germany is an exception, where we assumed a greater number of cold half-year EPEs (Beurton and Thieken, 2009), but in fact, most of the events occurred from May to September (the NW cluster) or during the spring and autumn (the R cluster). The top 10 central European EPEs were exclusively classified into the ED or O clusters. The events are exceptional due to the combination of a large spatial extent and high return periods of precipitation totals, which always act together when producing major precipitation extremes (Figure 6a). Nevertheless, the area of central Europe is never affected as a whole. There exist high negative correlations between the values of the $s\mathrm{WEI}_{\mathrm{rel}}$, which suggest that the occurrence of precipitation is often mutually exclusive between some parts of the study area (Figure 7). On the other hand, high correlations are evident between the neighbouring subcatchments and the regions connected by similar effects of orography.

The spatial structure of the precipitation extremity is crucial for runoff processes and thus for flood generation at different locations. As stated by Nied *et al*. (2017), precipitation and associated weather patterns are mostly responsible for some of the flood characteristics including, for example, a number of gauges with an at least 10-year flood. This can be explained by an exceedance of the infiltration capacity (Merz and Plate, 1997) when the runoff starts depending only on precipitation. The discharges of shorter return periods of approximately 2 years are governed rather by soil moisture conditions (Nied *et al*., 2017). However, the severity of a flood event may be significantly influenced by the pre-event soil moisture content, as it was during the flood of 2013 (Schröter *et al*., 2015). Although the extremity of the EPEs in 2002 and 2013 was almost the same (Table 2), the severity of the 2013 flood seems to be much greater, with the extremity index of Uhlemann *et al*. (2010) reaching the value 1.5 versus 1.09 in 2002 (Gvoždíková and Müller, 2017). While the 2002 and 2013 events are highly ranked according to both the precipitation and flood extremity indices, the two maximum EPEs of 1981 and 1997 are at the 18–19th positions in the list of major floods (Gvoždíková and Müller, 2017). The pre-event soil moisture conditions can explain the difference, but a limitation of the study area may play a role in the case of 1997 event, which also affected parts of the Vistula basin (Kundzewicz *et al*., 1999). It is likely that the $\mathrm{WEI}_{\mathrm{rel}}$ value of 1997 EPE would increase as well if we consider the Vistula basin. This may also apply to the May 2010 EPE, which is well described by Bissolli *et al*. (2011) as an event of a large extent and high intensity, but it is ranked only as the 50th EPE and it does not appear in the list of major floods (Gvoždíková and Müller, 2017). In contrast, the highly ranked flood events of March 1988 and 1981 do not appear among the 53 maximum EPEs, as probably a combination of soil saturation, rainfall, and snowmelt generated the floods. Generally, the majority of the extreme central European floods occur in the cold half-year (Uhlemann *et al*., 2010; Gvoždíková and Müller, 2017), especially in the northwest of the area.

However, the number of cold half-year events in the list of the maximum central European EPEs is significantly smaller, related to generally higher return periods of precipitation totals during the warm half-year events. Nevertheless, few EPEs occurred between December and April, and they exclusively belonged to the NW, R, and RD clusters (Figure 8a). It is noteworthy that these events occurred in a relatively short period of approximately 15 years, suggesting some changes in the seasonality of the events during the study period. Certain shifts in the seasonality are evident even at the subcatchment level, when, for example, spring EPEs replaced the summer ones in the case of the Danube-a subcatchment (Figure 9). There are no similar seasonal shifts detected in central Europe, although some seasonal trends of precipitation extremes were found in the past (Frei and Schär, 2001). Generally, it is quite difficult to analyse trends of very rare events due to the relatively small datasets available. The detected seasonality shifts would need further investigations in different areas.

5 | CONCLUSIONS

Using the WEI, we found the maximum precipitation events occurring in central Europe between 1961 and 2013. The

index reflects the return periods of the precipitation totals and also the event duration and extent, which is a great advantage, as well as the adaptability of the affected area and duration to individual events.

The WEI identified EPEs at the different spatial levels: central Europe, individual basins, and their subcatchments. The detailed spatial structure of the precipitation extremity was particularly useful for finding analogous events with similar spatial distributions. Even at the level of two clusters, the agglomerative hierarchical clustering method sharply divided the EPEs into western and eastern central European events that clearly produced five different clusters in other hierarchical levels.

Though evaluated by return periods of precipitation totals, the 11 maximum events exclusively belong to the ED and O clusters, where the extreme precipitation affected mainly the Danube, Elbe, and/or Oder basins. The ED and O clusters are exceptional in their seasonality because they are concentrated only in the warmer half-year. Within the E-CE group, the only winter cases appear in the RD cluster, when mainly the Upper Rhine and Danube without the Morava basin are affected. The W-CE group generally comprises the non-alpine Rhine and Weser/Ems events, which also affect the Elbe-c subcatchment. The seasonal pattern is not so obvious, although the greater concentration of the Rhine events (R) is particularly noticeable in May and from September to October. Despite the expectations, most of the EPEs affecting the northwest of the area (NW) occur in the warm half-year.

As a result, the 53 central European EPEs were distributed over the whole year but with higher concentration and extremity in its warmer half. This is in contrast with the distribution of central European flood extremes. Therefore, future tasks will focus on the identification of a relationship between floods, the presented extreme precipitation events, and the circulation conditions producing them. We expect that similar features in the spatial distribution of the precipitation extremity are due to similarities in the causal atmospheric conditions and that they determine a similar distribution of flooding.

ACKNOWLEDGEMENTS

This work was supported by the Czech Science Foundation (Grant No. 17-23773S). We would also like to acknowledge the European Climate Assessment & Dataset project (ECA&D), Czech Hydrometeorological Institute (CHMI), Deutscher Wetterdienst (DWD), Instytut Meteorologii i Gospodarki Wodnej (IMGW), Zentralanstalt für Meteorologie und Geodynamik (ZAMG), Austrian data portal eHYD, Météo-France and MeteoSwiss for providing rain gauge data.

ORCID

Blanka Gvoždíková https://orcid.org/0000-0001-6465-4917

REFERENCES

van Bebber, W.J. (1891) Die Zugstrassen der barometrischen Minima nach den Bahnenkarten der deutschen Seewarte für den Zeitraum 1875–1890. *Meteorologische Zeitschrift*, 8, 361–366.

Beurton, S. and Thieken, A.H. (2009) Seasonality of floods in Germany. *Hydrological Sciences Journal*, 54, 62–76. https://doi.org/10.1623/hysj.54.1.62.

Bissolli, P., Friedrich, K., Rapp, J. and Ziese, M. (2011) Flooding in eastern central Europe in May 2010—reasons, evolution and climatological assessment. *Weather*, 66, 147–153. https://doi.org/10.1002/wea.759.

Black, A.R. and Werritty, A. (1997) Seasonality of flooding: a case study of North Britain. *Journal of Hydrology*, 195, 1–25.

Blöschl, G., Nester, T., Komma, J., Parajka, J. and Perdigão, R.A.P. (2013) The June 2013 flood in the Upper Danube Basin, and comparisons with the 2002, 1954 and 1899 floods. *Hydrology and Earth System Sciences*, 17, 5197–5212. https://doi.org/10.5194/hess-17-5197-2013.

Fowler, H.J. and Kilsby, C.G. (2003) A regional frequency analysis of United Kingdom extreme rainfall from 1961 to 2000. *International Journal of Climatology*, 23, 1313–1334. https://doi.org/10.1002/joc.943.

Frei, C. and Schär, C. (2001) Detection probability of trends in rare events: theory and application to heavy precipitation in the Alpine region. *Journal of Climate*, 14, 1568–1584.

Gibson, P.B., Perkins-Kirkpatrick, S.E., Alexander, L.V. and Fischer, E.M. (2017) Comparing Australian heat waves in the CMIP5 models through cluster analysis. *Journal of Geophysical Research: Atmospheres*, 122, 3266–3281. https://doi.org/10.1002/2016JD025878.

Gong, X. and Richman, M.B. (1995) On the application of cluster analysis to growing season precipitation data in North America east of the Rockies. *Journal of Climate*, 8, 897–931.

Grams, C.M., Binder, H., Pfahl, S., Piaget, N. and Wernli, H. (2014) Atmospheric processes triggering the central European floods in June 2013. *Natural Hazards and Earth System Sciences*, 14, 1691–1702. https://doi.org/10.5194/nhess-14-1691-2014.

Gvoždíková, B. and Müller, M. (2017) Evaluation of extensive floods in western/central Europe. *Hydrology and Earth System Sciences*, 21, 3715–3725. https://doi.org/10.5194/hess-21-3715-2017.

Hofstätter, M., Lexer, A., Homann, M. and Blöschl, G. (2017) Large-scale heavy precipitation over central Europe and the role of atmospheric cyclone track types. *International Journal of Climatology*, 38(Suppl. 1), e497–e517. https://doi.org/10.1002/joc.5386.

IPCC. (2014) *Climate Change 2014: Synthesis Report. Contribution of Working Groups I, II and III to the Fifth Assessment Report of the Intergovernmental Panel on Climate Change*. Geneva: IPCC.

Jacobeit, J., Homann, M., Philipp, A. and Beck, C. (2017) Atmospheric circulation types and extreme areal precipitation in southern central Europe. *Advances in Science and Research*, 14, 71–75. https://doi.org/10.5194/asr-14-71-2017.

Kašpar, M., Müller, M., Crhová, L., Holtanová, E., Polášek, J.F., Popa, L. and Valeriánová, A. (2017) Relationship between Czech windstorms and air temperature. *International Journal of Climatology*, 37, 11–24. https://doi.org/10.1002/joc.468.

Keef, C., Svensson, C. and Tawn, J.A. (2009) Spatial dependence in extreme river flows and precipitation for Great Britain. *Journal of Hydrology*, 378, 240–252. https://doi.org/10.1016/j.jhydrol.2009.09.026.

Konrad, C.E. (2001) The most extreme precipitation events over the eastern United States from 1950 to 1996: considerations of scale. *Journal of Hydrometeorology*, 2, 309–325.

Kundzewicz, Z.W., Szamalek, K. and Kowalczak, P. (1999) The great flood of 1997 in Poland. *Hydrological Sciences Journal*, 44, 855–870. https://doi.org/10.1080/02626669909492285.

Kyselý, J. (2009) Trends in heavy precipitation in The Czech Republic over 1961–2005. *International Journal of Climatology*, 29, 1745–1758. https://doi.org/10.1002/joc.1784.

Kyselý, J. and Picek, J. (2007) Regional growth curves and improved design value estimates of extreme precipitation events in The Czech Republic. *Climate Research*, 33, 243–255.

Lhotka, O. and Kyselý, J. (2014) Characterizing joint effects of spatial extent, temperature magnitude and duration of heat waves and cold spells over central Europe. *International Journal of Climatology*, 35, 1232–1244. https://doi.org/10.1002/joc.4050.

Marx, S. (1980) Die im Gebiet der DDR aufgetretenen extrem hohen Tagessummen des Niederschlages (1907 bis 1978) mit Angaben über die Ausmaße des

starken Dauerregens vom 7./8. August 1978. *Zeitschrift für Meteorologie*, 30, 318–328.

Merz, B. and Plate, E.J. (1997) An analysis of the effects of spatial variability of soil and soil moisture on runoff. *Water Resources Research*, 33, 2909–2922.

Messmer, M., Gómez-Navarro, J.J. and Raible, C.C. (2015) Climatology of Vb cyclones, physical mechanisms and their impact on extreme precipitation over central Europe. *Earth System Dynamics*, 6, 541–553. https://doi.org/10.5194/esd-6-541-2015.

Minářová, J., Müller, M., Clappier, A. and Kašpar, M. (2018) Comparison of extreme precipitation characteristics between the Ore Mountains and the Vosges Mountains (Europe). *Theoretical and Applied Climatology*, 133, 1249–1268. https://doi.org/10.1007/s00704-017-2247-x.

Müller, M. and Kašpar, M. (2011) Association between anomalies of moisture flux and extreme runoff events in the south-eastern Alps. *Natural Hazards and Earth System Sciences*, 11, 915–920. https://doi.org/10.5194/nhess-11-915-2011.

Müller, M. and Kašpar, M. (2014) Event-adjusted evaluation of weather and climate extremes. *Natural Hazards and Earth System Sciences*, 14, 473–483. https://doi.org/10.5194/nhess-14-473-2014.

Müller, M., Kašpar, M. and Matschullat, J. (2009) Heavy rains and extreme rainfall–runoff events in central Europe from 1951 to 2002. *Natural Hazards and Earth System Sciences*, 9, 441–450. https://doi.org/10.5194/nhess-9-441-2009.

Müller, M., Kašpar, M., Valeriánová, A., Crhová, L., Holtanová, E. and Gvoždíková, B. (2015) Novel indices for the comparison of precipitation extremes and floods: an example from the Czech territory. *Hydrology and Earth System Sciences*, 19, 4641–4652. https://doi.org/10.5194/hess-19-4641-2015.

Munich Re. (2011) *NATHAN World Map of Natural Hazards*. Munich: Munich Reinsurance Company.

Nied, M., Schröter, K., Lüdtke, S., Nguyen, V.D. and Merz, B. (2017) What are the hydro-meteorological controls on flood characteristics? *Journal of Hydrology*, 545, 310–326. https://doi.org/10.1016/j.jhydrol.2016.12.003.

Nissen, K.M., Ulbrich, U. and Leckebusch, G.C. (2014) Vb cyclones and associated rainfall extremes over central Europe under present day and climate change conditions. *Meteorologische Zeitschrift*, 22, 649–660. https://doi.org/10.1127/0941-2948/2013/0514.

Piniewski, M., Szcześniak, M., Kundzewicz, Z.W., Mezghani, A. and Hov, Ø. (2017) Changes in low and high flows in the Vistula and the Odra basins: model projections in the European-scale context. *Hydrological Processes*, 31, 2210–2225. https://doi.org/10.1002/hyp.11176.

Ramos, A.M., Trigo, R.M. and Liberato, M.L.R. (2017) Ranking of multi-day extreme precipitation events over the Iberian Peninsula. *International Journal of Climatology*, 37, 607–620. https://doi.org/10.1002/joc.4726.

Ren, F., Cui, D., Gong, Z., Wang, Y., Zou, X., Li, Y., Wang, S. and Wang, X. (2012) An objective identification technique for regional extreme events. *Journal of Climate*, 25, 7015–7027. https://doi.org/10.1175/JCLI-D-11-00489.1.

Roberts, J.F., Champion, A.J., Dawkins, L.C., Hodges, K.I., Shaffrey, L.C., Stephenson, D.B., Stringer, M.A., Thornton, H.E. and Youngman, B.D. (2014) The XWS open access catalogue of extreme European windstorms from 1979 to 2012. *Natural Hazards and Earth System Sciences*, 14, 2487–2501. https://doi.org/10.5194/nhess-14-2487-2014.

Schröter, K., Kunz, M., Elmer, F., Mühr, B. and Merz, B. (2015) What made the June 2013 flood in Germany an exceptional event? A hydro-meteorological evaluation. *Hydrology and Earth System Sciences*, 19, 309–327. https://doi.org/10.5194/hess-19-309-2015.

Seibert, P., Frank, A. and Formayer, H. (2007) Synoptic and regional patterns of heavy precipitation in Austria. *Theoretical and Applied Climatology*, 87, 139–153. https://doi.org/10.1007/s00704-006-0198-8.

Stucki, P., Rickli, R., Brönnimann, S., Martius, O., Wanner, H., Grebner, D. and Luterbacher, J. (2012) Weather patterns and hydro-climatological precursors of extreme floods in Switzerland since 1868. *Meteorologische Zeitschrift*, 21, 531–550. https://doi.org/10.1127/0941-2948/2012/36.

Tibshirani, R., Walther, G. and Hastie, T. (2001) Estimating the number of clusters in a data set via the gap statistic. *Journal of the Royal Statistical Society: Series B*, 63, 411–423. https://doi.org/10.1111/1467-9868.00293.

Uhlemann, S., Thieken, A.H. and Merz, B. (2010) A consistent set of trans-basin floods in Germany between 1952–2002. *Hydrology and Earth System Sciences*, 14, 1277–1295. https://doi.org/10.5194/hess-14-1277-2010.

Ulbrich, U., Brücher, T., Fink, A.H., Leckebusch, G.C., Krüger, A. and Pinto, J.G. (2003) The central European floods of August 2002: part 1—rainfall periods and flood development. *Weather*, 58, 371–377. https://doi.org/10.1256/wea.61.03A.

Ustrnul, Z., Wypych, A., Henek, E., Czekierda, D., Walawender, J., Kubacka, D., Pyrc, R. and Czernecki, B. (2014) *Meteorological hazard atlas of Poland*. Kraków: Instytut Meteorologii i Gospodarki Wodnej, Wydawnictwo Attyka.

Valeriánová, A., Crhová, L., Holtanová, E., Kašpar, M., Müller, M. and Pecho, J. (2017) High temperature extremes in The Czech Republic 1961–2010 and their synoptic variants. *Theoretical and Applied Climatology*, 127, 17–29. https://doi.org/10.1007/s00704-015-1614-8.

Wilks, D.S. (2006) *Statistical Methods in the Atmospheric Sciences*, 2nd edition. Amsterdam: Academic Press.

Zhang, X., Alexander, L., Hegerl, G.C., Jones, P., Klein Tank, A., Peterson, T.C., Trewin, B. and Zwiers, F.W. (2011) Indices for monitoring changes in extremes based on daily temperature and precipitation data. *WIREs: Climate Change*, 2, 851–870. https://doi.org/10.1002/wcc.147.

How to cite this article: Gvoždíková B, Müller M, Kašpar M. Spatial patterns and time distribution of central European extreme precipitation events between 1961 and 2013. *Int J Climatol*. 2019;1–16. https://doi.org/10.1002/joc.6019

5 Moisture flux anomalies

Paper IV: Gvoždíková, B., Müller, M., 2021. Moisture fluxes conducive to central European extreme precipitation events. Atmospheric Research, 248. https://doi.org/10.1016/j.atmosres.2020.105182.

Atmospheric Research 248 (2021) 105182

Contents lists available at ScienceDirect

Atmospheric Research

journal homepage: www.elsevier.com/locate/atmosres

Moisture fluxes conducive to central European extreme precipitation events

Blanka Gvoždíková[a,*], Miloslav Müller[a,b]

[a] Charles University, Faculty of Science, Department of Physical Geography and Geoecology, Albertov 6, Prague 2, 128 43, Czech Republic
[b] Institute of Atmospheric Physics CAS, Department of Meteorology, Boční II 1401, Prague 4, 141 31, Czech Republic

ARTICLE INFO

Keywords:
Moisture flux
Vertical velocity
Extreme precipitation
Central Europe

ABSTRACT

For the emergence of central European extreme precipitation events (EPEs), moisture supply mainly from the Atlantic or Mediterranean and an ascent of moist air are the most important ingredients. In the present study, we aim to define groups of EPEs with characteristic moisture flux conditions in the area of extra high upward vertical velocity, as well as to find the connection between the variants of moisture flux conditions and the spatio-seasonal distribution of extreme precipitation. Using ERA5 reanalysis data, we assigned one of three moisture flux variants to the set of 43 EPEs from 1979 to 2013 and thus specified (i) events with dominating moisture flux from the north (*Nf*), (ii) events with dominating moisture flux from the west (*Wf*), and (iii) other low-flux events (*Ot*). The classification of EPEs corresponds perfectly with seasonal and spatial patterns of extreme precipitation: while *Nf* events were concentrated only in the warm half-year and affected mainly eastern central Europe, *Wf* events occurred in the west and exclusively from September to March. Mainly in the case of *Nf* events, a direct link existing between anomalies in moisture flux and precipitation extremes can be beneficial for improving skill in forecasting EPEs.

1. Introduction

Large-scale extreme precipitation events in central Europe are usually associated with anomalies of atmospheric conditions at the synoptic scale. Meteorological variables, including potential vorticity, vertical velocity, and moisture flux, are studied in connection with the occurrence of hydrometeorological extremes (Martius et al., 2006; Kašpar and Müller, 2014) when the interaction of several anomalous variables allows the emergence of heavy rainfall or flooding in central Europe (Müller et al., 2009).

In elevated parts of the study area of central Europe, intense integrated vapour transport seems to be directly connected to extreme floods, as was demonstrated by Froidevaux and Martius (2016) in the Swiss Alps. Similar results were found in the southeastern Alps by Müller and Kašpar (2011), who revealed a close relationship between extreme flood events and moisture flux at the 850 hPa level in the respective area.

Both the Atlantic and the Mediterranean are important sources of moisture for precipitation in central Europe (Sodemann and Zubler, 2010). Warm-conveyor-belt advection and shallow convection in mid-latitude cyclones help move moisture into the free troposphere and transport it over long distances (Boutle et al., 2011). Apart from the large-scale moisture transport from distant water bodies, local land evaporation may play a crucial role in the emergence of heavy precipitation. This effect was shown in the case of extreme precipitation in August 2002 (Sodemann et al., 2009; Stohl and James, 2004) as well as during other mostly summer precipitation events (Sodemann and Zubler, 2010). In this study, we focus only on synoptic-scale processes of moisture transport that are major contributors to heavy precipitation throughout the year.

Cyclones moving along the Vb track (Van Bebber, 1891) are one of the main synoptic patterns controlling large-scale summer precipitation extremes in central Europe (Messmer et al., 2015). During the Vb events, cyclones move from the region of Genoa to the northeast and bring Mediterranean air into central Europe. The warm and moist air turns around the centre of the cyclone, so we actually experience moisture flux from the north or the northeast in the lower troposphere (Müller and Kašpar, 2010). Orographically enhanced precipitation induced by the Vb cyclone often results in extensive flooding on the northern slopes of the Alps and other west-east oriented mountain ranges in central Europe. Flooding then also affects the lowlands north of them, especially the Elbe and Oder basins and parts of the Danube basin (Nissen et al., 2014). Compared to the flood of August 2002 (Řezáčová et al., 2005), the more recent flood of May/June 2013 did not have the classic Vb character, but multiple cyclones tracked rather westward into central Europe, affecting mainly the Elbe and Danube

* Corresponding author.
E-mail address: blanka.gvozdikova@natur.cuni.cz (B. Gvoždíková).

https://doi.org/10.1016/j.atmosres.2020.105182
Received 8 April 2020; Received in revised form 23 June 2020; Accepted 30 July 2020
Available online 03 August 2020
0169-8095/ © 2020 Elsevier B.V. All rights reserved.

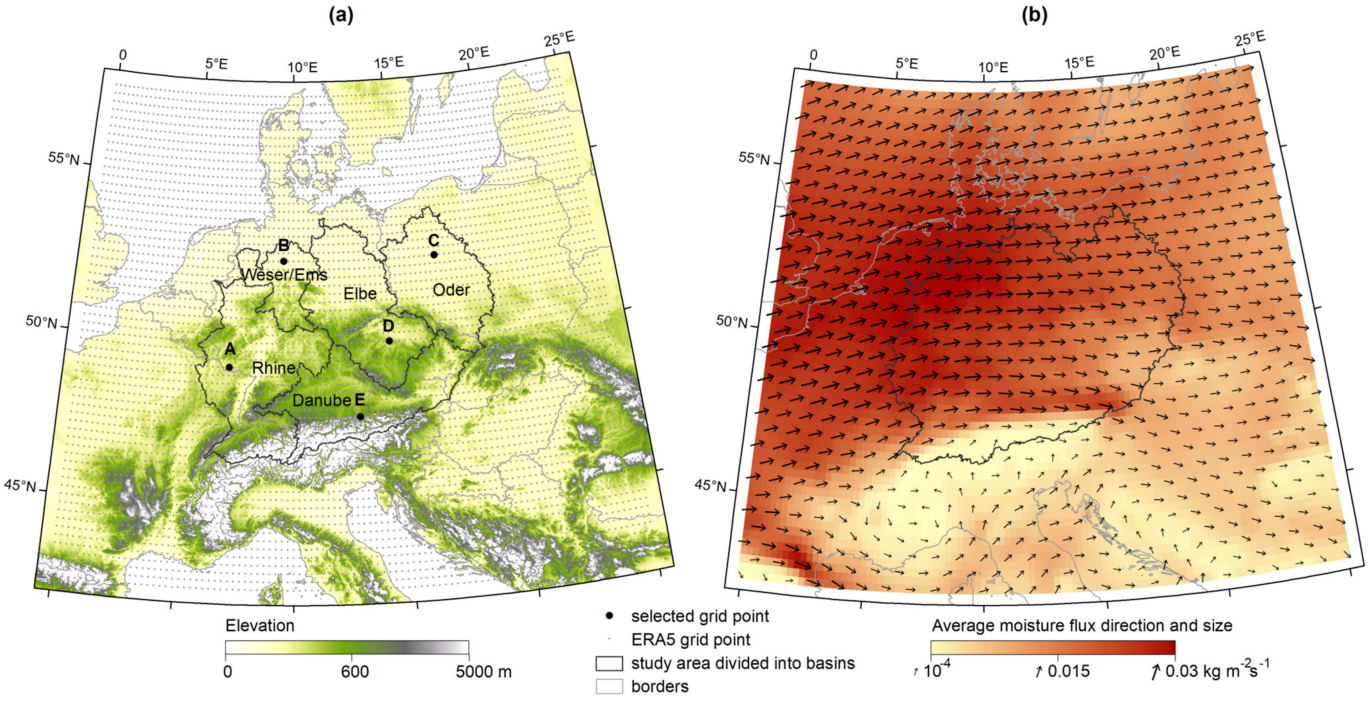

Fig. 1. (a) Elevation and (b) average moisture fluxes ($kg\,m^{-2}\,s^{-1}$) between 1979 and 2017 at the isobaric level of 850 hPa within and around the study area of central Europe. The arrow angle represents the average direction of moisture flux. Five grid points selected for further study (Table 2) are marked by capital letters.

basins (Grams et al., 2014). Nevertheless, a persistent northern moisture flux was a common feature for the development of heavy precipitation in 2013.

Another type of synoptic pattern brings moisture from the western sector with Atlantic frontal systems. Their influence is the largest in northwestern central Europe, and it decreases towards the southeast. The pattern is mostly related to winter precipitation extremes (Beurton and Thieken, 2009; Hofstätter et al., 2017). An intense moisture flux during these situations is induced by associated mid-latitude cyclones with a generally strong flow from the western sector. In winter, extreme winds tend to be connected to precipitation extremes mainly in northwestern central Europe (Martius et al., 2016), where the simultaneous occurrence of extreme events is often associated with low-pressure systems over the North Sea (Pfahl, 2014).

Mean moisture fluxes at the 850 hPa level have mostly western directions in central Europe (Fig. 1) in accordance with the prevailing winds from the west to the east in the mid-latitudes. The same is true for the mean vertically integrated water vapour flux (IWVF; Wypych et al., 2018), which confirms the significance of western zonal fluxes. The meridional component of the mean moisture flux is much less intense, especially in winter; however, July shows a slightly negative (northern) IWVF in southeastern central Europe, when the northwestern part tends to have positive values in July and October (Wypych et al., 2018). Differences in the significance of zonal and meridional moisture fluxes are the reason for concentrating on moisture flux anomalies that deviate from expected values and allow us to compare moisture fluxes from different directions. However, the question remains to what extent the occurrence of precipitation extremes can be explained by the presence of moisture flux extremes.

For the emergence of extreme precipitation, the moisture supply is not sufficient because only sustained ascent of moist air provides suitable conditions (Doswell III et al., 1998; Froidevaux and Martius, 2016). In the present study, selected extreme precipitation events (EPEs) from 1979 to 2013 are classified with respect to moisture flux magnitudes and direction in the area of extra high upward vertical velocity, which helps to distinguish various circulation types of the EPEs. The resulting variants of moisture flux conditions are assumed to correspond with spatial clusters of EPEs (Gvoždíková et al., 2019). By connecting EPEs to extremes of moisture flux, we want to explain the spatial occurrence and distribution of these events during the year, as there are great differences in the origin of "summer" and "winter" EPEs. At the spatial level of central Europe, we show the correspondence between the seasonality of moisture flux extremes from different directions and the seasonal variability in extreme precipitation events in the study area.

2. Data and methods

2.1. Reference precipitation events

Reference events are represented by a set of extreme precipitation events (EPEs), which were selected in our previous study (Gvoždíková et al., 2019) focusing on the spatial and temporal characteristics of central European EPEs. In the area of five main river basins (Rhine, Weser/Ems, Elbe, Danube, and Oder; see Fig. 1a), 53 maximum precipitation events were selected in 53 years between 1961 and 2013 by the value of the weather extremity index (WEI; Müller et al., 2015), combining the rarity of precipitation totals within an event-adjusted area and the spatial extent of the area. The determination of the WEI was done by maximizing the variable E_{ta} (Müller and Kašpar, 2014), which is the product of the radius of a circle, equivalent to the step-by-step increased considered area, and the mean common logarithm of the return periods of precipitation totals within the respective area. Not only the size of the considered area but also the duration of the event was optimized for each event by selecting the time window (from 1 to 10 days) in which the variable E_{ta} was maximum. Therefore, long-lasting large-scale precipitation is preferred over short-term local rains in the dataset.

Because of the time range of the reanalysis data used for the analysis of moisture fluxes (Section 2.2), the set of reference EPEs was limited to the period since 1979. Among the 43 EPEs that occurred between 1979 and 2013, most are summer extremes (Table 1), which often resulted in severe floods (Gvoždíková and Müller, 2017). The WEI was calculated not only within the whole study area but also within the five river

Table 1
Extreme precipitation events in central Europe from 1979 to 2013 ranked by precipitation extremeness (WEI) (Gvoždíková et al., 2019).

Ranking	Precipitaion event	Duration (days)	WEI	Ranking	Precipitaion event	Duration (days)	WEI
1	17 Jul 1981	4	0.235	23	22 Jul 2010	3	0.106
2	4 Jul 1997	5	0.200	24	27 Sep 2007	3	0.103
3	30 May 2013	4	0.195	25	28 Jun 1981	2	0.102
4	11 Aug 2002	2	0.194	26	16 Jun 1991	2	0.102
5	6 Aug 1985	4	0.176	27	11 Jun 1993	2	0.101
6	1 Aug 1983	5	0.165	28	24 Jun 2013	2	0.101
7	3 Aug 2006	6	0.153	29	13 Feb 1990	3	0.100
8	5 Sep 2007	2	0.144	30	6 Oct 1982	2	0.095
9	25 Sep 2010	3	0.140	31	12 Apr 1994	2	0.094
10	20 Oct 1986	3	0.140	32	21 Dec 1991	2	0.089
11	20 Jul 2011	3	0.138	33	23 May 1983	3	0.089
12	15 Jul 1997	7	0.137	34	27 May 2007	3	0.089
13	6 Aug 2002	2	0.137	35	12 Sep 1998	4	0.088
14	16 Jul 2002	2	0.128	36	7 Aug 2007	3	0.087
15	8 Jul 1996	1	0.123	37	21 Aug 2005	2	0.087
16	19 Dec 1993	2	0.121	38	28 Dec 1986	3	0.085
17	19 Mar 2002	4	0.119	39	21 Aug 2007	1	0.085
18	31 Jul 1991	3	0.117	40	3 Jun 1981	1	0.084
19	7 Aug 1981	4	0.115	41	16 May 2010	3	0.084
20	17 Jun 1979	1	0.110	42	8 Jun 1990	3	0.083
21	27 Oct 1998	2	0.107	43	25 Feb 1997	1	0.082
22	4 Sep 1984	8	0.106				

basins (shown in Fig. 1a) and their subcatchments. The values were then used as a similarity measure for clustering the events with respect to the spatial pattern of precipitation (Gvoždíková et al., 2019).

2.2. Reanalysis data

Our study employs ERA5 reanalysis data (Copernicus Climate Change Service, 2017) from 1979 to 2017. To recognize various circulation types of the EPEs, the fields of moisture fluxes are analysed and combined with vertical velocity. From the global hourly ERA5 dataset, we use the 6-h-resolution data of vertical velocity w (Pa s^{-1}) at the isobaric level of 700 hPa and several other meteorological variables at the 850 hPa level: air temperature T (K), specific humidity q (kg kg^{-1}), the zonal component of wind u (m s^{-1}), and the meridional component of wind v (m s^{-1}). All data are on a regular grid with a spatial resolution of 0.25° and processed in the area 0° − 25°E, 42.5° − 57.5°N.

The zonal and meridional moisture flux, F_{qu} and F_{qv}, respectively (kg m^{-2} s^{-1}), are calculated as a product of the air density ρ, specific humidity q, and the zonal or meridional component of wind (u or v) as follows:

$$F_{qu} = \rho q u \quad (1)$$

$$F_{qv} = \rho q v \quad (2)$$

Fluxes from the east and the north are negative, and we mark them as F_E and F_N, respectively. Correspondingly, for positive values, F_W refers to western and F_S to southern fluxes. Eqs. (1) and (2) suggest a significant decrease in moisture flux with altitude (Müller and Kašpar, 2011), which has discouraged us from using isobaric levels higher than 850 hPa. Nevertheless, lower levels are also not suitable due to higher mountainous terrain in some parts of the study area (Fig. 1a). To distinguish upward motions, values of vertical velocity at the 700 hPa isobaric level are used.

Instead of individual values of the vertical velocity and the components of moisture fluxes (F_{qu} and F_{qv}), we calculated daily means from 0600, 1200, 1800 UTC and 0000 UTC of the following day to make it comparable with daily precipitation totals (from 0600 to 0600 UTC) used for the selection of reference EPEs.

2.3. Anomalies of moisture flux

The magnitude and direction of moisture flux were chosen as decisive criteria for creating groups of EPEs of similar circulation conditions. For the list of reference events, we aim to determine the moisture flux anomaly from daily means of F_E, F_W, F_N and F_S. However, Fig. 1b shows the prevalence of western moisture fluxes in most parts of the study area except for the southern edge, where we observe some deformation by the Alps. To suppress the dominance of western fluxes, we need to transform the daily absolute values of moisture flux into relative values with respect to its climatology. In terms of the cumulative distribution function, we estimate cumulative probabilities corresponding to the i^{th} order statistic in the given pixel and thus make the values of fluxes comparable:

$$P(x_i) = \frac{i}{I+1} \quad (3)$$

In Eq. (3), P is the probability of x_i in its distribution function being equal to or lower than it, where i is the rank order and I is the total number of values (I = 14,245; i.e. the number of days in the whole period from 1979 to 2017). Cumulative probabilities close to 0 correspond to extreme eastern or northern fluxes in Eq. (3) (for x equal to F_{qu} or F_{qv}, respectively), while values of P close to 1 have opposite directions. Fig. 2 shows some examples of cumulative distribution functions derived from F_{qu} and F_{qv} values in five selected grid points of the study area (see Fig. 1a).

Daily means of vertical velocity w are transformed in terms of cumulative probabilities, according to Eq. (3), when negative values of vertical velocity indicating ascending motion have P close to 0. As heavy precipitation is mainly a result of ascending low-level moist air (Doswell III et al., 1998), we decided to combine the information about vertical velocity and moisture flux for the evaluation of moisture transport during reference EPEs. For this purpose, only grid points that have $P(w_i) \leq 0.1\%$ are considered (marked with *). A geometric mean G of cumulative probabilities of the components of moisture fluxes (F_{qu} and F_{qv}) over all such grid points is calculated as

$$G^*_e = \left(\prod_1^n P(x_i)^*\right)^{\frac{1}{n}} \quad (4)$$

for negative moisture fluxes F_E and F_N and

$$G^*_e = \left(\prod_1^n 1 - P(x_i)^*\right)^{\frac{1}{n}} \quad (5)$$

for positive moisture fluxes F_W and F_S. Thus, G^*_e values close to zero indicate extreme moisture fluxes from any directional sector within the area with extra high upward vertical motions.

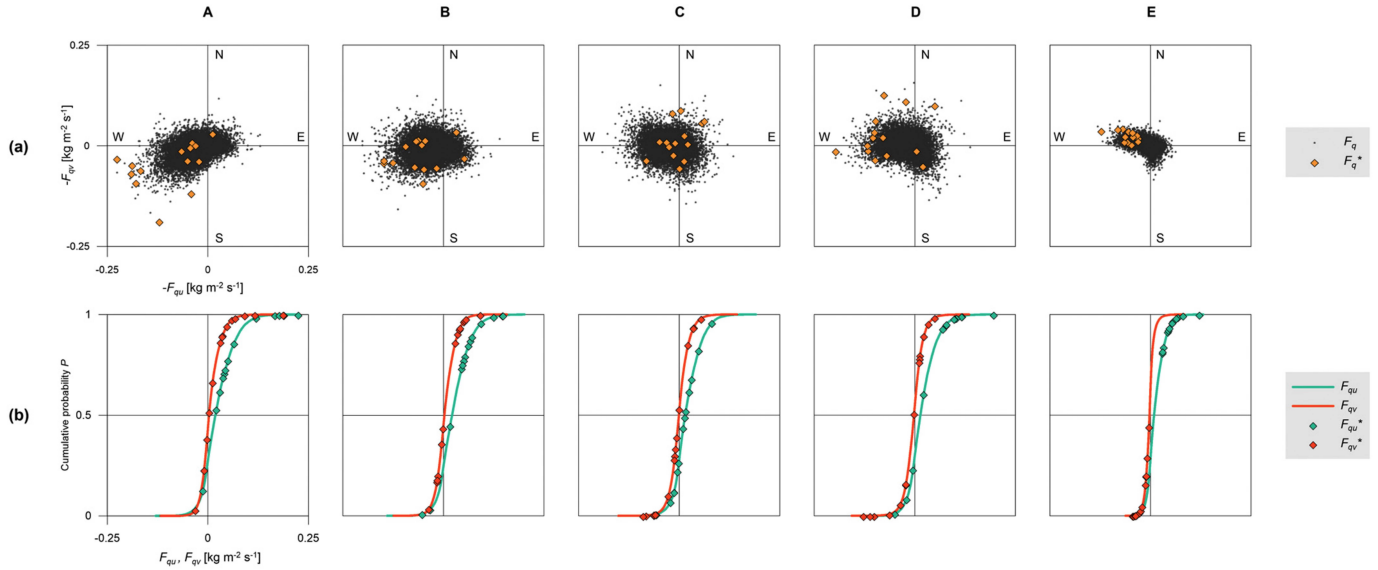

Fig. 2. Daily mean moisture fluxes F_q at the 850 hPa level from 1 January 1979, to 31 December 2017, at five selected grid points in the study area (A – E, see Fig. 1a and Table 2). If extra high upward vertical velocity ($P(w_i) \leq 0.1\%$) simultaneously occurred at the 700 hPa level at the grid point, the moisture flux is highlighted by a larger symbol and marked with * in the caption. (a) Magnitude and direction of the moisture flux on each day expressed by the distance and position of the symbol to the centre of the diagram. (b) Cumulative distribution function values of F_{qu} and F_{qv} at the 850 hPa level.

The total number of considered grid points in the geometric mean equals n during a single EPE, which can last one day but is usually a multi-day event, indicating that more than one day of data can be counted in Eqs. (4) and (5) according to the length of the reference event e (see Table 1). In the case of, e.g., a two-day event, the geometric mean is taken over all grid points that had $P(w_i) \leq 0.1\%$ in the first or the second day of the event. If the condition is met on both days, two values are included for one grid point.

2.4. Spatially accumulated moisture flux

Although the geometric means calculated by Eqs. (4) and (5) represent the rarity of moisture flux values, they do not reflect the real total amount of transported water vapour during the event over a certain area. A small value of G_e^* can be obtained by averaging cumulative probabilities over large areas as well as over only a few grid points. Therefore, we introduce a variable called spatially accumulated moisture flux T_d (kg s^{-1}), which is defined as

$$T_d = \sqrt{(S(F_{EW>}))^2 + (S(F_{NS>}))^2} \tag{6}$$

where S (kg s^{-1}) represents spatially accumulated moisture flux from one direction F (F_E, F_W, F_N, or F_S) on day d calculated as

$$S_d(F) = a \sum_1^n |F| \tag{7}$$

In Eq. (7), $n = 1163$ is the number of grid points covering the study area, and a indicates the average pixel size within the study area ($a \approx 5 \times 10^8$ m^2). In Eq. (6), $S(F_{EW>})$ represents the larger of the pair $S(F_E)$ and $S(F_W)$; $S(F_{NS>})$ is the larger of $S(F_N)$ and $S(F_S)$.

For the EPEs, the spatially accumulated moisture flux can be summed up over more than one day in accordance with the length of the reference event e; the variables in Eqs. (6) and (7) are then labelled T_e and S_e.

Analogous to the G_e^* parameter, we are also interested in moisture flux accumulations over areas of extra high upward vertical velocity. Therefore, in addition to T_d, T_e, S_d, and S_e, we introduce T_d^*, T_e^*, S_d^*, and S_e^*, where only grid points that have $P(w_i) \leq 0.1\%$ are considered in the calculation.

2.5. Division of extreme precipitation events with respect to moisture flux conditions

One of the main tasks is to find variants of moisture flux conditions leading to large-scale extreme precipitation in central Europe. The division of EPEs is easily made by the comparison of G_e^* calculated for four directional sectors F_E, F_W, F_N, and F_S with respect to Eqs. (4) and (5). The smallest (= the most significant) value of G_e^* then determines which sector outweighs others during some event, when the theoretical indication of events is as follows: *Ef* in the case of the smallest G_e^* for F_E, and similarly *Wf*, *Nf*, and *Sf* for western, northern and southern fluxes, respectively. However, in the case of small moisture fluxes, the direction is not significant. Therefore, we propose an additional group of "other" events *Ot* that includes EPEs with values of T_e^* lower than 10^9 kg s^{-1} and thus separates low-flux events.

3. Climatology of moisture fluxes in central Europe

In the lower troposphere, western directions of moisture flux dominate over central Europe, as demonstrated in Fig. 1b, presenting average moisture fluxes at the 850 hPa level. The Alpine region is characterized by some deformation due to higher altitudes, but the values of moisture flux could be biased considering that the 850 hPa level is sometimes below the model terrain. The dominance of western fluxes is again evident in Fig. 2a, showing the direction and magnitude of mean daily moisture fluxes at five different locations. Selected grid points (Table 2) with a model altitude from 51 to 835 m a.s.l. represent different parts of the study area.

The westernmost locations (points A and B) are characterized by the most pronounced dominance of western moisture fluxes both in size

Table 2
Spatial characteristics of the selected grid points (see Fig. 1).

Location	Latitude	Longitude	Altitude (m a.s.l.)	Basin	Closest city
A	49.25°N	7°E	278	Rhine	Saarbrücken
B	52.5°N	9.5°E	51	Weser/Ems	Hannover
C	52.5°N	17°E	86	Oder	Poznań
D	50°N	14.5°E	325	Elbe	Praha
E	47.75°N	13°E	835	Danube	Salzburg

and frequency. Mainly in the region west from the Rhine River (point A), the southwest sector has the greatest frequency of measurements, and the southeast is poorly represented. Towards the east (points C and D), northern moisture fluxes also become significant, not so much in frequency but in extreme values. In some cases of grid points C and D, extreme fluxes from the northern directions are comparable to those from the western directions. At these locations, the southeast moisture fluxes equal or even exceed the southwest moisture fluxes in size. The location at the northern foothills of the Alps (point E) shows specific behaviour, where moisture fluxes are mostly aligned with the zonal direction. However, southwestern moisture fluxes weaken, and the northwest directions prevail due to the Alpine ridge position and the topographically induced anticyclone west to northwest of the Alps.

In some cases, the extremes of moisture flux correspond with extra high upward vertical velocity situations (Fig. 2a). At location A, this relationship applies mostly to fluxes from the southwest sector. It is similar for location B but with two exceptions from the northeast and southeast directions. Towards the east, there is a greater proportion of days with more pronounced northern fluxes at high upward vertical velocity situations (points C and D). Finally, extra high upward vertical velocity at point E solely occurred together with moisture flux from the northwest sector.

Fig. 2b shows the same data transformed into cumulative probabilities (see Section 2.3). The prevalence of the western directions over the eastern directions is evident from the shift of the median (0.5 of the cumulative probability) to positive values of F_{qu}. The figure shows the advantage of the transformation, as the extreme values of these western and eastern moisture fluxes have the same distance from the median, which makes the extreme fluxes from different directions comparable and suitable for grouping EPEs according to moisture flux anomalies.

However, if studied with respect to large-scale precipitation events, moisture fluxes need to be evaluated within the whole study area instead of only at individual points. Therefore, spatially accumulated moisture flux T_d is calculated and presented in Fig. 3. The western sector is represented most frequently among the directions of daily accumulations of moisture flux. The dominance of western fluxes becomes even more pronounced if only higher values are considered: almost all daily mean moisture fluxes above $5 \times 10^{10}\,\mathrm{kg\,s^{-1}}$ are from the west. The gaps along the major axes in Fig. 3 are due to the spatial

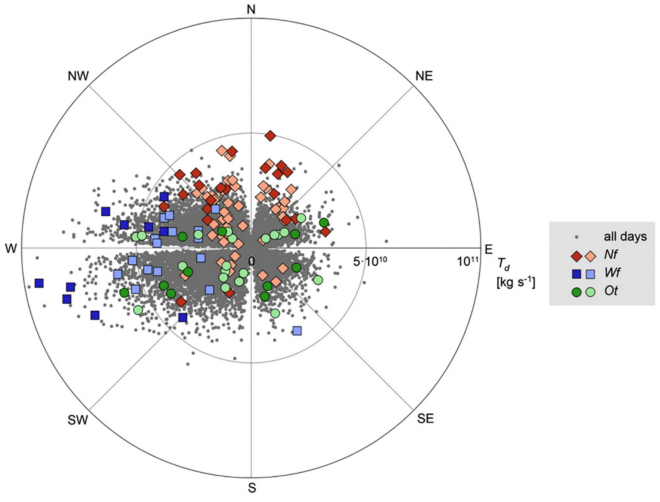

Fig. 3. Spatially accumulated moisture flux T_d on all days between 1979 and 2017 summed across the study area of central Europe. The magnitude and mean direction of the moisture flux on each day are expressed by the distance and position of the symbol to the centre of the diagram. Values reached during EPEs are marked with larger symbols differentiated into the variants *Wf*, *Nf* and *Ot*; darker symbols indicate the maximum magnitude reached during the event.

Table 3
Extreme precipitation events (EPEs, see Table 1) differentiated by their spatial clusters (Section 4.2) and variants of the prevailing moisture flux (Section 4.1).

EPEs ranking	Spatial cluster	G^*_e for				T^*_e	Moisture flux variant
		F_E	F_W	F_N	F_S	($10^9\,\mathrm{kg\,s^{-1}}$)	
1	ED	**0.124**	0.377	**0.028**	0.427	7.990	Nf
2	O	**0.064**	0.624	**0.001**	0.840	11.718	Nf
3	ED	**0.226**	0.434	**0.003**	0.830	3.236	Nf
4	ED	0.389	**0.110**	**0.003**	0.766	9.152	Nf
5	O	**0.238**	0.597	**0.002**	0.898	6.302	Nf
6	ED	**0.381**	0.413	**0.010**	0.352	4.300	Nf
7	O	**0.399**	0.593	**0.031**	0.999	2.139	Nf
8	ED	**0.152**	0.531	**0.002**	0.998	5.261	Nf
9	ED	**0.350**	0.728	**0.135**	0.909	1.125	Nf
10	R	0.986	**0.016**	0.886	**0.096**	3.590	Wf
11	O	0.382	**0.048**	**0.002**	0.723	4.935	Nf
12	O	**0.111**	0.704	**0.074**	0.774	1.911	Nf
13	ED	**0.060**	0.638	**0.009**	0.941	1.180	Nf
14	NW	**0.099**	0.970	**0.096**	0.960	1.043	Nf
15	O	**0.041**	0.685	**0.016**	0.401	3.467	Nf
16	R	0.945	**0.155**	0.762	**0.425**	7.733	Wf
17	RD	0.968	**0.018**	**0.097**	0.652	5.850	Wf
18	ED	**0.138**	0.279	**0.005**	1.000	1.657	Nf
19	R	**0.290**	0.888	**0.351**	0.498	0.594	Ot
20	ED	**0.033**	0.877	**0.002**	0.986	3.014	Nf
21	R	0.998	**0.001**	0.873	**0.071**	12.646	Wf
22	R	0.736	**0.347**	0.897	**0.546**	0.593	Ot
23	O	0.564	**0.473**	**0.032**	0.864	1.342	Nf
24	NW	**0.043**	0.937	**0.153**	0.932	0.908	Ot
25	NW	**0.156**	0.705	**0.050**	0.314	0.511	Ot
26	RD	**0.250**	0.409	**0.371**	0.468	0.361	Ot
27	O	0.629	**0.284**	**0.044**	0.941	0.586	Ot
28	O	**0.087**	0.721	**0.004**	0.980	3.973	Nf
29	RD	0.980	**0.067**	**0.419**	0.685	6.049	Wf
30	R	0.830	**0.069**	0.559	**0.154**	1.381	Wf
31	NW	0.352	**0.146**	**0.027**	0.898	1.331	Nf
32	RD	0.914	**0.022**	**0.106**	0.537	3.341	Wf
33	R	**0.199**	0.813	**0.041**	0.496	0.194	Ot
34	NW	0.555	**0.252**	**0.039**	0.584	2.823	Nf
35	R	0.632	**0.077**	**0.179**	0.236	2.111	Wf
36	R	**0.146**	0.958	**0.046**	0.959	0.051	Ot
37	RD	0.891	**0.049**	**0.023**	0.998	0.124	Ot
38	NW	0.973	**0.016**	**0.102**	0.816	3.035	Wf
39	NW	**0.112**	0.635	0.297	**0.115**	0.267	Ot
40	NW	**0.048**	0.941	0.709	**0.200**	0.351	Ot
41	O	**0.243**	0.526	**0.002**	0.995	1.829	Nf
42	O	**0.243**	0.767	**0.050**	0.953	1.788	Nf
43	R	0.995	**0.003**	0.965	**0.013**	5.853	Wf

Each event is characterized by the total amount of moisture flux (T^*_e) and the parameter G^*_e for moisture fluxes from four directional sectors. For both the meridional and zonal components of the flux, the smaller value is highlighted in bold; the underlined number shows the minimum.

character of the variable T_d when it is very unlikely for the spatially accumulated moisture flux to be exclusively zonal or meridional.

4. Moisture flux size and direction during EPEs

4.1. Variants of EPEs with respect to moisture flux conditions

There are 43 selected EPEs between 1979 and 2013 (Table 1) ranked by precipitation extremeness (WEI; Gvoždíková et al., 2019) when we are able to assign one of five variants of moisture flux conditions to each of them (Section 2.5). In fact, all EPEs could be classified into only three variants, namely, *Nf*, *Wf* or *Ot* (Table 3), which means that western and northern moisture fluxes are especially important for extreme precipitation in central Europe. No *Sf* or *Ef* cases were detected, although the geometric mean G^*_e reached the smallest values for the eastern moisture flux during several EPEs. However, the spatially accumulated moisture flux T^*_e was quite low during these cases, and we finally classified them as *Ot* events.

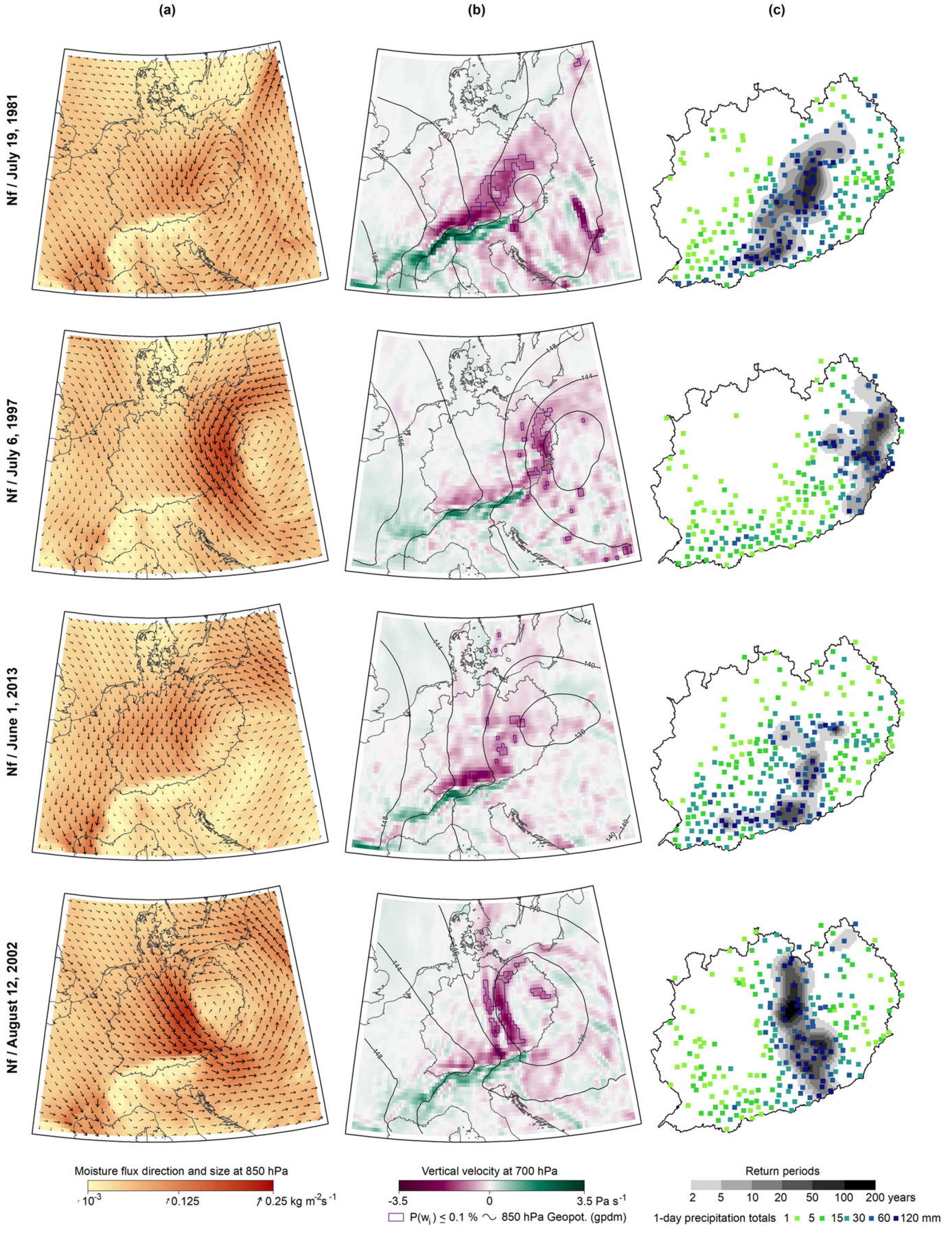

(caption on next page)

Fig. 4. Moisture flux, vertical velocity and precipitation during the four largest EPEs of the *Nf* variant (July 1981, July 1997, May/June 2013, August 2002). The day with the maximum amount of moisture flux is displayed for each event. (a) Average daily moisture fluxes ($kg\,m^{-2}\,s^{-1}$); the arrow angle represents the average direction of moisture flux during the day in the given pixel. (b) Vertical velocity ($Pa\,s^{-1}$) at 700 hPa and geopotential height (gpdm) of the 850 hPa level; the area enclosed by the solid line indicates grid points with extra high upward vertical velocity ($P(w_i) \leq 0.1\%$). (c) One-day precipitation totals (mm) and their return periods at selected gauges.

Approximately 50% of events (22) belong to the *Nf* group when pronounced northern fluxes are most frequently combined with the eastern fluxes (Table 3). These EPEs are generally the largest precipitation extremes according to the WEI; we have 16 of them among the 20 largest events. The spatially accumulated moisture flux T_e^* generally decreases with decreasing precipitation extremeness, with the maximum reached during the five-day event in July 1997. The second largest value of T_e^* was reached in August 2002 within only two days, which stresses the rarity of the circulation conditions during this event. The third maximum value of T_e^* among *Nf* events corresponds with the maximum event according to precipitation extremity in July 1981; the maximum daily value of the spatially accumulated moisture flux T_d^* was detected on July 19 (Fig. 4a). Large northern fluxes occurred mainly in the southeastern part of the study area in the rear of a cyclone, where the values overlapped with extra high upward vertical velocity (Fig. 4b). The same area was affected by heavy rainfall with daily totals exceeding 100 mm at some stations – up to 100-year return period precipitation (Fig. 4c). Together with events in 1997, 2002, and 2013, the greatest impact is in the eastern half of the territory, with the 1997 case being significantly shifted to the east compared to others. However, all events are very similar (Fig. 4), with significant precipitation in the area of extra high upward vertical velocity combined with large northern fluxes. The ascending motions on the windward side of the Alps are always accompanied by descent behind the Alpine ridge.

Group *Wf* consists of 10 events with the most significant fluxes from the west, which are combined with both northern and southern fluxes as a secondary direction (Table 3). The largest fluxes (both in absolute and relative terms) were reported during the two-day event in October 1998, while there were three other *Wf* events of higher precipitation extremity, including October 1986, December 1993, and March 2002. Days with maximum T_d^* of all these EPEs are shown in Fig. 5. Associated pronounced west and southwest fluxes (Fig. 5a) occurred mainly in the southern half of the study area (except the Alps), where the absolute values of moisture flux were much higher than in the case of *Nf* events (compare with Fig. 4a), apparently due to the higher wind velocity at 850 hPa. However, extra high upward vertical velocity sometimes affected rather smaller and discontinuous areas (Fig. 5b), clearly corresponding with the windward sides of central European middle mountains. In the strong zonal flow, almost the entire area was covered by rainfall of lower intensities that was not particularly significant in terms of 1-day precipitation totals (Fig. 5c). The largest precipitation often affected the Upper and Middle Rhine. Only in March 2002 did the northwestern flow contribute to higher precipitation totals on the windward side of the Alps in the Danube basin.

Eleven of the 43 EPEs (Table 3) have been marked as “others”, which is a mixed group of EPEs of various synoptic causes or even convective events. There are 5 EPEs with the most significant eastern fluxes and 5 other events similar to the *Nf* group but with weaker overall flux. All the EPEs of the *Ot* group have a relatively small spatially accumulated moisture flux T_e^*, although the geometric means of ordered values are sometimes very small, indicating significant fluxes. This size can be due to generally weaker eastern fluxes, which show a great abnormality but a small sum, or due to a limited area considered in the geometric mean. A small number of grid points with $P(w_i) \leq 0.1\%$ within the study area is typical for the four largest EPEs of the *Ot* group shown in Fig. 6. However, the great variability in events is evident from the 850 hPa geopotential heights and the direction of moisture fluxes in Fig. 6b and a, respectively. The moisture fluxes and vertical velocity fields are clearly weaker compared to those in Figs. 4 and 5. Some events may be more of a local character, such as the largest EPE in August 1981, with precipitation concentrated in a relatively smaller area in the lower Rhine basin (Fig. 6c). A weak pressure gradient in this case suggests the rather convective nature of the event.

4.2. Correspondence between moisture flux variants and precipitation spatial patterns among EPEs

In our previous study (Gvoždíková et al., 2019), we clustered the EPEs listed in Table 1 with respect to the spatial distribution of precipitation. In an agglomerative hierarchical clustering procedure, we merged the closest single- or multiple-member groups of EPEs into a final number of five clusters (spatial clusters in Table 3). The spatial similarity was assessed based on the relative weather extremity index (WEI_{rel}) calculated for individual smaller segments of the study area. Detailed information on clustering of EPEs, including the clustering dendrogram, is provided in Gvoždíková et al., 2019, section 3.2. Fig. 7 and Table 4 show the significant correspondence between the five spatial clusters and the moisture flux variants.

The maximum extreme central European precipitation events belong to clusters *ED* and *O*, comprising EPEs with precipitation concentrated mainly in the Elbe-Danube area and Oder basin, respectively. In both these clusters, the relationship with the northern moisture flux is extra strong: 19 of 20 *ED* and *O* events belong to the variant *Nf*; the only rather weak event belonging to the *Ot* group (in June 1993) was still connected with moisture flux from the north, though not so strong (Table 3).

In contrast, the variant *Nf* is represented by none of the 15 events belonging to the other two spatial clusters *R* and *RD*, comprising EPEs with precipitation concentrated mainly in the middle part of the Rhine basin (*R*) and in the alpine parts of the Rhine and Danube basins (*RD*). The moisture flux variant *Wf* prevails in both of these clusters.

Finally, the *NW* cluster of events with precipitation concentrated mainly in the northwestern part of the study area is the least pronounced in terms of moisture flux variants. Moisture fluxes during these events were generally not extra strong, with a large spread of directions (Fig. 7b). Unlike other spatial clusters, half of the *NW* events experienced substantial moisture flux from the eastern or even the southeastern sector.

4.3. Comparison of moisture fluxes during and without EPEs

Whereas the spatially accumulated moisture flux connected with extra high upward vertical velocity T_e^* generally decreases with decreasing precipitation extremeness, we can assume smaller values of T_e^* in days without EPEs. However, when we want to compare moisture flux conditions during and without EPEs, we need to compare individual days due to the variable length of precipitation events. The signs in Fig. 7a represent the spatially accumulated moisture flux according to Eq. (6) calculated for individual days (referred to as T_d^*). The values of T_d^* calculated only over grid points with extra high upward vertical velocity are in contrast with the T_d values in Fig. 3, which are summed up regardless of the magnitude of the vertical velocity. The daily values in Fig. 7 are concentrated mainly between 10^7 and $10^9\,kg\,s^{-1}$ and from the southwest to the northwest, where the angle symbolizes the average direction of moisture flux in a given day with $P(w_i) \leq 0.1\%$ in at least one pixel in the study area. Values greater than $10^9\,kg\,s^{-1}$ occur almost only between the west-southwest and northeast directions.

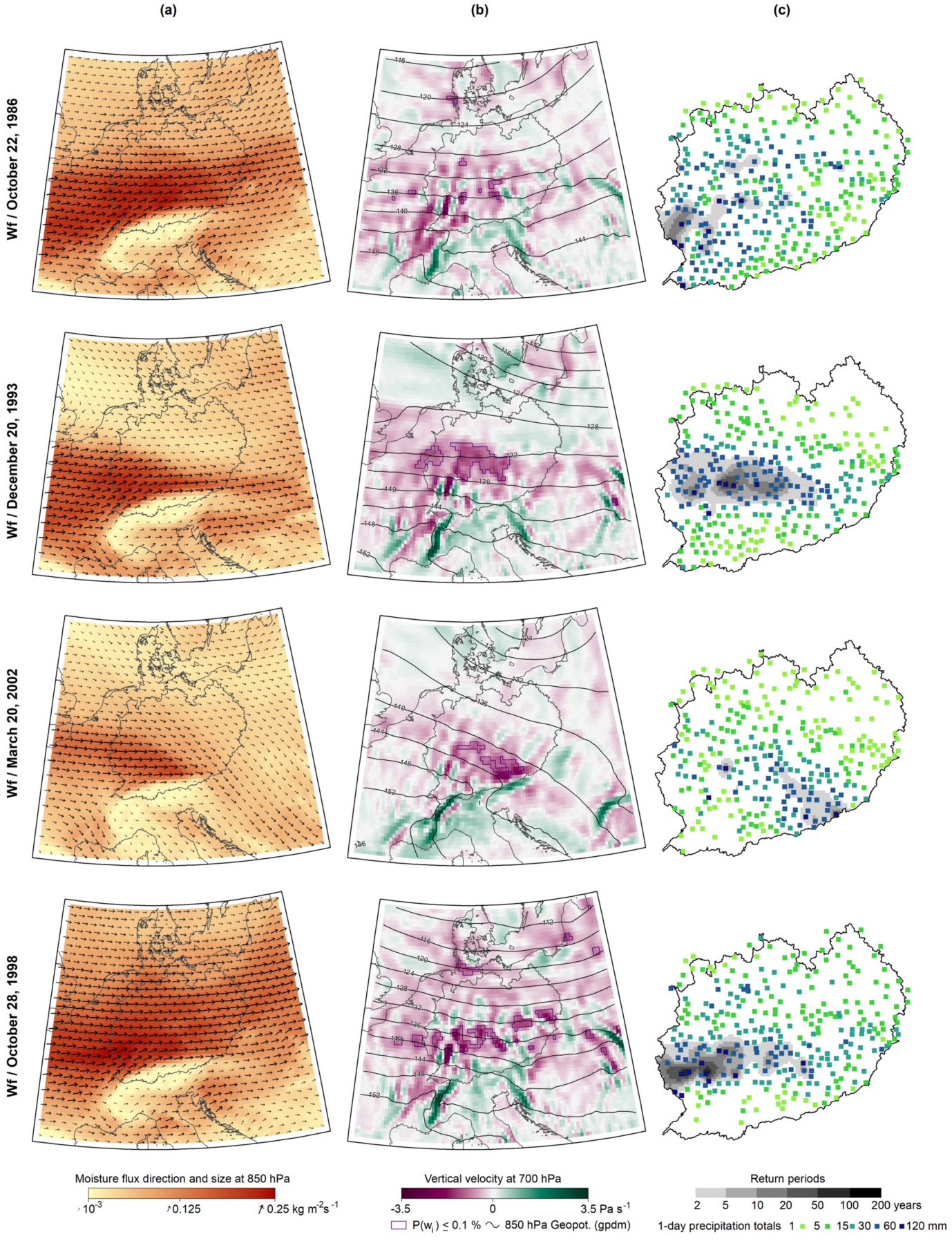

Fig. 5. Same as Fig. 4 but for the four largest EPEs of the *Wf* variant (October 1986, December 1993, March 2002, October 1998).

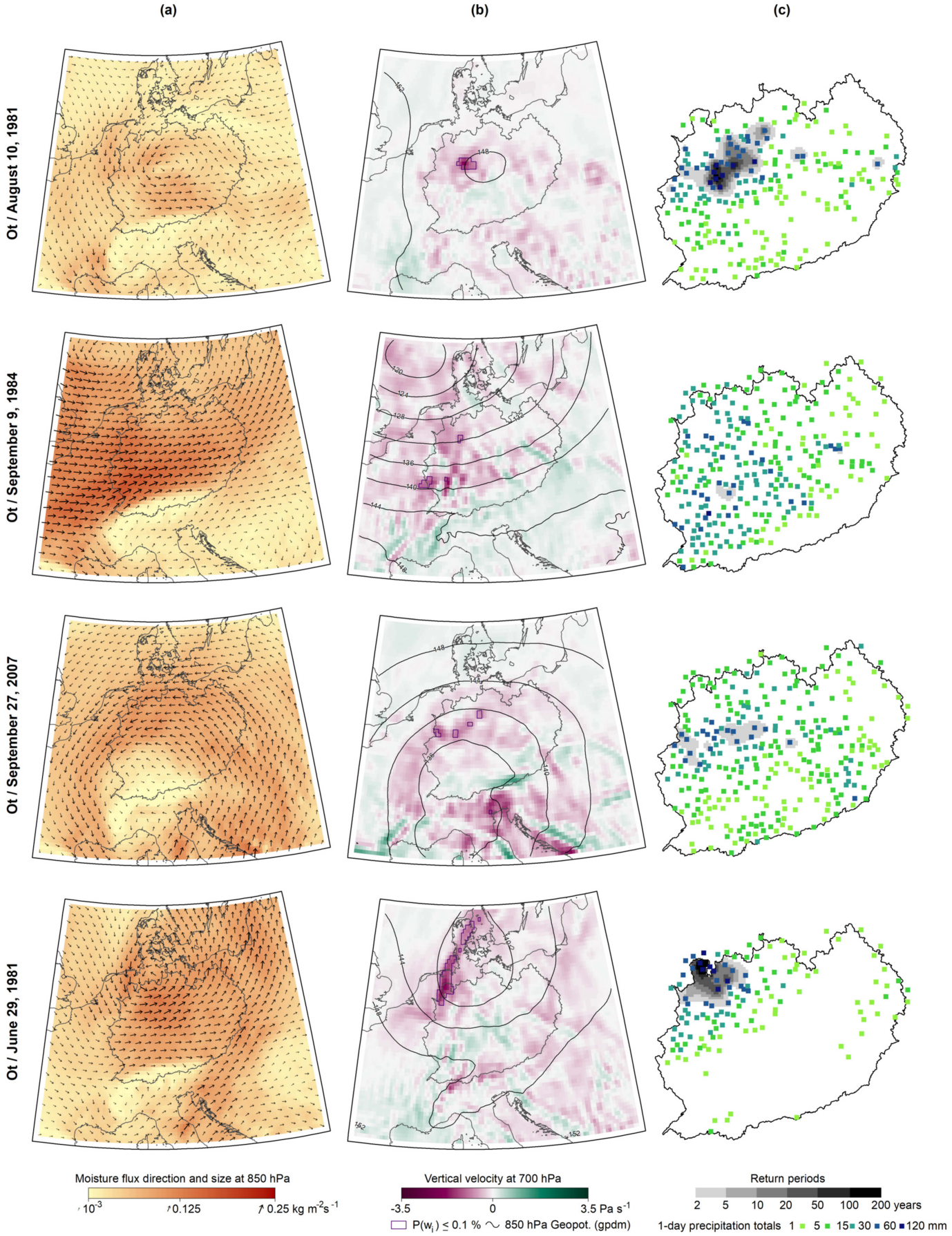

Fig. 6. Same as Fig. 4 but for the four largest EPEs of the *Ot* variant (August 1981, September 1984, September 2007, June 1981).

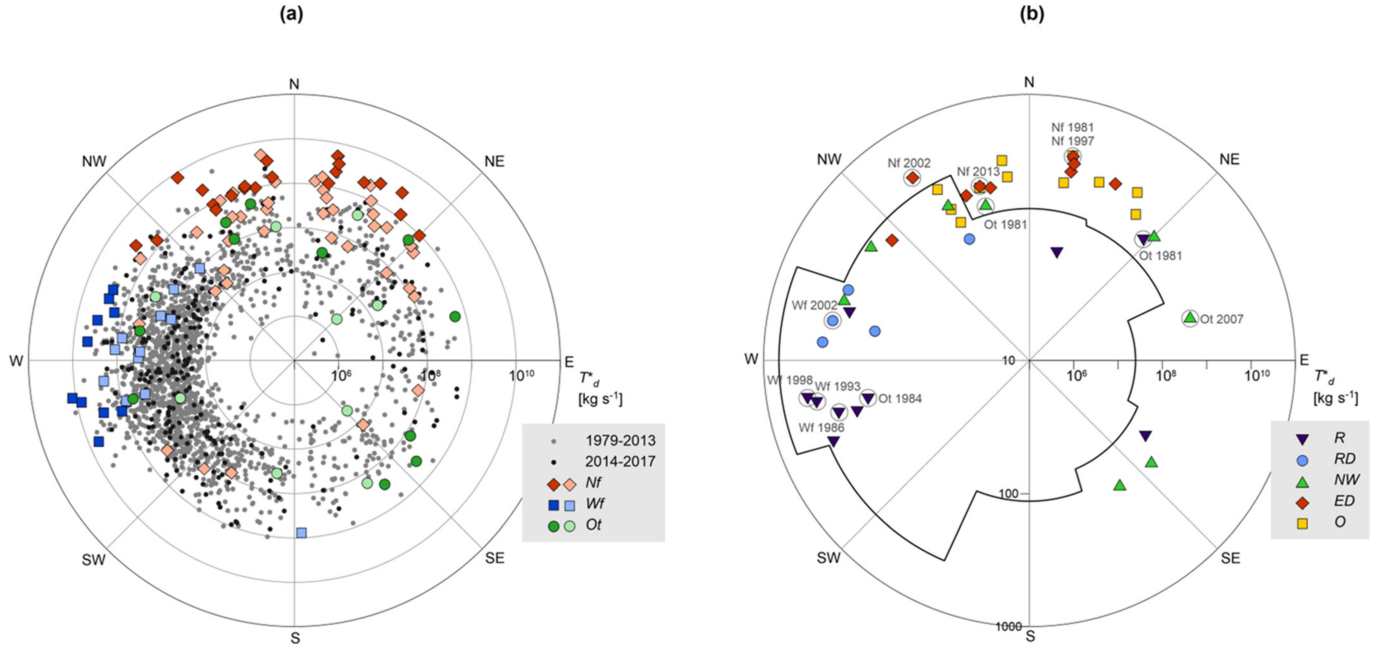

Fig. 7. Spatially accumulated moisture flux T^*_d on all days between 1979 and 2017 summed across the area of extra high upward vertical velocity ($P(w_i) \leq 0.1\%$). The magnitude and mean direction of the moisture flux on each day are expressed by the distance and position of the symbol to the centre of the diagram. (a) All days when the criterion was fulfilled at least at one grid point are presented. Values reached during EPEs are marked with symbols as in Fig. 3. (b) Only days with maximum moisture fluxes during individual EPEs are presented, differentiated by their membership to spatial clusters *R*, *RD*, *NW*, *ED*, and *O*. The largest EPEs are labelled (in accordance with Figs. 4, 5, and 6). The numbers of all T^*_d values in each directional sector are only indicated by the solid line.

Table 4
Numbers of corresponding EPEs within spatial clusters (*ED*, *O*, *R*, *RD*, and *NW*) and moisture flux variants (*Nf*, *Wf*, and *Ot*).

	Nf	Wf	Ot	Total
ED	9	0	0	9
O	10	0	1	11
R	0	6	4	10
RD	0	3	2	5
NW	3	1	4	8
Total	22	10	11	43

The maximum values of T^*_d during both *Nf* and *Wf* events are roughly above the magnitude of 10^9 kg s^{-1}, the angle is however different for *Wf* events concentrating between west-southwest and west-northwest and *Nf* events approximately between northwest and northeast. Despite the considerable angular differences, moisture flux variants cannot simply be read from the angle. It is given by the way the events are divided into groups (using relative values of G^*_e, which are averaged over several days, instead of the absolute amount T^*_e) and demonstrated by the position of two *Nf* points that are closer to the west than to the north in Fig. 7a. In these cases, the western flux was larger in an absolute manner, but it still did not exceed the northern flux in terms of abnormality. Generally, the points around the northwest direction (until approximately 325°) are a mixture of points that could potentially be assigned to either the *Wf* or *Nf* group.

There are only a few unclassified points (= days not related to any EPE from Table 1) left in the sector between 325° and 45° and above 7.5×10^8 kg s^{-1}, which is the smallest maximum value of T^*_d measured during any *Nf* event. This outcome indicates a good match between the maximum moisture flux values and the EPEs from the *Nf* group. Two of the eight unclassified points (seven unclassified events) in this sector of Fig. 7 were recorded after the end of 2013 (14 July 2016, and 16 May 2014), so the events do not appear in our database but had considerable precipitation amounts according to station reports. August 13, 2002, is the day after a major two-day event in August 2002; the total daily amount of moisture flux was close to 5×10^9 kg s^{-1}, but the respective point is unclassified because the event was assessed as a two-day event within central Europe (Gvoždíková et al., 2019). Nevertheless, using the same algorithm in the area of the Czech Republic (Müller et al., 2015), the event lasted three days from August 11 to 13, so this sign would belong. Two of the remaining four unclassified events then had considerable WEI values, but they did not appear in the basic list of the largest precipitation events (Gvoždíková et al., 2019).

In the case of *Wf* events, the correspondence between maximum moisture flux values and EPEs is not as obvious, with a much higher proportion of unclassified points in the range of approximately 250° to 290° and above 10^9 kg s^{-1} (Fig. 7a). This greater number of points is related to the method of deriving moisture flux in Eqs. (1) and (2), where it is directly proportional to wind velocity, causing the frequent appearance of windstorms among the points within the western sector of Fig. 7. From five maximum unclassified points, three were among the largest wind events in the Czech Republic (Kašpar et al., 2017), while the storm Kyrill in January 2007 and the November 1984 storm were even the most intense. Together with another unclassified point representing the January 1995 event, they are also among the most extreme windstorms hitting Europe (Roberts et al., 2014).

5. Seasonality of EPEs and moisture fluxes

Groups of extreme precipitation events, differentiated according to moisture flux conditions, also substantially differ in terms of their seasonal distribution (Fig. 8a): *Wf* events occurred exclusively from September to March, while *Nf* and *Ot* events occurred mostly in the warm part of the year (from April to September). This difference can be interpreted in terms of the seasonal distribution of moisture fluxes under extra high upward vertical velocity conditions. In general, the period from May to August experiences many more such days than the other months do, and this is the case for fluxes from individual sectors as well (Fig. 8b). However, extra strong western fluxes (more than 10^9 kg s^{-1}) occur almost exclusively from October to March when almost all *Wf* events appeared. In contrast, such extra strong northern

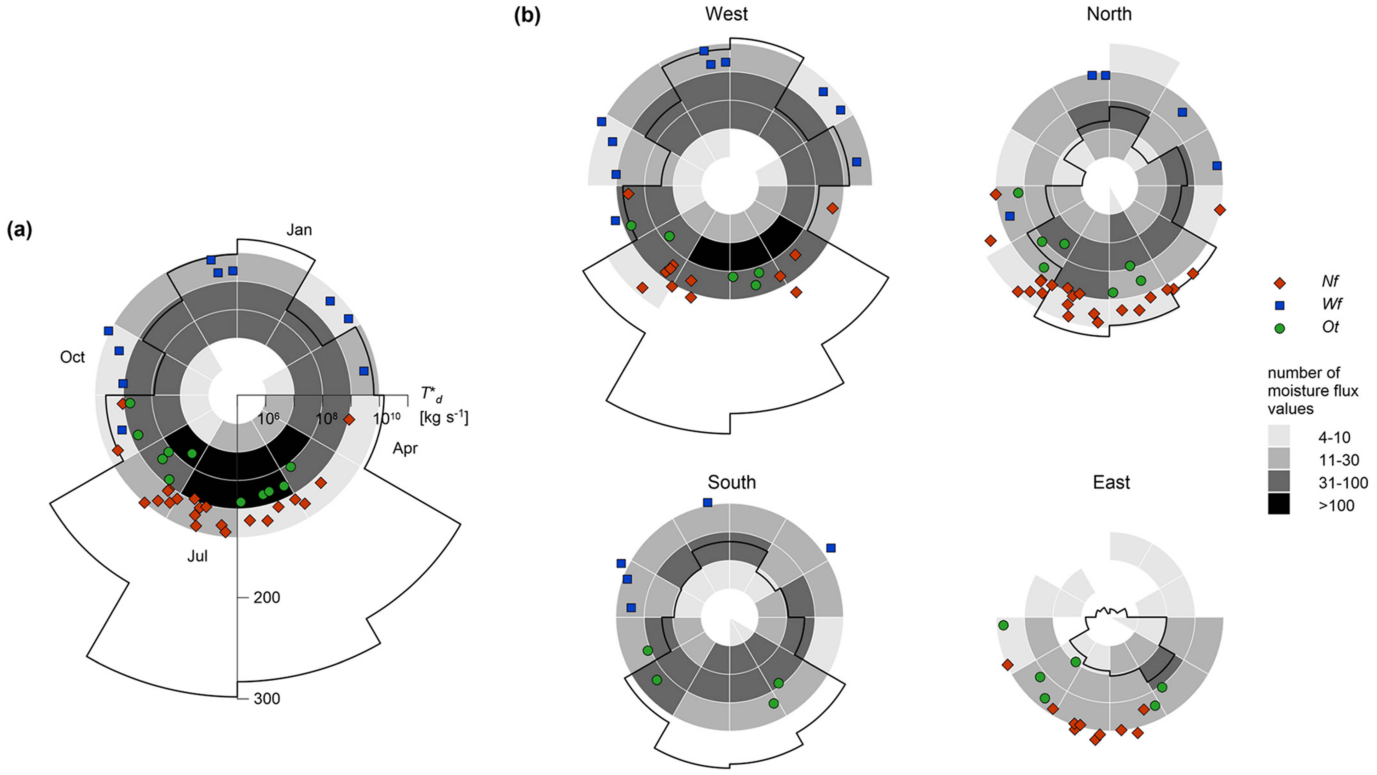

Fig. 8. The seasonal distribution of spatially accumulated moisture flux T^*_d on all days between 1979 and 2017 summed across the area of extra high upward vertical velocity ($P(w_i) \leq 0.1\%$) within the whole study area: (a) all moisture fluxes regardless of their directions; and (b) fluxes from four directional sectors (only the largest meridional and zonal flux for one day is counted). Values reached in days with maximum moisture fluxes during individual EPEs are marked by symbols as in Fig. 3. The solid line represents the number of values in each month. Shading indicates the number of values in four size categories.

fluxes are represented mostly in summer months when *Nf* events are concentrated. The fluxes from the south and the east are usually not as strong, but the eastern fluxes are especially strongly dependent on the season: values of more than $10^8\,\mathrm{kg\,s^{-1}}$ appear only in the warm half-year when they contribute to the *Nf* and possibly to the *Ot* events.

The seasonal difference among the variants of EPEs with respect to moisture flux conditions explains the differences in the seasonal distribution of EPEs among the five studied river basins (Fig. 9a), already mentioned in our previous study (Gvoždíková et al., 2019). Because maximum events in the Oder, Elbe, and Danube river basins belong almost exclusively to the *Nf* variant, the EPEs are concentrated in the warm half-year there. EPEs in the other two subregions of the study area (Weser/Ems and Rhine river basins) belong mainly to the *Wf* and *Ot* groups. As a result, EPEs occur in both the warm and the cold half-years there.

The detailed analysis of the seasonal distribution of moisture fluxes from various sectors in the five subregions (Fig. 9b) further clarifies the seasonal distribution of EPEs there. The significant concentration of EPEs into July and the first half of August in the Oder River basin seems to be related to the concentration of strong northern fluxes during these two months in this region. The northern fluxes are usually combined with the eastern fluxes during EPEs there. In the Elbe and Danube River basins where EPEs also belong mainly to the *Nf* group, EPEs are spread more throughout the warm half-year as well as the strong northern and western fluxes, which contribute more to extreme precipitation there than in the Oder basin. In contrast, the Rhine *Wf* events seem to be related to more frequent strong western and southern moisture fluxes in autumn and winter. Finally, the *Ot* events in the Weser/Ems subregion could be related to all flux directions, including the eastern warm-half-year moisture fluxes.

6. Discussion

6.1. The role of the vertical velocity

In central Europe, mainly western and northern moisture fluxes are connected to precipitation extremes. However, the supply of moisture itself needs to be supported by the upward motion of air. These are two basic components of heavy precipitation that are often studied together (Giannakaki and Martius, 2015; Doswell III et al., 1998).

In the present study, we decided to overlap the fields of moisture flux and vertical velocity to explain the occurrence of extreme precipitation events in central Europe. We look at the total amount of moisture flux in the area of extra high upward vertical velocity that corresponds to the lowest 0.1% of the vertical velocity values at each grid point. Other options were considered as well with cumulative probabilities of $P(w_i) \leq 0.5\%$ and $P(w_i) \leq 1\%$ when we wanted to obtain the best ratio between events and unclassified values of the spatially accumulated moisture flux (Fig. 7a) above a certain threshold. The aim was to separate the extremes of moisture flux that would lead to precipitation extremes in most cases, which was best accomplished using the strongest vertical velocity limit of 0.1%. Without the vertical velocity limit, the signal is not clear, and a direct relationship between moisture flux and precipitation extremes is not observed (compare Figs. 3 and 7a).

6.2. Relevance of moisture flux size

The individual EPEs were divided into three groups according to the causal flux of moisture from a given direction. There are only two

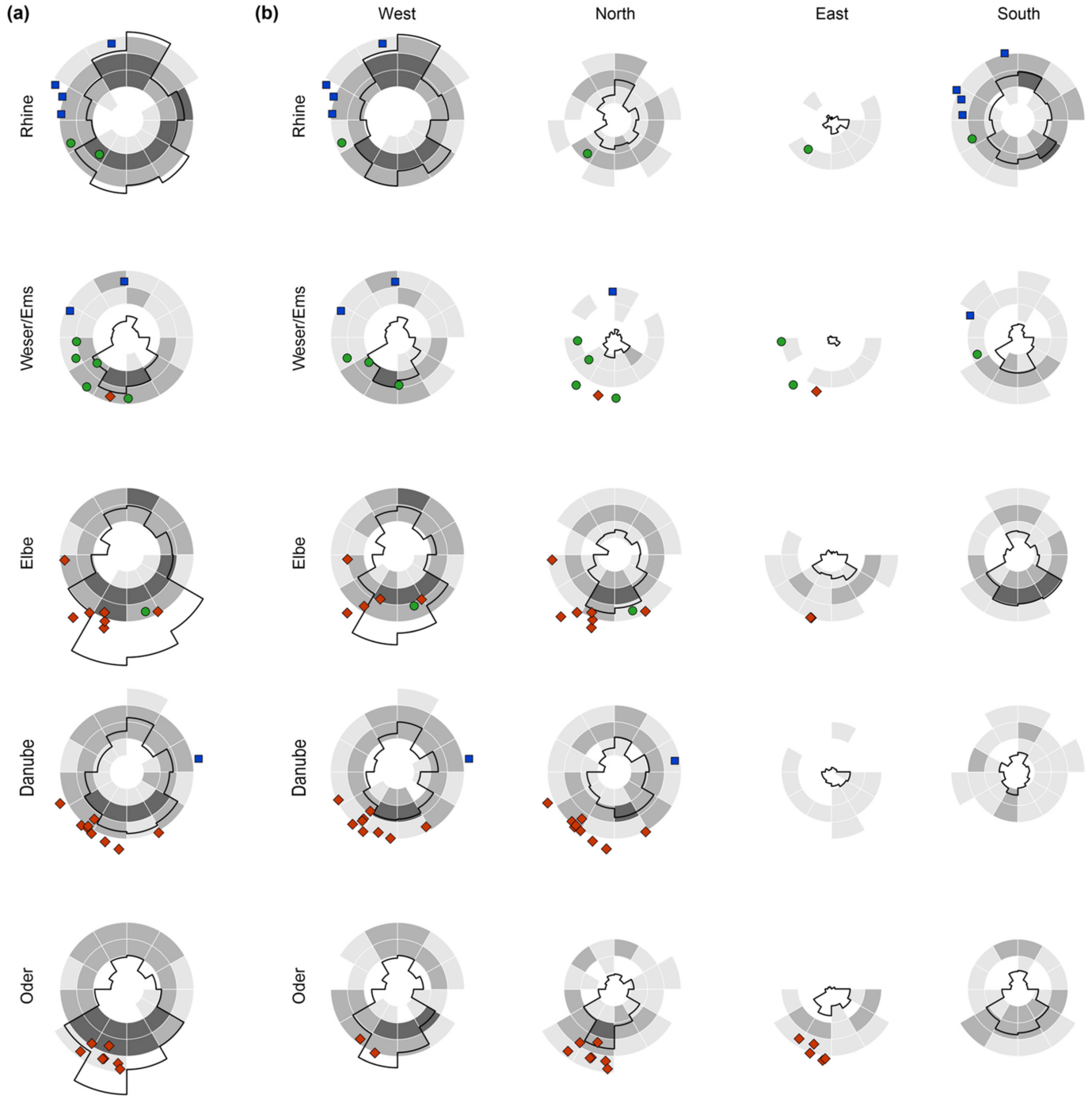

Fig. 9. Same as Fig. 8 but for individual river basins; only the largest events in each basin (according to Gvoždíková et al., 2019) are depicted by symbols. The legend and axis labels correspond to Fig. 8.

significant directions – western and northern – that create *Wf* and *Nf* groups of events and correspond to the main synoptic patterns bringing moisture either from the Atlantic or Mediterranean to central Europe (Hofstätter et al., 2017).

The *Ot* group is made up of other events with weaker overall moisture flux. The decisive criterion was the value of spatially accumulated moisture flux available for the event ($T_e^s = 10^9\,\mathrm{kg\,s^{-1}}$). We have chosen the value subjectively based on a subjective assessment of individual events, whose synoptic causes substantially differ and often have a convective character.

Of all groups, *Nf* best explained the occurrence of relevant precipitation extremes. Western fluxes are often too large even on days without significant precipitation extremes (Fig. 7a). The reason could be that the moisture flux is directly proportional to wind velocity (Eqs. (1) and (2)), which is usually stronger in the case of western fluxes and therefore allows windstorms to be accompanied by extra high moisture flux values. Although wind and precipitation extremes occur relatively often simultaneously during the winter months and mainly over northwestern central Europe (Martius et al., 2016), some strong western moisture flux events do not correspond with extreme values of the WEI. Fig. 10 clarifies the role of the two variables when calculating the moisture flux value. Fig. 10a shows that during EPEs, high moisture flux values are either due to high wind velocity or due to high values of the specific humidity. The groups of EPEs rather differ in terms of the

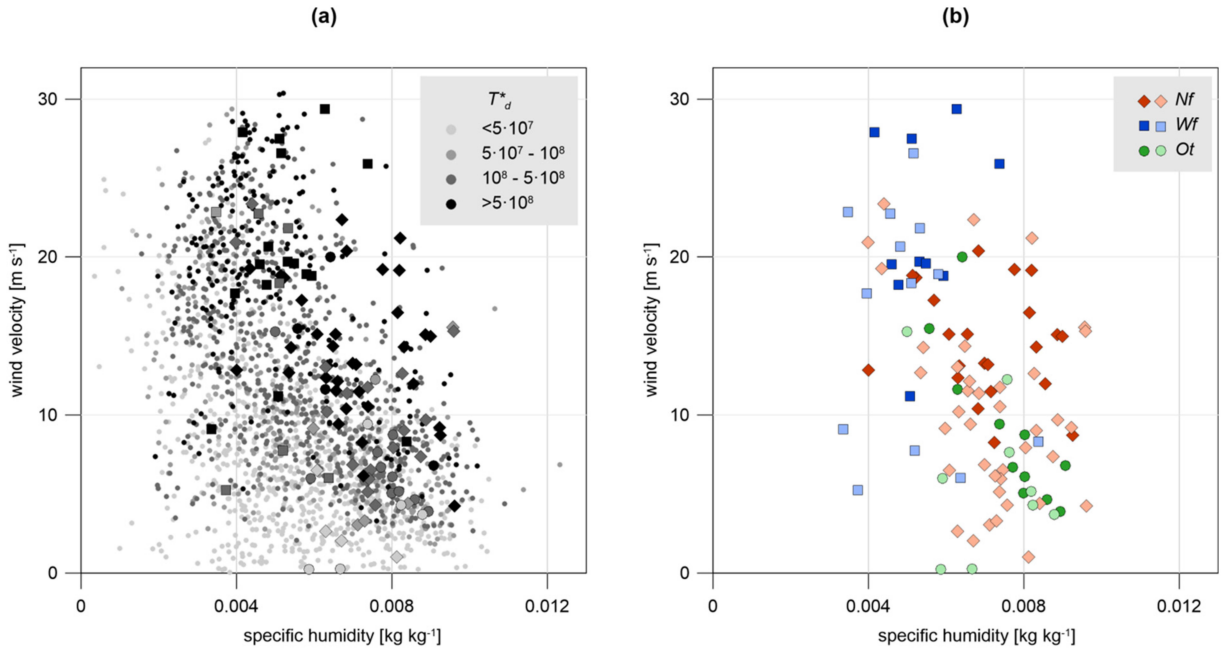

Fig. 10. Contribution of average wind velocity and average specific humidity at 850 hPa to the spatially accumulated moisture flux T^*_d on all days between 1979 and 2017 summed across the area of extra high upward vertical velocity ($P(w_i) \leq 0.1\%$). (a) The values of T^*_d are depicted by shading; all days when the criterion was fulfilled at least at one grid point are presented; values reached during EPEs are highlighted by larger symbols. (b) Only days during EPEs are presented; the variants of the moisture flux are differentiated by symbols as in Fig. 3.

contribution of the two variables (Fig. 10b): *Wf* events are concentrated in the upper half of the scatterplot, which shows a more crucial role of high winds, while *Nf* and even the *Ot* group show lower average wind velocities against higher specific humidity values. This fact corresponds with the presented difference in the seasonal distribution among the three groups because the values of the wind velocity are generally higher in the cold half-year than in the warm half-year, while the specific humidity exhibits the opposite trend. Nevertheless, a number of extra high values of the moisture flux not related to the EPEs are shown in Fig. 10a. All of them are due to rather high wind velocities, which suggests that in the case of strong winds, the extra high moisture flux values can partly overestimate the expectation of the magnitude of the precipitation event.

7. Concluding remarks

- We used the ERA5 reanalysis data to divide a set of 43 central European extreme precipitation events from 1979 to 2013 into three groups (Table 3) representing (i) events with dominating moisture flux from the northern sector (*Nf*), (ii) events with dominating moisture flux from the western sector (*Wf*), and (iii) low flux events (*Ot*). The classification was based on the moisture flux magnitudes and direction in the area of extra high upward vertical velocity, which are both important ingredients for the emergence of heavy precipitation.
- Approximately 50% of events (22) belong to the *Nf* group, which are mostly the largest precipitation extremes according to the WEI (Table 3). The *Wf* group is represented by 10 events, and the remaining 11 EPEs belong to the *Ot* group. Examples of events from each group (Fig. 4) highlight the differences in moisture flux direction and size.
- The division of EPEs according to moisture flux conditions fits well with the spatially differentiated clusters of EPEs, when events occurring in the Elbe-Danube area and Oder basin are connected with the abnormal values of moisture flux from the north (*Nf* events), while *Wf* events often affected the Rhine-Danube area (Fig. 7).
- The seasonal distribution of EPEs follows the moisture flux variants, with *Nf/Ot* events occurring regularly in summer and *Wf* events occurring only from September to March (Fig. 8a). The difference can be interpreted in terms of the seasonal distribution of extra high values of moisture flux from the respective sectors. Moreover, the seasonal differences among the groups of EPEs with respect to moisture flux conditions explain the differences in the seasonal distribution of EPEs among the five studied river basins.
- Mainly in the case of *Nf* events, anomalies of moisture flux almost always led to extremes in precipitation, as there are just a few unclassified points (events) among the EPE values in Fig. 7a. This outcome is more evident when considering only grid points with extra high upward vertical velocity (compare Figs. 3 and 7a). However, due to higher wind velocity (Fig. 10), the correspondence between moisture flux values and *Wf* cases is not as obvious as that in *Nf* cases.
- Because northern moisture flux seems to be directly connected to extremes in precipitation, there is a potential to use it as a predictor of EPEs. Future tasks will thus involve finding additional circulation anomalies important for the emergence of precipitation extremes and concentration on the forecast skill of the circulation anomalies, which could be even better than the skill of the quantitative precipitation forecast.

Declaration of Competing Interest

The authors declare that they have no known competing financial interests or personal relationships that could have appeared to influence the work reported in this paper.

Acknowledgments

This work was supported by the Czech Science Foundation (Grant No. 19-05011S). We would also like to acknowledge ECMWF for providing ERA5 reanalysis.

References

Beurton, S., Thieken, A.H., 2009. Seasonality of floods in Germany. Hydrol. Sci. J. 54, 62–76. https://doi.org/10.1623/hysj.54.1.62.

Boutle, I.A., Belcher, S.E., Plant, R.S., 2011. Moisture transport in midlatitude cyclones. Q. J. Roy. Meteor. Soc. 137, 360–373. https://doi.org/10.1002/qj.783.

Copernicus Climate Change Service (C3S), 2017. ERA5: Fifth generation of ECMWF atmospheric reanalyses of the global climate. In: Copernicus Climate Change Service Climate Data Store (CDS), https://cds.climate.copernicus.eu/cdsapp#!/home.

Doswell III, C.A., Ramis, C., Romero, R., Alonso, S., 1998. A diagnostic study of three heavy precipitation episodes in the western Mediterranean region. Weather Forecast. 13, 102–124.

Froidevaux, P., Martius, O., 2016. Exceptional integrated vapour transport toward orography: an important precursor to severe floods in Switzerland. Q. J. Roy. Meteor. Soc. 142, 1997–2012. https://doi.org/10.1002/qj.2793.

Giannakaki, P., Martius, O., 2015. Synoptic-scale flow structures associated with extreme precipitation events in northern Switzerland. Int. J. Climatol. 36, 2497–2515. https://doi.org/10.1002/joc.4508.

Grams, C.M., Binder, H., Pfahl, S., Piaget, N., Wernli, H., 2014. Atmospheric processes triggering the central European floods in June 2013. Nat. Hazards Earth Syst. Sci. 14, 1691–1702. https://doi.org/10.5194/nhess-14-1691-2014.

Gvoždíková, B., Müller, M., 2017. Evaluation of extensive floods in western/central Europe. Hydrol. Earth Syst. Sci. 21, 3715–3725. https://doi.org/10.5194/hess-21-3715-2017.

Gvoždíková, B., Müller, M., Kašpar, M., 2019. Spatial patterns and time distribution of central European extreme precipitation events between 1961 and 2013. Int. J. Climatol. 39, 3282–3297. https://doi.org/10.1002/joc.6019.

Hofstätter, M., Lexer, A., Homann, M., Blöschl, G., 2017. Large-scale heavy precipitation over central Europe and the role of atmospheric cyclone track types. Int. J. Climatol. 38 (Suppl. 1), e497–e517. https://doi.org/10.1002/joc.5386.

Kašpar, M., Müller, M., 2014. Combinations of large-scale circulation anomalies conducive to precipitation extremes in the Czech Republic. Atmos. Res. 138, 205–212. https://doi.org/10.1016/j.atmosres.2013.11.014.

Kašpar, M., Müller, M., Crhová, L., Holtanová, E., Polášek, J.F., Pop, L., Valeriánová, A., 2017. Relationship between Czech windstorms and air temperature. Int. J. Climatol. 37, 11–24. https://doi.org/10.1002/joc.4682.

Martius, O., Zenklusen, E., Schwierz, C., Davies, H.C., 2006. Episodes of alpine heavy precipitation with an overlying elongated stratospheric intrusion: a climatology. Int. J. Climatol. 26, 1149–1164. https://doi.org/10.1002/joc.1295.

Martius, O., Pfahl, S., Chevalier, C., 2016. A global quantification of compound precipitation and wind extremes. Geophys. Res. Lett. 43, 7709–7717. https://doi.org/10.1002/2016GL070017.

Messmer, M., Gómez-Navarro, J.J., Raible, C.C., 2015. Climatology of Vb cyclones, physical mechanisms and their impact on extreme precipitation over central Europe. Earth Syst. Dynam. 6, 541–553. https://doi.org/10.5194/esd-6-541-2015.

Müller, M., Kašpar, M., 2010. Quantitative aspect in circulation type classifications – an example based on evaluation of moisture flux anomalies. Phys. Chem. Earth 35, 484–490. https://doi.org/10.1016/j.pce.2009.09.004.

Müller, M., Kašpar, M., 2011. Association between anomalies of moisture flux and extreme runoff events in the south-eastern Alps. Nat. Hazards Earth Syst. Sci. 11, 915–920. https://doi.org/10.5194/nhess-11-915-2011.

Müller, M., Kašpar, M., 2014. Event-adjusted evaluation of weather and climate extremes. Nat. Hazards Earth Syst. Sci. 14, 473–483. https://doi.org/10.5194/nhess-14-473-2014.

Müller, M., Kašpar, M., Řezáčová, D., Sokol, Z., 2009. Extremeness of meteorological variables as an indicator of extreme precipitation events. Atmos. Res. 92, 308–317. https://doi.org/10.1016/j.atmosres.2009.01.010.

Müller, M., Kašpar, M., Valeriánová, A., Crhová, L., Holtanová, E., Gvoždíková, B., 2015. Novel indices for the comparison of precipitation extremes and floods: an example from the Czech territory. Hydrol. Earth Syst. Sci. 19, 4641–4652. https://doi.org/10.5194/hess-19-4641-2015.

Nissen, K.M., Ulbrich, U., Leckebusch, G.C., 2014. Vb cyclones and associated rainfall extremes over central Europe under present day and climate change conditions. Meteorol. Z. 22, 649–660. https://doi.org/10.1127/0941-2948/2013/0514.

Pfahl, S., 2014. Characterising the relationship between weather extremes in Europe and synoptic circulation features. Nat. Hazards Earth Syst. Sci. 14, 1461–1475. https://doi.org/10.5194/nhess-14-1461-2014.

Řezáčová, D., Kašpar, M., Müller, M., Sokol, Z., Kakos, V., Hanslian, D., Pešice, P., 2005. A comparison of the flood precipitation episode in August 2002 with historic extreme precipitation events on the Czech territory. Atmos. Res. 77, 354–366. https://doi.org/10.1016/j.atmosres.2004.10.008.

Roberts, J.F., Champion, A.J., Dawkins, L.C., Hodges, K.I., Shaffrey, L.C., Stephenson, D.B., Stringer, M.A., Thornton, H.E., Youngman, B.D., 2014. The XWS open access catalogue of extreme European windstorms from 1979 to 2012. Nat. Hazards Earth Syst. Sci. 14, 2487–2501. https://doi.org/10.5194/nhess-14-2487-2014.

Sodemann, H., Zubler, E., 2010. Seasonal and inter-annual variability of the moisture sources for Alpine precipitation during 1995–2002. Int. J. Climatol. 30, 947–961. https://doi.org/10.1002/joc.1932.

Sodemann, H., Wernli, H., Schwierz, C., 2009. Sources of water vapour contributing to the Elbe flood in August 2002 – a tagging study in a mesoscale model. Q. J. Roy. Meteor. Soc. 135, 205–223. https://doi.org/10.1002/qj.374.

Stohl, A., James, P., 2004. A Lagrangian analysis of the atmospheric branch of the global water cycle. Part I: Method description, validation, and demonstration for the August 2002 flooding in central Europe. J. Hydrometeorol. 5, 656–678. https://doi.org/10.1175/1525-7541(2004)005<0656:ALAOTA>2.0.CO;2.

Van Bebber, W.J., 1891. Die Zugstrassen der barometrischen Minima nach den Bahnenkarten der deutschen Seewarte für den Zeitraum 1875–1890. Meteorol. Z. 8, 361–366.

Wypych, A., Bochenek, B., Rózycki, M., 2018. Atmospheric moisture content over Europe and the Northern Atlantic. Atmosphere 9, 18. https://doi.org/10.3390/atmos9010018.

6 Application in forecasting

Paper V: Gvoždíková, B., Müller, M. Predictability of moisture flux anomalies indicating central European extreme precipitation events. Submitted to Quarterly Journal of the Royal Meteorological Society.

Predictability of moisture flux anomalies indicating central European extreme precipitation events

Blanka Gvoždíková[1], Miloslav Müller[1,2]

[1]Faculty of Science, Charles University, Prague, Czech Republic
[2]Institute of Atmospheric Physics AS CR, Prague, Czech Republic

Correspondence to: Blanka Gvoždíková (blanka.gvozdikova@natur.cuni.cz)

Abstract

Forecasting heavy precipitation has an important role in mitigating floods and associated hazards, but it remains one of the main challenges in operational meteorology. Our previous study confirmed the close connection between large-scale extreme precipitation events and anomalous moisture fluxes in central Europe. Therefore, we propose a variable that is referred to as accumulated ascending moisture flux, which could potentially support extreme precipitation event forecasts. The variable reflects the total amount of transported water vapour in combination with extra high upward vertical velocity, which are important factors required for extreme precipitation occurrence. The aim of this study was to determine the predictability of the variable and what affects its quality. While the predictability of moisture flux is satisfactory, generally less accurate forecasts of the vertical velocity negatively affect the predictability of accumulated ascending moisture flux, especially in the case of summer precipitation events with prevailing northern moisture flux. Nevertheless, the forecast of the variable was adequate and stable up to 6 days in advance in all cases of maximum events that produced major central European summer floods. There was no such continuity in high accumulated ascending moisture flux forecasts for less extreme or false-alarm precipitation events. Thus, we assume that the calculation of the accumulated ascending moisture flux from numerical weather prediction could be useful as a supporting tool in extreme precipitation warnings in central Europe.

Keywords: moisture flux, extreme precipitation, predictability, central Europe, ERA-Interim

1 Introduction

Numerical weather prediction (NWP) models exhibit insufficient forecast skill for extreme precipitation events (EPEs), particularly due to the high spatial and temporal variability of precipitation (Sukovich et al., 2014). However, accurate forecasts of precipitation, particularly extreme events, are essential for mitigating the impact of possible precipitation extremes as well as subsequent floods, which can cause serious damage to society and ecosystems.

Our focus is large-scale extreme precipitation in central Europe, where events can be connected to synoptic-scale processes of moisture transport mainly from the Atlantic and the Mediterranean. The transport of moisture is often considered essential for the emergence of hydrometeorological extremes in this area. A close relationship between extreme floods and intense moisture transport has been demonstrated in the Alps by Froidevaux and Martius (2016), who examined the vertically integrated variable, and by Müller and Kašpar (2011), who focused on the moisture flux at single pressure levels. However, extreme precipitation requires moisture supply supported by a sustained lifting of air, which has been considered in our previous study (Gvoždíková, Müller, 2021), where we examined the moisture flux conditions in the area of extra high upward vertical velocity. Results showed that extreme moisture flux might be a suitable indicator of EPEs, especially events with dominating northern moisture flux (*Nf*). The EPEs that belong to the *Nf* type represented a large group of EPEs that affect the eastern parts of central Europe in the warm half-year and that cause severe floods in the Oder, Elbe and Danube basins (Gvoždíková, Müller, 2017). On the other hand, there were several EPEs with dominating western moisture flux (*Wf*), which occurred only from September to March (Gvoždíková, Müller, 2021) and mostly affected the western half of central Europe. However, the correspondence between extreme western moisture flux and *Wf* EPEs was not as strong due to cases when high values of moisture flux from the west occurred due to extra high wind velocities despite rather small amounts of air moisture.

Given that the moisture flux is related to a larger-scale circulation, we can assume that its predictability will be better than in the case of precipitation, which is driven by more complex small-scale atmospheric processes (Lavers et al., 2016). There is already evidence from previous studies that integrated vapour transport (IVT) is more predictable than precipitation (Lavers et al., 2014). The finding was based on the comparison of the degree of linear association between forecasted fields and observed fields measured by the Pearson correlation coefficient. Since the correlation coefficient is a dimensionless value, it may be useful for comparing the quality of forecasts for different atmospheric variables.

There are a large number of verification methods that have been employed for precipitation or moisture fluxes (Wilks, 2011; Rossa et al., 2008). However, many of them do not allow a comparison of precipitation and moisture flux predictability. For the verification of spatial fields, which are typically produced by numerical NWP models, anomaly correlation is one of the most common traditional measures of forecast accuracy (Wilks, 2011). Anomaly correlation is utilized as one of

the main verification measures at European Centre for Medium-Range Weather Forecasts (ECMWF; Owens, Hewson, 2018), although it is not directly employed for precipitation. There may be a problem with forecasts that indicate smaller-scale precipitation patterns that are somewhat misplaced and are penalized twice for showing precipitation at the wrong location and not showing precipitation at the correct location (Ebert, 2008). Therefore, new verification methods that account for spatial translation and suppress the double penalty issue were developed (Gilleland et al., 2009). However, this issue is more problematic for high-resolution forecasts.

For the purposes of this study, we decided to use the anomaly correlation coefficient to compare the predictability of precipitation, moisture flux and vertical velocity in central Europe. We focus on the predictability of selected EPEs and compare it with nonextreme precipitation days since 1979. Because some EPEs were directly linked to extremes in moisture flux accompanied by a high upward vertical velocity (Gvoždíková, Müller, 2021), we aim to assess the use of the combination of vertical velocity and moisture flux to predict extreme precipitation. We assume that the combined variable could support extreme precipitation warnings even at longer lead times and improve preparedness for these extremes.

2 Data and methods

2.1 Study area and reference precipitation events

In central Europe, a moisture supply from both the Atlantic and the Mediterranean relates to the emergence of precipitation extremes (Sodemann and Zubler, 2010; Hofstätter et al., 2017). Based on our previous study (Gvoždíková, Müller, 2021), there were three essential types of events of different origins that affect the area of five main river basins (Rhine, Weser/Ems, Elbe, Danube, and Oder), which define our area of interest (Figure 1).

The examined extreme precipitation events (Table 1) were always large-scale extremes that were selected by the value of the weather extremity index (WEI; Müller et al., 2015) combining the information about precipitation intensity, the area affected by precipitation and the duration of the event. The WEI is equal to the maximum value of the variable E_{ta} (Müller and Kašpar, 2014), which is calculated for the day-by-day expanding time window (from 1 day to 10 days) as the product of the radius of a circle (equivalent to the enlarging area) and the mean common logarithm of the return periods of precipitation totals within the considered area. Although the identified EPEs had a variable length, mostly up to five days, the course of multiday events can always be analysed by the one-day E_{ta}.

The final list of central European EPEs published by Gvoždíková et al. (2019) consisted of three types of events of different moisture flux conditions that prevail during their lifetimes. A geometric mean of relative moisture flux values (separately from each of the four cardinal directions) specified the following division: (i) events with dominating moisture flux from the northern sector (*Nf*),

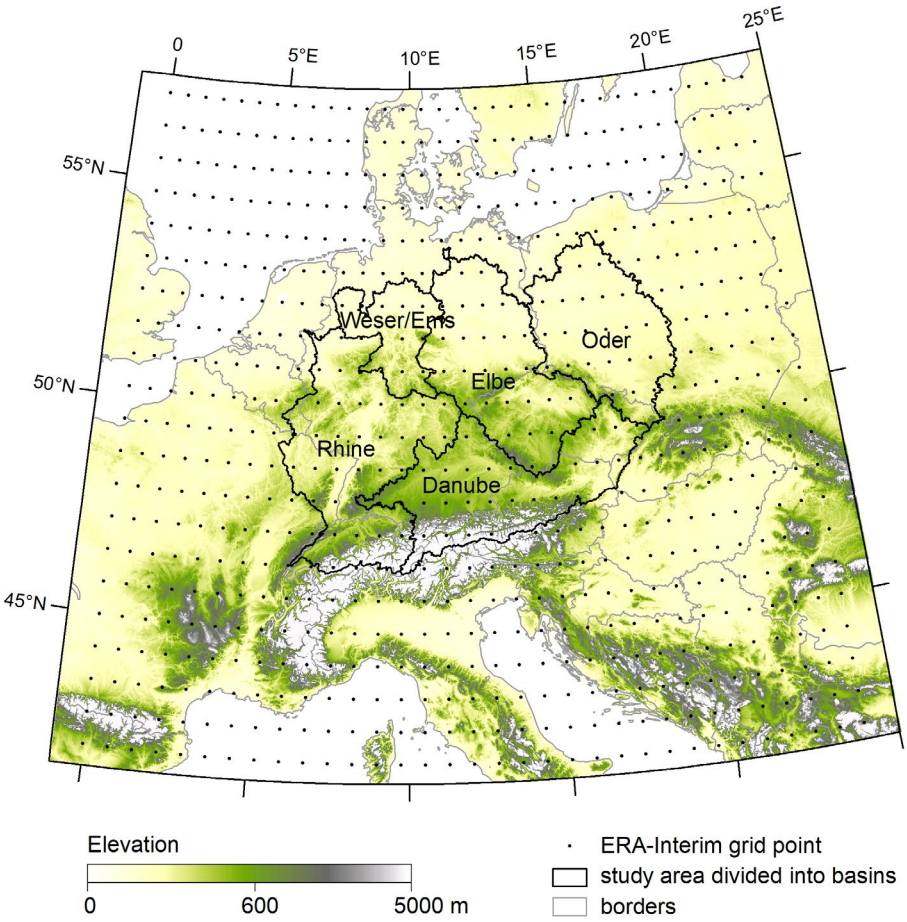

Figure 1: Elevation and ERA-Interim grid points in the study area

(ii) events with dominating moisture flux from the western sector (*Wf*), and (iii) low flux events (*Ot*) (Gvoždíková, Müller, 2021). Considering that the geometric mean was taken only over grid points of extra high upward vertical velocity, no *Sf* events or *Ef* events were detected (i.e., events with dominating southern moisture fluxes or eastern moisture fluxes, respectively). As a result, we identified 22 *Nf* events, 10 *Wf* events, and 11 *Ot* events between 1979 and 2013. In this study, we focused on two of these three type: EPEs of *Nf* and *Wf* moisture flux variants, which completely differ in their origin.

2.2 ERA-Interim reanalysis and forecasts

Data from the ERA-Interim reanalysis based on the ECMWF Integrated Forecast System (IFS) were retrieved from January 1979 to December 2018 over the area 0°–24°E, 42°–57°N with a horizontal grid spacing of 0.75° on a regular latitude/longitude grid (Figure 1). Reanalysis of the vertical velocity w (Pa s^{-1}) at a pressure level of 700 hPa (with negative values indicating ascending motion) and air temperature T (K), specific humidity q (kg kg^{-1}), zonal component of wind u (m s^{-1}), and meridional component of wind v (m s^{-1}) at the 850 hPa level were retrieved at 0000 and 1200 UTC. The same variables were retrieved from ERA-Interim forecasts for a maximum period of 10 days,

Table 1: Extreme precipitation events of *Nf* (left and central panel) and *Wf* (right panel) moisture flux variants in central Europe from 1979 to 2013 ranked by precipitation extremeness (WEI).

EPEs Ranking	Precipitation event	Duration (days)	Moisture flux variant	EPEs Ranking	Precipitation event	Duration (days)	Moisture flux variant	EPEs Ranking	Precipitation event	Duration (days)	Moisture flux variant
1	17 Jul 1981	4	Nf	13	6 Aug 2002	2	Nf	10	20 Oct 1986	3	Wf
2	4 Jul 1997	5	Nf	14	16 Jul 2002	2	Nf	16	19 Dec 1993	2	Wf
3	30 May 2013	4	Nf	15	8 Jul 1996	1	Nf	17	19 Mar 2002	4	Wf
4	11 Aug 2002	2	Nf	18	31 Jul 1991	3	Nf	21	27 Oct 1998	2	Wf
5	6 Aug 1985	4	Nf	20	17 Jun 1979	1	Nf	29	13 Feb 1990	3	Wf
6	1 Aug 1983	5	Nf	23	22 Jul 2010	3	Nf	30	6 Oct 1982	2	Wf
7	3 Aug 2006	6	Nf	28	24 Jun 2013	2	Nf	32	21 Dec 1991	2	Wf
8	5 Sep 2007	2	Nf	31	12 Apr 1994	2	Nf	35	12 Sep 1998	4	Wf
9	25 Sep 2010	3	Nf	34	27 May 2007	3	Nf	38	28 Dec 1986	3	Wf
11	20 Jul 2011	3	Nf	41	16 May 2010	3	Nf	43	25 Feb 1997	1	Wf
12	15 Jul 1997	7	Nf	42	8 Jun 1990	3	Nf				

when the forecasts were initiated at 0000 UTC and thus the forecast lead times ranged from 24 to 240 hours. Zonal and meridional moisture fluxes (kg m^{-2} s^{-1}) were obtained from the retrieved data as $F_{qu} = \rho q u$ and $F_{qv} = \rho q v$, respectively. Fluxes from the west and south are positive, while the negative values refer to eastern and northern fluxes. Daily means of the reanalysis and forecasts of the vertical velocity and the components of moisture fluxes were calculated using 0000, 1200 UTC and 0000 UTC of the following day. In addition to these fields on pressure levels, total surface precipitation forecasts were obtained in 24-hour steps, with daily values accumulated to 0000 UTC. In this case, the 24-hour forecast represented the observation.

The advantage of comparing ERA-Interim forecasts with its reanalysis is that the same physics can be employed for both, which is guaranteed by a fixed IFS cycle (Cy31r2), on which the ERA-Interim is based (Dee et al., 2011). The approach allows us to determine the capability of the model for prediction, and thus, presents the upper limit of the predictive skill—rather idealized predictability—which could be achieved if the model had the same physics as the real world (Luo and Wood, 2006). However, real physical processes are much more complex, which implies that the actual predictive skill will be less than the idealized predictability.

2.3 Idealized predictability calculation

For the set of EPEs as well as the whole study period, we aimed to compare the predictability of the daily values of the vertical velocity at the 700 hPa pressure level, the zonal and meridional moisture flux at the 850 hPa level, and the total surface precipitation. Computing the Pearson correlation coefficient between the grid points of a single pair of reanalysis/forecast fields allows such a comparison. However, the commonly employed measure operates more often on anomalies of values, when the climatological mean value c_i of each of I grid points is subtracted from both reanalysis r_i and forecasts f_i of different lead times: $r'_i = r_i - c_i$, and $f'_i = f_i - c_i$, respectively. The centred anomaly correlation AC is then calculated according to Wilks (2011) as the usual Pearson correlation:

$$AC = \frac{\sum_{i=1}^{I}(f'_i - \overline{f'})(r'_i - \overline{r'})}{\sqrt{\sum_{i=1}^{I}(f'_i - \overline{f'})^2 \sum_{i=1}^{I}(r'_i - \overline{r'})^2}} \quad (1).$$

As a result, AC measures the similarities in anomaly patterns, but it is not sensitive to absolute or conditional biases, and thus, reflects potential predictive skill.

2.4 Accumulated ascending moisture flux

As shown in our previous study (Gvoždíková, Müller, 2021), the combination of the vertical velocity and moisture flux worked better than the moisture flux as a potential predictor of extreme precipitation in central Europe. We introduced a variable, which is here referred to as the accumulated ascending moisture flux T^*_d (kg s^{-1}) and reflects the total amount of transported water vapour during day d over grid points with extra high upward vertical velocity. The size of T^*_d is calculated by the vector sum of the accumulated zonal flux (the larger of the western and eastern fluxes, $F_{W/E}$) and the meridional flux (the larger of the southern and northern fluxes, $F_{S/N}$):

$$T^*_d = \sqrt{\left(a\sum_1^n |F_{W/E}|\right)^2 + \left(a\sum_1^n |F_{S/N}|\right)^2} \quad (2).$$

In Equation 2, a refers to the average pixel size within the study area ($a \approx 4.5\times10^9$ m^2), and n is the variable number of grid points with extra high upward vertical velocity, which represents the vertical velocity within 0.5% of the lowest reanalysis values for a particular grid point from 1979 to 2018.

When the accumulated ascending moisture flux derived from the reanalysis has previously confirmed a correspondence to extreme precipitation (especially *Nf* events), we want to determine whether the calculation of T^*_d is reliable even in the case of forecasts with different lead times. Knowing the smallest maximum T^*_d for the set of EPEs, we can consider that the daily forecast is dichotomous (yes/no forecast)—indicates if an event will or will not happen according to exceedance of the T^*_d threshold. The four possible combinations of forecasts (yes/no) and reanalysis (yes/no) are specified in elements of a 2×2 contingency table: hits, false alarms, misses and correct negatives (Wilks, 2011), which can be used to calculate a large variety of categorical statistics. As an example, we present the hit rate and false-alarm ratio, which we apply later in this study. The hit rate is a rather positively oriented score that indicates the proportion of yes events that was actually forecasted: $hit\ rate = \frac{hits}{hits+misses}$. As it disregards false alarms, it is often combined with the false-alarm ratio, which measures the proportion of yes forecasts that did not occur: $false\ alarm\ ratio = \frac{false\ alarms}{hits+false\ alarms}$ (Rossa et al., 2008).

To analyse the advantages and limitations of T^*_d forecasts, we also introduce the accumulated moisture flux, which is referred to as T_d and is accumulated over all grid points in the study area, and therefore, is not conditioned by the extra high value of the upward vertical velocity.

3 Relation of accumulated ascending moisture flux to precipitation

3.1 Relation to extreme precipitation events

Due to the position in mid-latitudes, western directions of moisture flux prevail in the study area, which also applies to the highest values of T^*_d in general and to maximum T^*_d values during *Wf* EPEs (upper left diagram in Figure 2). To evaluate the representation of EPEs among high T^*_d values, we separately defined sectors within the diagram for *Nf* and *Wf* events so that N1 and W1 sectors comprise maximum T^*_d values during all EPEs of the respective type. The more limited sectors N2 and W2 comprise only a part of them (for more details, refer to Table 2). The agreement between high T^*_d values and EPEs of the given type was tested for the reanalysis and forecasts within the sectors in two ways: (i) percentage of the T^*_d values due to the EPEs in the total number of T^*_d values; (ii) percentage of the EPEs with T^*_d values within the sector in the total number of EPEs of the respective type.

The results for the reanalysis are depicted by the signs on the far left in Figure 3a. Almost half of the T^*_d values in sector N1 and all of the T^*_d values in N2 are due to *Nf* EPEs. Although only 40% of *Nf* EPEs reached the more limited sector, they included the 5 largest precipitation events (Table 1), which led to significant floods in central Europe during warmer half-years (Gvoždíková, Müller, 2017). Regarding the *Wf* precipitation events, only a minority (15%) of the values in the larger W1

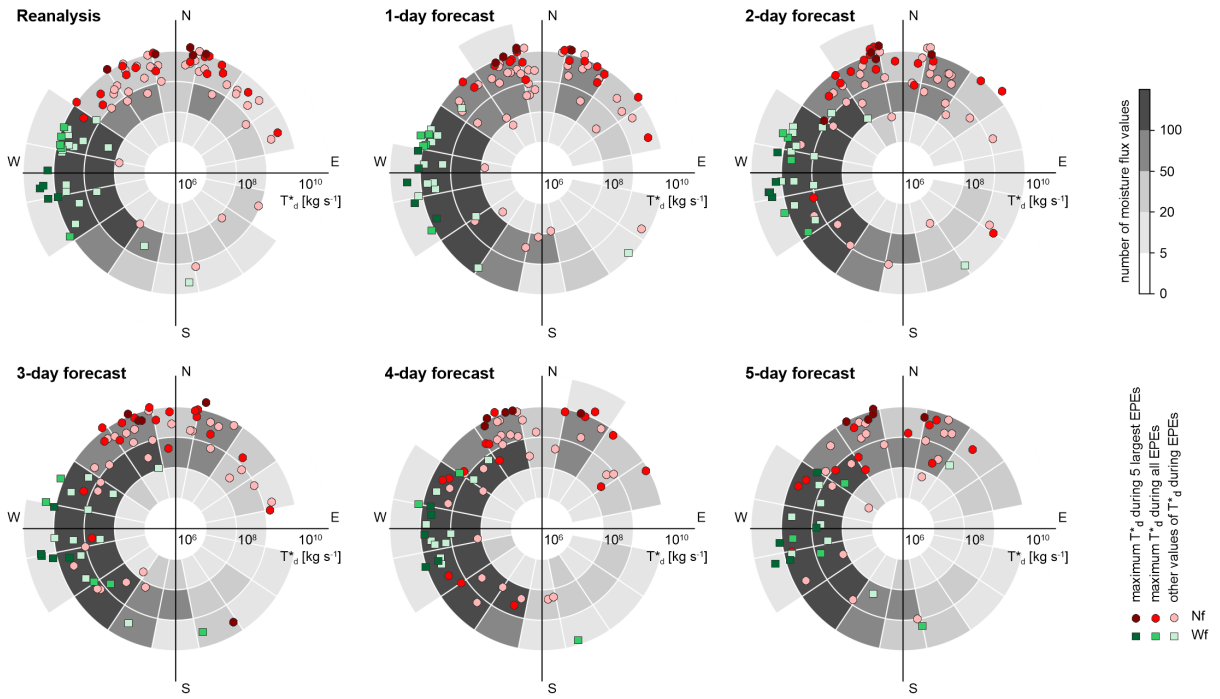

Figure 2: Reanalysis and forecasts of accumulated ascending moisture flux (T^*_d) during EPEs in comparison with the frequency of T^*_d values on all days between 1979 and 2018, when the criterion of extra high upward vertical velocity was fulfilled at least in one grid point. Values reached during EPEs are marked with symbols different for the variants *Nf* and *Wf*; magnitude and mean direction of the moisture flux are expressed by the distance and position to the centre of the diagram. Shading depicts the frequency of T^*_d values on all days within the given intervals and directional sectors.

Table 2: Directional sectors considered for the reanalysis and forecasts of accumulated ascending moisture flux (T^*_d) and accumulated moisture flux (T_d).

Sectors	N1	N2	W1	W2
Range of angles	300° - 70°	325° - 20°	235° - 295°	250° - 280°
Threshold of T^*_d (kg s^{-1})	$2{\cdot}10^9$	$9{\cdot}10^9$	$7{\cdot}10^9$	$2{\cdot}10^{10}$
Threshold of T_d (kg s^{-1})	$2{\cdot}10^{10}$	$3{\cdot}10^{10}$	$4{\cdot}10^{10}$	$7{\cdot}10^{10}$

sector were due to EPEs. If we consider the more limited sector W2 with only 40% of the *Wf* EPEs, their percentage in the total number of such high T^*_d values increases to 50%. Note that these events were the largest *Wf* precipitation events since 1979. A substantial portion of T^*_d values in sectors W1 and W2, which were not accompanied by EPEs, was recorded on days when strong moisture fluxes were generated by extra high wind velocity combined with rather low values of air humidity.

In general, high T^*_d values became more frequent when computed from the forecast outputs (Figure 2). As a result, the proportion of EPEs in high T^*_d forecasts decreased already for 1-day and 2-day forecasts (Figure 3a) compared to the reanalysis. The decrease was more pronounced for the northern moisture fluxes, in which the proportion of values related to *Nf* EPEs decreased to 26% and 69% in the N1 sector and N2 sector, respectively. Nevertheless, the forecasts of T^*_d associated with *Nf* events remained quite satisfactory for 1- to 3-day forecasts and even longer in the case of the 5 largest events, although their T^*_d values slightly decreased (Figure 2).

The situation was rather different for the forecasts of moisture fluxes from the western direction. The proportion of T^*_d values associated with *Wf* EPEs to the total number of measurements even increased slightly within the first two days of the forecast and approached the values in the northern sectors (Figure 3a). However, the number of included events in the defined sectors generally decreased faster with longer forecast lead times.

An interesting comparison is offered by Figure 3b, which displays the moisture flux (T_d) accumulated over all grid points and not only over points with extra high upward vertical velocity. There was no significant decline with longer forecast lead times, which could indicate the problem that forecasted vertical velocity values affect the size of accumulated ascending moisture flux (T^*_d) shown in Figure 3a. However, despite the better correspondence of reanalysis and forecasts in Figure 3b, extra high accumulated moisture flux (T_d) is less related to the EPEs than T^*_d, as the percentage of the T_d values due to EPEs was very low in all sectors.

3.2 Relation to one-day precipitation extremity

The analysis of T^*_d values in Figure 2 shows that all significant precipitation events had an extra high value of accumulated ascending moisture flux at least on one day. However, the direct connection between the T^*_d variable and the daily precipitation extremity (given by real one-day E_{ta}; Gvoždíková et al. 2019) is less significant. Even during the selected precipitation events, the peak of the daily E_{ta} values often did not coincide in time with the peak of T^*_d but was shifted mostly one day forward or

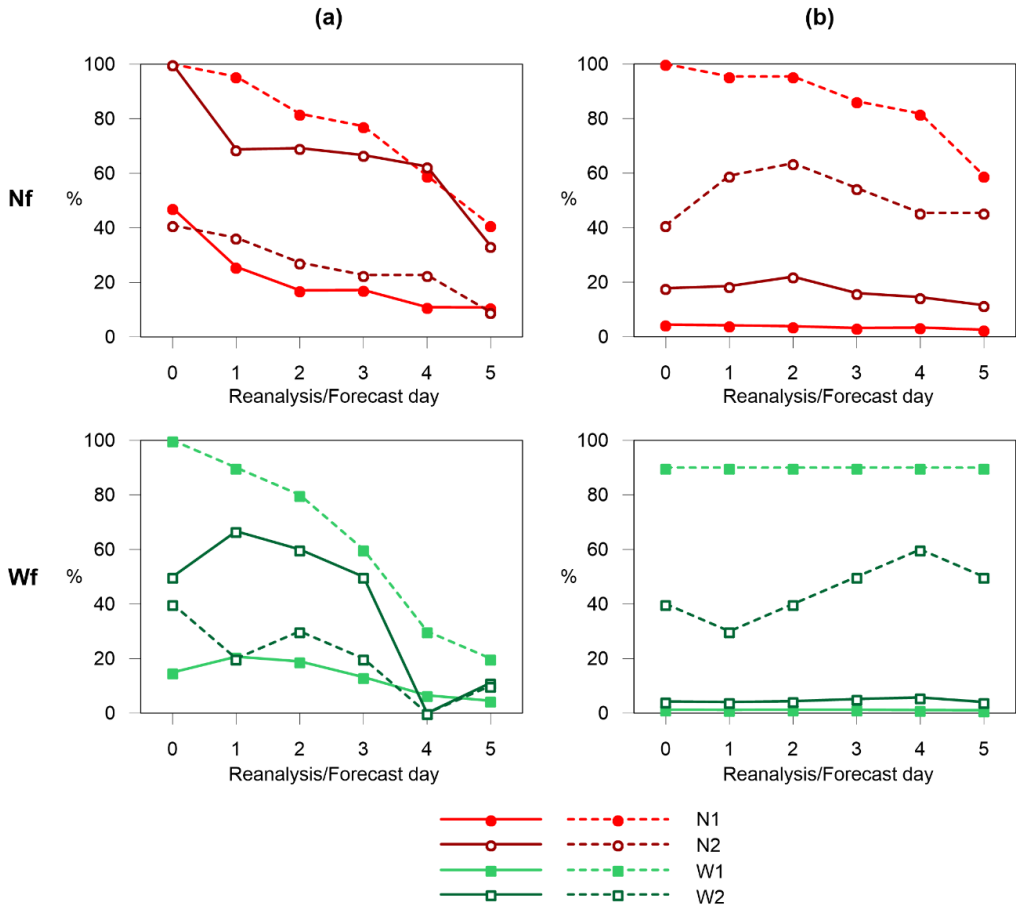

Figure 3: (a) Reanalysis and forecasts of the proportion of *Nf* and *Wf* event points to the total number of accumulated ascending moisture flux values (T^*_d) in sectors N1, N2, W1, and W2 (refer to Table 2). The percentage of events in the sector is depicted by the dashed line. (b) The same as (a) but for accumulated moisture flux (T_d) without the condition of extra high vertical velocity.

one day backward. Therefore, we also analyse the relation between T^*_d values and E_{ta} values on individual days.

The number of cases when extra high accumulated ascending moisture fluxes were related to extreme precipitation at the daily resolution from 1979 to 2013 is indicated in Figure 4. In its left upper part (Figure 4a), we considered only days with reanalysed T^*_d values of the northern moisture flux (range of angles is the same for sector N1). The total number of these days was divided into 5% intervals with respect to T^*_d and E_{ta} distributions. Figure 4b represents the same result but for the western moisture flux directions (W1). We focused on days when T^*_d and E_{ta} values exceeded their medians (Figure 4a, and similarly, 4b). The relation between high T^*_d values and high E_{ta} values is obvious. In the case of northern moisture fluxes (Figure 4a), as many as 60% of days with T^*_d above the 80th percentile were accompanied by E_{ta} values above the 80th percentile, and vice versa. The corresponding percentage was lower for western moisture fluxes (43%, Figure 4b). A similar agreement exists on the opposite side of both tables between small T^*_d and E_{ta}; for values below the 65th percentile, 80% of the days matched in Figure 4a and 74% of the days matched in Figure 4b.

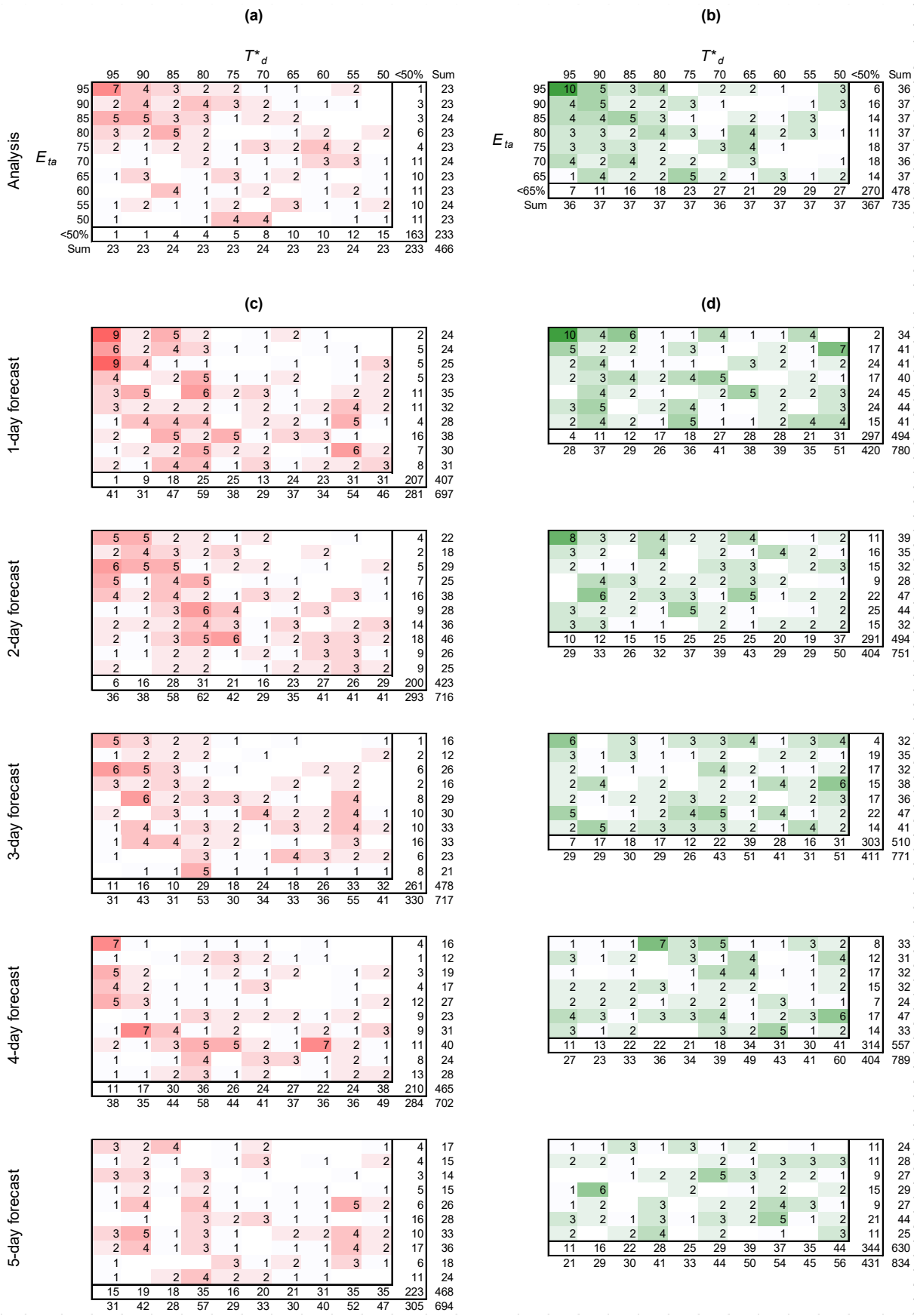

Figure 4: Relationship between one-day precipitation extremity, which is expressed by E_{ta}, and accumulated ascending moisture flux (T^*_d) of a given range of angles as for sectors (a), (c) N1 and (b), (d) W1 (refer to Table 2). T^*_d values are derived either from (a), (b) reanalysis or (c), (d) forecasts. The sorted data are divided into equal parts, which represent 5% of the total number of values.

The results for the forecasting data are shown in Figure 4c and 4d, where the values of both variables used for division into intervals remained the same as shown in Figures 4a and 4b, respectively. Thus, the measured precipitation expressed by one-day E_{ta} and the forecasted values of T^*_d are compared. However, the number of days considered in Figure 4c (N1 angles) was much greater than that in the case of reanalysis, which was due to a larger number of days with forecasted extra high upward vertical velocity. Even on the first forecast day, the number of days in individual intervals of T^*_d sometimes doubled, but most of the false-alarm T^*_d values were below the 50th percentile of E_{ta}. Due to this increase in the number of days considered in Figure 4c, only 33% of days on the first forecast day had T^*_d and E_{ta} values above the 80th percentile simultaneously. Compared to the reanalysis, a decrease of nearly half was obtained. In the case of western moisture fluxes (Figure 4d), the corresponding percentage remained approximately the same size on the first forecast day as that in the reanalysis.

Although the maxima of T^*_d did not correspond exactly to the precipitation maxima, the agreement between high T^*_d and E_{ta} in a daily step was satisfactory in the reanalysis and mainly for northern moisture fluxes. Based on the forecasts, the close connection quickly disappeared. This finding was related to a large increase in the number of days with forecasted extra high upward vertical velocity, which was typical only for the northern moisture flux directions. This result indicates that forecasts may overestimate vertical velocity values mostly on days with a predominant northern moisture flux.

4 Predictability of considered variables

4.1 Influence of vertical velocity on accumulated ascending moisture flux predictability

The previous section indicated that the vertical velocity may reduce the quality of the accumulated ascending moisture flux forecast. To confirm the presumption, we decided to compare the accuracy of the T^*_d and T_d forecasts (Figure 5) using two selected scores: hit rate and false-alarm ratio (refer to Section 2.4). The thresholds for the YES events correspond to T^*_d and T_d values that reached the N1/W1 sector thresholds in Table 2.

The poor forecast of T^*_d in sector N1 was caused by a large number of false alarms, which is demonstrated by a high false-alarm ratio (Figure 5b). Even on the first forecast day, false alarms almost doubled the number of hits (Table 3). This finding corresponds to the increase in the number of days considered in Figure 4c. For sector W1, the forecast was better according to a lower false-alarm ratio, but a slightly higher number of missed events (and lower hit rate) had the opposite effect and worsened T^*_d forecasts.

In contrast, the daily forecast of T_d seems to be quite accurate. Both the hit rate and the false-alarm ratio showed much better results than when we considered the condition of extra high upward vertical velocity (Figure 5). However, as Figure 3b shows, only a small part of the high T_d values in the defined sectors were associated with EPEs. Therefore, it is not possible to use it as a supporting

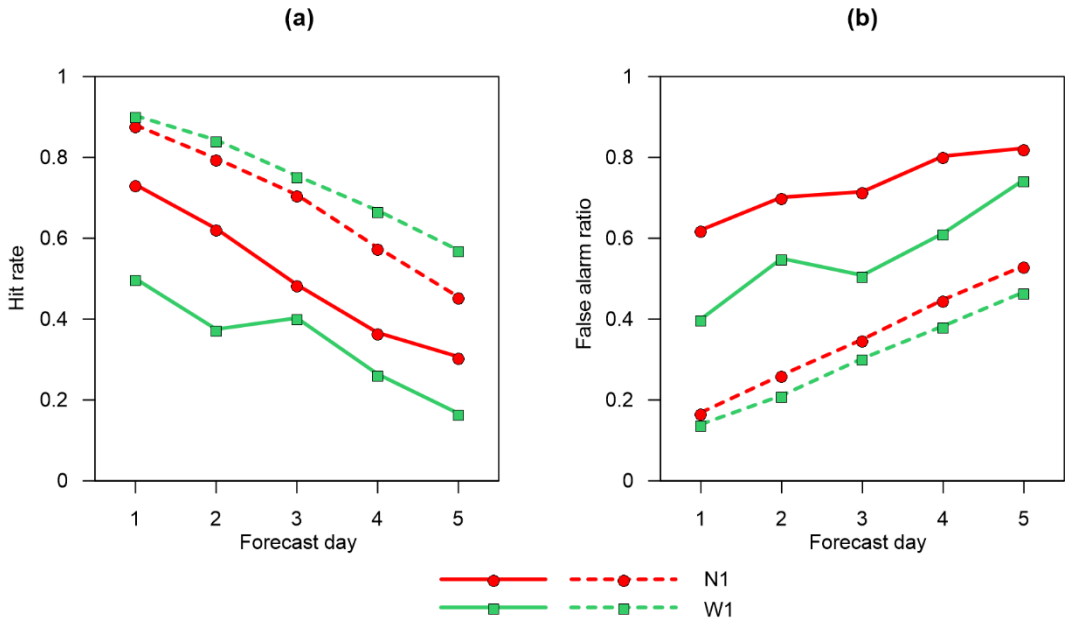

Figure 5: (a) Hit rate and (b) False-alarm ratio calculated for pairs of reanalysis/forecast of accumulated ascending moisture flux (T^*_d). YES events are set to the occurrence in sectors N1 and W1 (refer to Table 2). Dashed lines depict the same measures for the accumulated moisture flux (T_d) without the condition of extra high vertical velocity.

forecasting tool for extreme precipitation warnings. Simultaneously, working with T^*_d is also problematic due to the lower forecast accuracy.

Nevertheless, the forecasts of T^*_d during the 5 largest EPEs seem quite stable even if vertical velocity is included (Figure 2). There was consistency in forecasting high values of T^*_d, especially in the case of *Nf* extreme precipitation events. For the 5 largest EPEs, the model began to forecast high T^*_d 6 days in advance (we take into account the forecast for the same day with a possible one-day shift; Figure 6). Except for EPEs, there were only few cases when forecasts continuously indicated high T^*_d for at least 6 consecutive days. Apart from the largest *Nf* events, these cases included the 4th largest *Wf* event (Table 1), several less extreme spring events and two February precipitation events (some of them outside the largest EPEs in Table 1). Only one case in April remained without a precipitation response.

Table 3: Contingency tables for verification of 1-day forecasts of (a), (c) accumulated ascending moisture flux (T^*_d) and (b), (d) accumulated moisture flux (T_d) from 1979 to 2018. Tables are divided according to the sector in which we evaluate the occurrence of daily events: (a), (b) N1 sector and (c), (d) W1 sector. For sector thresholds, refer to Table 2.

(a) N1

		Reanalysis	
		yes	no
1-day forecast	yes	74	121
	no	27	14379

(b) N1

		Reanalysis	
		yes	no
1-day forecast	yes	1077	219
	no	147	13156

(c) W1

		Reanalysis	
		yes	no
1-day forecast	yes	36	24
	no	36	14505

(d) W1

		Reanalysis	
		yes	no
1-day forecast	yes	1445	235
	no	155	12764

4.2 Comparison of predictability of precipitation, vertical velocity and moisture fluxes

Considering the previous findings of this study, it can be assumed that the vertical velocities significantly affect the quality of the T^*_d forecast. Therefore, we examined individual variables and assessed their predictability by calculating anomaly correlations (refer to Section 2.3) between the grid points of the daily pairs of reanalysis/forecast fields. On average, the vertical velocity field predictability appears to be similar to that of precipitation, but both are much worse than the predictability of moisture flux (Figure 7a). Both zonal moisture flux and meridional moisture flux showed very similar results with anomaly correlations that were much higher than those for precipitation or vertical velocity. Even in the 5-day forecast, the AC values were approximately 0.6 compared to 0.4 for precipitation and vertical velocity.

In the case of the selected *Nf* and *Wf* events, the predictability of vertical velocity was only slightly better than that of precipitation (except for the 1-day forecast, compare Figure 7b and 7c). However, a significant difference occurred between the anomaly correlations for the *Nf* events and those for the *Wf* events, with much better results for the western moisture flux situations. The differences between the *Nf* events and *Wf* events were not apparent only in the case of the anomaly correlations for zonal moisture fluxes and meridional moisture fluxes, *fqu* (Figure 7d) and *fqv* (Figure 7e), respectively.

Excellent predictability of moisture fluxes and less accurate results for the vertical velocity suggest an explanation for a much worse agreement between EPEs and forecasted T^*_d than in the reanalysis (Figure 3a). Simultaneously, this finding agrees with the greater accuracy of the forecasts of T_d (Table 3, Figure 5), which are independent of the condition of extra high upward vertical velocity.

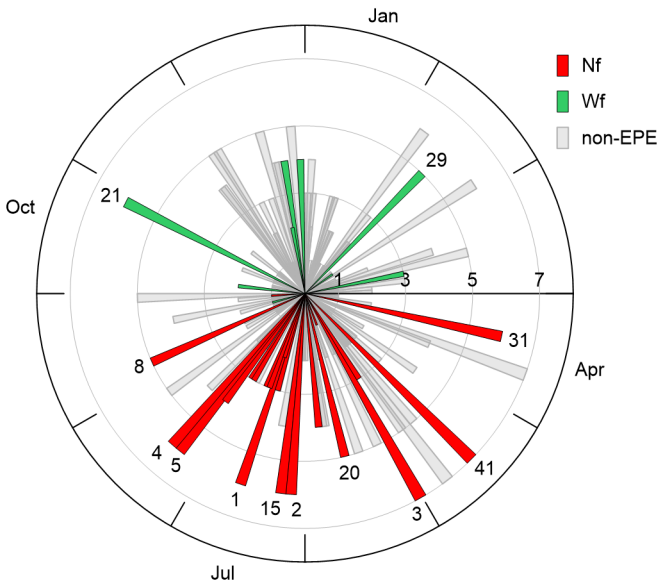

Figure 6: Quality of accumulated ascending moisture flux (T^*_d) forecasts for days when values reached sectors N1/W1 (refer to Table 2) on at least the first forecast day. The distance to the centre of the diagram expresses the number of days of consecutive forecasts of T^*_d within sectors. The directional angle represents the seasonal distribution of events. EPEs are highlighted in colour compared to cases that did not belong to EPEs. Selected EPEs are marked with a number that corresponds to the ranking in Table 1.

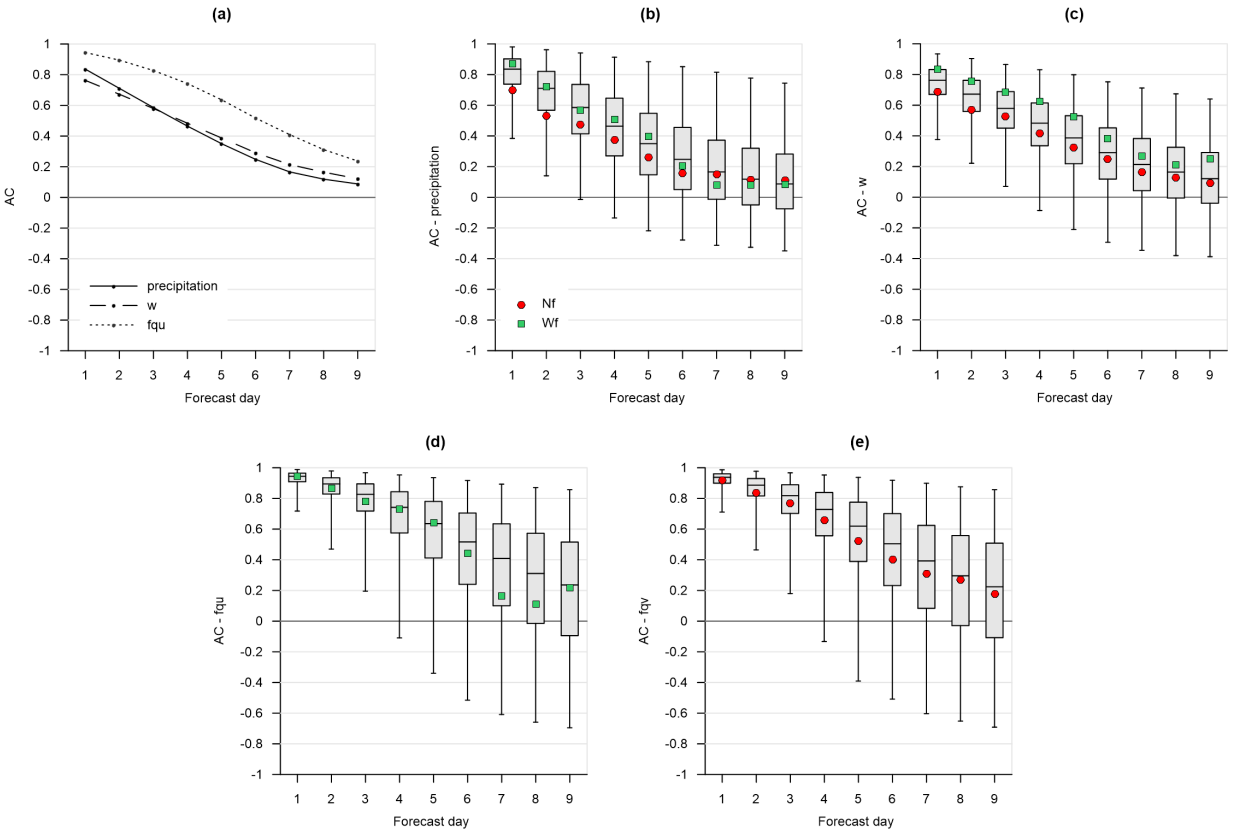

Figure 7: (a) Median values and (b), (c), (d), and (e) boxplots of anomaly correlations for (b) precipitation forecast, (c) vertical velocity (*w*) forecast at the 700 hPa level, (d) zonal (*fqu*) and (e) meridional moisture flux (*fqv*) forecast at the 850 hPa level. The whiskers go from each quartile to the 1st and 99th percentile values. The symbols represent the mean anomaly correlations for days during *Nf* or *Wf* events.

5 Discussion

Moisture flux forecasting can support the prediction of precipitation extremes, but first, it needs to be reasonably connected to these extremes, and second, the quality of its predictability must be sufficient (Froidevaux and Martius, 2016).

The close relationship between accumulated ascending moisture flux T^*_d and especially large EPEs of the northern moisture flux variant (*Nf*) was confirmed in this study. This result agrees with previous findings by Gvoždíková and Müller (2021), which were based on data from the recent ERA5 reanalysis. The agreement was even better using ERA5 data when expressed as the percentage of *Nf* event points to the total number of T^*_d values, which accounted for 68% in the sector that corresponds to N1 (Table 2) compared to 47% using ERA-Interim. Moreover, it seems that the relationship between T^*_d and the one-day E_{ta} was also stronger for the ERA5 reanalysis (not shown). Higher data resolution (0.25° spatial grid) may explain this stronger relationship, as it captures local extremes of accumulated ascending moisture flux, or the stronger relationship may be related to the selected vertical velocity threshold. In our previous study (Gvoždíková, Müller, 2021), extra high upward vertical velocity corresponded to only 0.1% of the lowest reanalysis values, which was not possible in the case of ERA-Interim data, where some EPEs would not be recorded.

In addition to the existing relation between extreme precipitation and T^*_d at lower tropospheric isobaric levels, research by other authors often links extreme precipitation and floods to intense IVT, which usually occurs in atmospheric river regions. Thus, IVT had a significant effect on extreme events in the western United States (Konrad, Dettinger, 2017) or western Europe (Lavers, Villarini, 2013). According to Froidevaux and Martius (2016), IVT perpendicular to orography also caused major floods in the Swiss Alps, although it was not always associated with atmospheric rivers. Simultaneously, the authors were aware of the strong vertical wind shear situations, which can affect the IVT direction and reduce its magnitude. A significant change in the wind direction with altitude is often related to EPEs in the eastern part of central Europe (Bližňák et al., 2019), where precipitation extremes are triggered by Vb cyclones that originate in the Mediterranean region (Messmer et al., 2015).

Despite the obvious connection between extreme moisture flux and precipitation, few studies have compared their predictability. Lavers et al. (2014, 2016) focused on IVT and confirmed the higher predictability of moisture flux compared to precipitation. They explained this finding by a connection of moisture flux to synoptic-scale circulation, which is more predictable than microphysical phenomena, such as precipitation. Our study demonstrates excellent predictability for zonal and meridional moisture fluxes at the 850 hPa level. However, combined with vertical velocity, the accumulated ascending moisture flux is not an appropriate forecasting tool due to the worse predictability of vertical velocity (Figure 7).

6 Concluding remarks

- The connection between extra high accumulated ascending moisture flux and EPEs exists mainly in the case of precipitation extremes with predominant northern moisture flux (*Nf* events), when a closer relationship occurred during larger precipitation extremes. In the case of high T^*_d in the western moisture flux directions, the correspondence to *Wf* EPEs was less significant due to the larger proportion of nonprecipitation events among these values caused by the high wind velocities with rather small air moisture.

- Due to the higher spatial resolution, ERA5 outperforms the ERA-Interim reanalysis and exhibits a closer connection between precipitation extremes and extra high T^*_d values.

- Forecasts of moisture fluxes are more reliable than those of precipitation, but this reliability does not apply to accumulated ascending moisture flux calculated in the area of extra high upward vertical velocity, which produces a large number of false-alarm situations with northern moisture flux. This finding was connected to a poorer vertical velocity forecast during these situations. Despite the worse predictability of T^*_d, there was continuity in forecasting extra high T^*_d values in the case of large *Nf* EPEs. For the 5 largest *Nf* events, high T^*_d values were forecasted at least 6 days in advance, when there was no such continuity for smaller or false-alarm events.

- We could use the continuity of high T^*_d forecasts as support for predicting large EPEs of the *Nf* type, such as in July 1981 and 1997, August 2002 or May/June 2013, which led to disastrous floods in central Europe. For less-extreme events, forecasts of accumulated ascending moisture flux are not reliable enough, and a forecasting tool that is based only on the moisture fluxes would be better. However, it seems that T^*_d accumulated in the area of extra high upward vertical velocity shows a better direct relationship to precipitation extremes than T_d independent of this condition.

Acknowledgements

We would like to thank Stephan Pfahl for his helpful insights and discussions on the topic. The ERA-Interim reanalysis and forecast data were retrieved from the ECMWF data server. This work was supported by The Ministry of Education, Youth and Sports grant LTC19043.

References

Bližňák, V., Kašpar, M., Müller, M., Zacharov, P. (2019) Sub-daily temporal reconstruction of extreme precipitation events using NWP model simulations. Atmospheric Research, 224, 65-80. https://doi.org/10.1016/j.atmosres.2020.105309.

Dee, D.P., Uppala, S.M., Simmons, A.J., Berrisford, P., Poli, P., Kobayashi, S., Andrae, U., Balmaseda, M.A., Balsamo, G., Bauer, P., Bechtold, P., Beljaars, A.C.M., van de Berg, L., Bidlot, J., Bormann, N., Delsol, C., Dragani, R., Fuentes, M., Geer, A.J., Haimberger, L., Healy, S.B., Hersbach, H., Hólm, E.V., Isaksen, L., Kållberg, P., Köhler, M., Matricardi, M., McNally, A.P., Monge-Sanz, B.M., Morcrette, J.-J., Park, B.-K., Peubey, C., de Rosnay, P., Tavolato, C., Thépaut, J.-N. and Vitart, F. (2011) The ERA-Interim reanalysis: configuration and performance of the data assimilation system. Quarterly Journal of the Royal Meteorological Society, 13, 553–597. https://doi.org/10.1002/qj.828.

Gilleland, E., Ahijevych, D., Brown, B.G., Casati, B., Ebert, E.E. (2009) Intercomparison of spatial forecast verification methods. Weather and Forecasting, 24, 1416–1430. https://doi.org/10.1175/2009WAF2222269.1.

Gvoždíková, B., Müller, M. (2017) Evaluation of extensive floods in western/central Europe. Hydrology and Earth System Sciences, 21, 3715–3725. https://doi.org/10.5194/hess-21-3715-2017.

Gvoždíková, B., Müller, M., Kašpar, M. (2019) Spatial patterns and time distribution of central European extreme precipitation events between 1961 and 2013. International Journal of Climatology, 39, 3282−3297. https://doi.org/10.1002/joc.6019.

Gvoždíková, B., Müller, M. (2021) Moisture fluxes conducive to central European extreme precipitation events. Atmospheric Research, 248. https://doi.org/10.1016/j.atmosres.2020.105182.

Ebert, E.E. (2008) Fuzzy verification of high resolution gridded forecasts: a review and proposed framework. Meteorological Applications. 15, 51–64. https://doi.org/10.1002/met.25.

Froidevaux, P., Martius, O. (2016) Exceptional integrated vapour transport toward orography: an important precursor to severe floods in Switzerland. Quarterly Journal of the Royal Meteorological Society, 142, 1997–2012. https://doi.org/10.1002/qj.2793.

Hofstätter, M., Lexer, A., Homann, M., Blöschl, G. (2017) Large-scale heavy precipitation over central Europe and the role of atmospheric cyclone track types. International Journal of Climatology, 38(Suppl. 1), e497–e517. https://doi.org/10.1002/joc.5386.

Konrad, C.P., Dettinger, M.D. (2017) Flood runoff in relation to water vapor transport by atmospheric rivers over the western United States, 1949–2015. Geophysical Research Letters, 44, 11456–11462. https://doi.org/10.1002/2017GL075399.

Lavers, D.A., Pappenberger, F., Zsoter, E. (2014) Extending medium-range predictability of extreme hydrological events in Europe. Nature Communications, 5, 5382, https://doi.org/10.1038/ncomms6382.

Lavers, D.A., Pappenberger, F., Richardson, D.S., Zsoter, E. (2016) ECMWF extreme forecast index for water vapor transport: a forecast tool for atmospheric rivers and extreme precipitation. Geophysical Research Letters, 43(22), 11852– 11858. https://doi.org/10.1002/2016gl071320.

Lavers, D.A., Villarini, G. (2013) The nexus between atmospheric rivers and extreme precipitation across Europe. Geophysical Research Letters, 40, 3259–3264. https://doi.org/10.1002/grl.50636.

Luo, L., Wood, E.F. (2006) Assessing the idealized predictability of precipitation and temperature in the NCEP Climate Forecast System. Geophysical Research Letters, 33, L04708. https://doi.org/10.1029/2005GL025292.

Messmer, M., Gómez-Navarro, J.J., Raible, C.C. (2015) Climatology of Vb cyclones, physical mechanisms and their impact on extreme precipitation over central Europe. Earth System Dynamics, 6, 541–553. https://doi.org/10.5194/esd-6-541-2015.

Müller, M., Kašpar, M. (2011) Association between anomalies of moisture flux and extreme runoff events in the south-eastern Alps. Natural Hazards and Earth System Sciences, 11, 915–920. https://doi.org/10.5194/nhess-11-915-2011.

Müller, M., Kašpar, M. (2014) Event-adjusted evaluation of weather and climate extremes. Natural Hazards and Earth System Sciences, 14, 473–483. https://doi.org/10.5194/nhess-14-473-2014.

Müller, M., Kašpar, M., Valeriánová, A., Crhová, L., Holtanová, E., Gvoždíková, B. (2015) Novel indices for the comparison of precipitation extremes and floods: an example from the Czech territory. Hydrology and Earth System Sciences, 19, 4641–4652. https://doi.org/10.5194/hess-19-4641-2015.

Owens, R.G., Hewson, T. (2018) ECMWF forecast user guide. Available at: https://www.ecmwf.int/node/16559. ECMWF [Accessed 28 April 2020]. https://doi.org/10.21957/m1cs7h

Rossa, A., Nurmi, P., Ebert, E. (2008) Overview of methods for the verification of quantitative precipitation forecasts. In: Michaelides S. (eds) Precipitation: Advances in Measurement, Estimation and Prediction. Springer, Berlin, Heidelberg. https://doi.org/10.1007/978-3-540-77655-0_16.

Sodemann, H., Zubler, E. (2010) Seasonal and inter-annual variability of the moisture sources for Alpine precipitation during 1995–2002. International Journal of Climatology, 30, 947–961. https://doi.org/10.1002/joc.1932.

Sukovich, E.M., Ralph, F.M., Barthold, F.E., Reynolds, D.W., Novak, D.R. (2014) Extreme quantitative precipitation forecast performance at the Weather Prediction Center from 2001 to 2011. Weather and Forecasting, 29, 894–911. https://doi.org/10.1175/WAF-D-13-00061.1.

Wilks, D.S. (2011) Statistical Methods in the Atmospheric Sciences. 3rd Edition. Elsevier, 676 pp.

7 Main results and discussion

7.1 Extreme large-scale hydrometeorological events

Although assessed in a similar way combining event magnitude and spatial extent, the lists of large-scale precipitation and flood extremes overlapped only to a limited extent. In case of extreme flood events, those of the cold half-year predominated with peaks in January and March. The secondary frequency maximum occurred in July, but in general, summer events accounted for only one-third of the major floods. Only when the threshold for the flood peak discharges was raised from two- to ten-year return period, warm half-year events accounted for almost half of the cases. In contrast, extreme precipitation events were distributed over the whole year but with higher concentration and extremity in its warmer half. The discrepancy between the lists of extreme precipitation and floods can be justified by a large number of winter floods that partially originated from snowmelt and did not depend only on extreme precipitation (Uhlemann et al., 2010). Although these floods generally reach lower return periods of discharge values, they may be very extensive (Brázdil et al., 2005), causing their frequent representation among the major flood events. The flood of March 1988 can be an example that ranked second in the list of the major floods and was even first by Uhlemann et al. (2010). However, the event did not occur among the extreme precipitation events. In fact, only a few cold half-year events appeared in both lists, e.g. the event at the end of 1993 or in October/November 1998, which affected only the western part of central Europe. On the other hand, the list of extreme floods included the summer precipitation extremes from July 1981 and 1997, June 2013 and August 2002, which (in this order) represented the maximum recorded precipitation events. In the list of extreme floods, these events belonged to the top twenty, the floods in 2013 and 2002 were even the first and the third largest, respectively. Such a high ranking may be related to the wet conditions before flooding events (Grams et al., 2014; James et al., 2004) and also to the unusually large affected area in 2013.

The size of the affected area largely controls the value of the flood extremity index of Uhlemann et al. (2010) and the Weather extremity index for the evaluation of precipitation extremes of Müller and Kašpar (2014), too. Therefore, some events that occurred on the edge of the study area could be underestimated. The flood of July 1997 is an example of the underestimation, as in addition to the

Oder River basin, the flood also affected the Vistula basin to the east of the study area (Kundzewicz et al., 1999). In the list of extreme floods, the 1997 event was at the 18th position and its rating would likely be higher if we consider the Vistula basin. This may also apply to the May 2010 flood, which was well described by Bissolli et al. (2011) as an event of a large extent and high intensity, but it did not appear in the list of extreme floods and was ranked only as of the 50th extreme precipitation event. At the same time, it is possible that some cold half-year events on the western edge of the study area was underestimated as well, and if a larger area is considered, their ranking would probably be a little different.

Regarding the seasonal distribution of extreme flood and precipitation events, there was a clear difference between the western and the eastern parts of the study area: the number of cold half-year events decreased towards the east, whereas the number of warm half-year events increased in the same direction. Many events resembled each other in where heavy precipitation occurred. Therefore, it was possible to divide the extreme precipitation events according to the similarity in the spatial patterns into two main types of events that basically occurred either in the west or in the east. The finer clustering then divided the events into five groups. Only two of them, namely ED (Elbe-Danube) and O (Oder), were represented among the top ten central European extreme precipitation events. These events were exceptional in their seasonality too, because they occurred exclusively from the end of May to the beginning of September. Three other groups consisted of generally lower extreme events rather equally distributed throughout the year, so their seasonal pattern was not so obvious. Within the eastern-type events, the only winter cases appeared in the RD (Rhine-Danube) group, when mainly the Upper Rhine and the Danube without the Morava basin were affected. Despite the expectations, the western-type precipitation events were not predominantly of a winter character as were the flood extremes (Beurton and Thieken, 2009), but in fact, a lot of these events occurred during the spring and autumn within the Rhine basin (R group) or even in summer months in case of the northwestern part of central Europe (NW group).

7.2 Circulation causes

Some studies previously indicated a connection between moisture transport and extreme precipitation (Lavers, Villarini, 2013; Müller and Kašpar, 2011). However, the supply of moisture itself needs to be supported by the upward motion of air (Giannakaki and Martius, 2015; Doswell et al., 1998). Therefore, in the presented thesis, the circulation conditions were analysed quantitatively by examining moisture flux magnitudes and direction in the area of extra high upward vertical velocity. Three types of events were recognized: (i) events with dominating moisture flux from the northern sector (*Nf*), (ii) events with dominating moisture flux from the western sector (*Wf*), and (iii) weak flux events (*Ot*). The two significant directions of moisture flux – western and northern – reflect the main synoptic patterns bringing moisture to central Europe from the Atlantic and Mediterranean, respectively (Hofstätter et al., 2017). Additional analysis showed that these types of moisture flux conditions corresponded perfectly with the seasonal and spatial patterns of extreme

precipitation events: events with prevailing northern moisture flux were concentrated only in the warm half-year and affected mainly eastern central Europe, while events with prevailing western moisture flux occurred in the west and exclusively from September to March. In summary, the difference between the two main groups of extreme precipitation events in central Europe can be explained by the seasonal distribution of extra high values of moisture flux from the respective sectors. The last group of weak flux events did not represent the largest precipitation extremes; the group consisted of events of various synoptic causes or even convective events that occurred usually during warm half-year in the western part of central Europe.

Mainly in case of *Nf* events, the extremity of circulation, i.e. anomalies of moisture flux, explained well the occurrence of relevant precipitation extremes. However, the degree of agreement between extreme circulation conditions and extreme precipitation depended on the threshold of the vertical velocity that determined the extra high values of that variable. Generally, a stricter threshold and higher data resolution of ERA5 reanalysis in comparison with ERA-Interim resulted in a closer relationship between circulation and precipitation extremes. In contrast, the relationship between anomalies of western moisture flux and the respective precipitation events was less clear. Western fluxes were often too large even on days without significant precipitation extremes. The reason could be that the moisture flux is directly proportional to wind velocity, which is usually stronger in the case of western fluxes; this fact allows windstorms to reach high moisture flux values, too. Although wind and precipitation extremes occur relatively often simultaneously during the winter months (Martius et al., 2016), some strong western moisture flux events did not correspond with precipitation extremes.

7.3 Predictability of events

Microphysical phenomena, such as precipitation, suffer from a lack of forecast skill in numerical weather prediction, especially in case of extreme precipitation (Herman and Schumacher, 2016). Due to a close connection between anomalies of northern moisture flux and extreme precipitation of the respective type, we could ask a question whether the predictability of moisture flux anomalies is good enough to support the correct prediction of extreme precipitation events.

In fact, only a few studies have compared the predictability of precipitation and moisture transport; e.g. Lavers et al. (2014, 2016) confirmed the higher predictability of integrated vapour transport compared to precipitation. Similarly, this thesis demonstrated excellent predictability for zonal and meridional moisture fluxes at the 850 hPa level. However, while the predictability of moisture flux itself proved to be very good and more reliable than of precipitation, generally less accurate forecasts of the vertical velocity negatively affected the predictability of moisture flux accumulated in the area of extra high upward vertical velocity. It produced a large number of false alarms, especially in case of summer precipitation events with prevailing northern moisture flux.

Despite the general inaccuracy, the forecast of moisture flux anomalies in the area of extra high upward vertical velocity was good and stable up to six days in advance in all cases of extreme events that produced major central European summer floods, such as in July 1981 and 1997, August 2002 and June 2013. There was no such continuity for less extreme or false alarm events, thanks to which we can conclude that the calculation of moisture flux anomalies from numerical weather prediction could be useful as a supporting tool at least for predicting large extreme precipitation events of *Nf* type. For less extreme events, forecasts were not reliable enough, and a worse vertical velocity forecast thus made a more general use impossible.

8 Conclusions

According to various studies, the number of extreme precipitation events is increasing and probably will increase in the future, but this is not so certain in the case of extreme floods. This thesis cannot approve or reject the statement, as the study period was quite short for analysing trends of very rare events. Generally, the extreme events rather accumulated in certain periods when also some shifts in the seasonal distribution were evident. However, the vulnerability of humans to extreme hydrometeorological events is increasing regardless of the trends, and therefore we should study these extremes, not only their consequences but also their causes.

Through the thesis, all of the parts of the "hydro-synoptic continuum" was considered. Thanks to the larger area of interest, it was possible to examine the spatial structure of events, possible differences between them, and their relation to conditions in the atmosphere. The application of the acquired knowledge in the forecasting of extreme precipitation events was the added value. The thesis emphasized the practical use of moisture flux forecast as a supporting tool for extreme precipitation warnings, which could improve preparedness for extreme precipitation and flood events.

Predominantly, the study focused on large-scale extreme precipitation and floods, for which the size of the affected area is as crucial in the extremity assessment as the magnitude of precipitation totals or flood discharges. The advantage of the extremity indices used is that they connect both aspects. However, even the same concept produced two different lists of extreme events. The lists matched perfectly only in case of major summer events that affected mainly Elbe, Danube and/or Oder basins and resulted in the largest and most damaging summer floods in central Europe. All of those summer extremes were associated with anomalous northern moisture fluxes in the lower troposphere, which were well predicted already six days in advance. In the future, the forecasts of moisture flux anomalies could complement the quantitative precipitation forecast for the prediction of high-impact summer events.

Although the contribution for summer extreme events is clear, the issue of cold half-year events with a prevailing western moisture flux remains unresolved. The problem is that the correspondence between extreme western moisture flux and the precipitation events of that type was not so strong because of the cases when high values of moisture flux from the west occurred due to extra high

wind velocities despite rather small air moisture. It is, therefore, necessary to look for other circulation anomalies or their combinations that would better suit the occurrence of these extremes.

The problematic forecast of vertical velocities is the second issue that should be addressed in further research. Worse vertical velocity forecast negatively affected the predictability of moisture flux anomalies especially in case of less extreme events. Alternatively and independently of the vertical velocity, it would be possible to employ integrated vapour transport, as the variable is often associated with flood and precipitation extremes in other studies. However, its use can be problematic due to the large wind shear that occurs during summer events with the flux of moisture from the northern sector. This statement would need to be confirmed, as well as the results obtained from ERA-Interim forecasts, which should be verified in the future using other numerical weather prediction models with finer horizontal resolution.

References (excluding Sections 2.3.2 and 3-6)

Barredo, J.I., 2007. Major flood disasters in Europe: 1950–2005. Natural Hazards, 42, 125–148. https://doi.org/10.1007/s11069-006-9065-2.

Beurton, S., Thieken, A.H., 2009. Seasonality of floods in Germany. Hydrological Sciences Journal, 54, 62–76. https://doi.org/10.1623/hysj.54.1.62.

Bissolli, P., Friedrich, K., Rapp, J., Ziese, M., 2011. Flooding in eastern central Europe in May 2010—reasons, evolution and climatological assessment. Weather, 66, 147–153. https://doi.org/10.1002/wea.759.

Blöschl, G., Nester, T., Komma, J., Parajka, J., Perdigão, R.A.P., 2013. The June 2013 flood in the Upper Danube Basin, and comparisons with the 2002, 1954 and 1899 floods. Hydrology and Earth System Sciences, 17, 5197–5212. https://doi.org/10.5194/hess-17-5197-2013.

Brázdil, R., Dobrovolný, P., Elleder, L., Kakos, V., Kotyza, O., Květoň, V., Macková, J., Štekl, V., Tolasz, R., Valášek, H., 2005. Historické a současné povodně v České republice. Masarykova Univerzita v Brně a Český hydrometeorologický ústav v Praze, Brno, Praha, 370 s.

Caspary, H.J., 1995. Recent winter floods in Germany caused by changes in the atmospheric circulation across Europe. Physics and Chemistry of the Earth, 20, 459–462.

Copernicus Climate Change Service (C3S), 2017. ERA5: Fifth generation of ECMWF atmospheric reanalyses of the global climate. In: Copernicus Climate Change Service Climate Data Store (CDS), https://cds.climate.copernicus.eu/cdsapp#!/home.

Čekal, R., 2005. Hydrosynoptická analýza povodňových situací v povodí Horní Ohře. Disertační práce. Katedra fyzické geografie a geoekologie Přf UK, Praha.

Dee, D.P., and Coauthors, 2011. The ERA-Interim reanalysis: configuration and performance of the data assimilation system. Quarterly Journal of the Royal Meteorological Society, 13, 553–597. https://doi.org/10.1002/qj.828.

Doswell III, C.A., Ramis, C., Romero, R., Alonso, S., 1998. A diagnostic study of three heavy precipitation episodes in the western Mediterranean region. Weather and Forecasting, 13, 102–124. https://doi.org/10.1175/1520-0434(1998)013<0102:ADSOTH>2.0.CO;2.

eHYD, 2021. Hydrographic data of Austria, http://ehyd.gv.at/ (last access: 9 May 2016).

Elleder, L., 2007. Historické extrémní případy povodní v povodí Labe a Vltavy. In: Langhammer, J. (ed.): Změny v krajině a povodňové riziko. Přírodovědecká fakulta Univerzity Karlovy, Praha.

EEA (European Environment Agency), 2019. Economic losses from climate-related extremes in Europe, https://www.eea.europa.eu/data-and-maps/indicators/direct-losses-from-weather-disasters-3/assessment-2 (last access: 23 November 2020).

Francou, J. and Rodier, J.-A.: Essai de classification des crues maximales observées dans le monde. Cahiers ORSTOM, Série Hydrologie, IV, 19–46, 1967.

Froidevaux, P., Martius, O., 2016. Exceptional integrated vapour transport toward orography: an important precursor to severe floods in Switzerland. Quarterly Journal of Royal Meteorological Society, 142, 1997–2012. https://doi.org/10.1002/qj.2793.

Giannakaki, P., Martius, O., 2015. Synoptic-scale flow structures associated with extreme precipitation events in northern Switzerland. International Journal of Climatology, 36, 2497–2515. https://doi.org/10.1002/joc.4508.

Grams, C.M., Binder, H., Pfahl, S., Piaget, N., Wernli, H., 2014. Atmospheric processes triggering the central European floods in June 2013. Natural Hazards and Earth System Sciences, 14, 1691–1702. https://doi.org/10.5194/nhess-14-1691-2014.

GRDC, 2020. River discharge data, http://www.bafg.de/GRDC/ (last access: 23 February 2017).

Herman, G.R., Schumacher, R.S., 2016. Extreme Precipitation in Models: An Evaluation. Weather and Forecasting, 31, 1853–1879. https://doi.org/10.1175/WAF-D-16-0093.1.

Herschy, R.W. (Ed.), 2003. World Catalogue of Maximum Observed Floods, IAHS Press, Wallingford, IAHS-AISH Publ. 284.

Hess, P., Brezowsky, H., 1952. Katalog der Großwetterlagen Europas. Ber. Dt. Wetterd. in der US-Zone 33.

Hladný, J., 2007. Fakta a mýty o povodních. In: Langhammer, J. (ed.): Povodně a změny v krajině. Katedra fyzické geografie a geoekologie Přírodovědecké fakulty Univerzity Karlovy a Ministerstvo životního prostředí ČR, Praha. ISBN 978-80-86561-86-8.

Hofstätter, M., Lexer, A., Homann, M. and Blöschl, G., 2017. Large-scale heavy precipitation over central Europe and the role of atmospheric cyclone track types. International Journal of Climatology, 38(Suppl. 1), e497–e517. https://doi.org/10.1002/joc.5386.

Huth, R., Beck, C., Philipp, A., Demuzere, M., Ustrnul, Z., Cahynová, M., Kyselý, J., Tveito, O.E., 2008. Classifications of atmospheric circulation patterns: recent advances and applications. Annals of the New York Academy of Sciences, 1146, 105–152. https://doi.org/10.1196/annals.1446.019.

IMGW-PIB, 2021. Central database, https://dane.imgw.pl/ (last access: 26 February 2017).

IPCC, 2014. Climate Change 2014: Synthesis Report. Contribution of Working Groups I, II and III to the Fifth Assessment Report of the Intergovernmental Panel on Climate Change [Core Writing Team, Pachauri, R.K., Meyer, L.A. (eds.)]. IPCC, Geneva, Switzerland, 151 pp.

Jacobeit, J., Glaser, R., Luterbacher, J., Wanner, H., 2003. Links between flood events in central Europe since AD 1500 and largescale atmospheric circulation modes, Geophysical Research Letters, 30, 1172–1175, https://doi.org/10.1029/2002GL016433.

Jacobeit, J., Philipp, A., Nonnenmacher, M., 2006. Atmospheric circulation dynamics linked with prominent discharge events in Central Europe. Hydrological Sciences Journal, 51, 946–965. https://doi.org/10.1623/hysj.51.5.946.

James, P., Stohl, A., Spichtinger, N., Eckhardt, S., Forster, C., 2004. Climatological aspects of the extreme European rainfall of August 2002 and a trajectory method for estimating the associated evaporative source regions. Natural Hazards and Earth System Sciences, 4, 733–746. https://doi.org/10.5194/nhess-4-733-2004.

Kašpar, M., Müller, M., 2010. Variants of synoptic-scale patterns inducing heavy rains in the Czech Republic. Physics and Chemistry of the Earth, 35, 477–483. https://doi.org/10.1016/j.pce.2009.11.004.

Kašpar, M., Müller, M., 2014. Combinations of large-scale circulation anomalies conducive to precipitation extremes in the Czech Republic. Atmospheric Research, 138, 205–212. https://doi.org/10.1016/j.atmosres.2013.11.014.

Kašpar, M., Müller, M., Crhová, L., Holtanová, E., Polášek, J.F., Popa, L., Valeriánová, A., 2017. Relationship between Czech windstorms and air temperature. International Journal of Climatology, 37, 11–24. https://doi.org/10.1002/joc.468.

Keef, C., Svensson, C., and Tawn, J.A., 2009. Spatial dependence in extreme river flows and precipitation for Great Britain. Journal of Hydrology, 378, 240–252.

Klein Tank, A.M.G., and Coauthors, 2002. Daily dataset of 20th-century surface air temperature and precipitation series for the European Climate Assessment. International Journal of Climatology, 22, 1441–1453. https://doi.org/10.1002/joc.773.

Konrad, C.E., 2001. The most extreme precipitation events over the eastern United States from 1950 to 1996: considerations of scale. Journal of Hydrometeorology, 2, 309–325.

Kundzewicz, Z.W., Pińskwar, I., Brakenridge, G.R., 2013. Large floods in Europe, 1985–2009, Hydrological Sciences Journal, 58, 1–7. https://doi.org/10.1080/02626667.2012.745082.

Kundzewicz, Z.W., Szamalek, K., Kowalczak, P., 1999. The great flood of 1997 in Poland. Hydrological Sciences Journal, 44, 855–870. https://doi.org/10.1080/02626669909492285.

Kyselý, J., 2009. Trends in heavy precipitation in The Czech Republic over 1961–2005. International Journal of Climatology, 29, 1745–1758. https://doi.org/10.1002/joc.1784.

Lavers, D.A., Pappenberger, F., Richardson, D.S., Zsoter, E., 2016. ECMWF extreme forecast index for water vapor transport: a forecast tool for atmospheric rivers and extreme precipitation. Geophysical Research Letters, 43(22), 11852– 11858. https://doi.org/10.1002/2016gl071320.

Lavers, D.A., Pappenberger, F., Zsoter, E., 2014. Extending medium-range predictability of extreme hydrological events in Europe. Nature Communications, 5, 5382, https://doi.org/10.1038/ncomms6382.

Lavers, D.A., Villarini, G., 2013. The nexus between atmospheric rivers and extreme precipitation across Europe. Geophysical Research Letters, 40, 3259–3264. https://doi.org/10.1002/grl.50636.

Lhotka, O., Kyselý, J., 2014. Characterizing joint effects of spatial extent, temperature magnitude and duration of heat waves and cold spells over central Europe. International Journal of Climatology, 35, 1232–1244. https://doi.org/10.1002/joc.4050.

Łupikasza, E.B., 2017. Seasonal patterns and consistency of extreme precipitation trends in Europe, December 1950 to February 2008. Climate Research, 72, 217–237. https://doi.org/10.3354/cr01467.

Martius, O., Pfahl, S., Chevalier, C., 2016. A global quantification of compound precipitation and wind extremes. Geophysical Research Letters, 43, 7709–7717. https://doi.org/10.1002/2016GL070017.

Martius, O., Zenklusen, E., Schwierz, C., Davies, H.C., 2006. Episodes of alpine heavy precipitation with an overlying elongated stratospheric intrusion: a climatology. International Journal of Climatology, 26, 1149–1164. https://doi.org/10.1002/joc.1295.

Messmer, M., Gómez-Navarro, J.J. and Raible, C.C., 2015. Climatology of Vb cyclones, physical mechanisms and their impact on extreme precipitation over central Europe. Earth System Dynamics, 6, 541–553. https://doi.org/10.5194/esd-6-541-2015.

Minářová, J., Müller, M., Clappier, A., Kašpar, M., 2018. Comparison of extreme precipitation characteristics between the Ore Mountains and the Vosges Mountains (Europe). Theoretical and Applied Climatology, 133, 1249–1268. https://doi.org/10.1007/s00704-017-2247-x.

Mudelsee, M., Börngen, M., Tetzlaff, G., Grünewald, U., 2004. Extreme floods in central Europe over the past 500 years: Role of cyclone pathway Zugstrasse Vb. Journal of Geophysical Research, 109, D23101. https://doi.org/10.1029/2004JD005034.

Müller, M., Kašpar, M., 2010. Quantitative aspect in circulation type classifications – an example based on evaluation of moisture flux anomalies. Physics and Chemistry of the Earth, 35, 484–490. https://doi.org/10.1016/j.pce.2009.09.004.

Müller, M., Kašpar, M., 2011. Association between anomalies of moisture flux and extreme runoff events in the south-eastern Alps. Natural Hazards and Earth System Sciences, 11, 915–920. https://doi.org/10.5194/nhess-11-915-2011.

Müller, M., Kašpar, M., 2014. Event-adjusted evaluation of weather and climate extremes. Natural Hazards and Earth System Sciences, 14, 473–483. https://doi.org/10.5194/nhess-14-473-2014.

Müller, M., Kašpar, M., Matschullat, J., 2009a. Heavy rains and extreme rainfall–runoff events in Central Europe from 1951 to 2002. Natural Hazards and Earth System Sciences, 9, 441–450. https://doi.org/10.5194/nhess-9-441-2009.

Müller, M., Kašpar, M., Řezáčová, D., Sokol, Z., 2009b. Extremeness of meteorological variables as an indicator of extreme precipitation events. Atmospheric Research, 92, 308–317. https://doi.org/10.1016/j.atmosres.2009.01.010.

Nissen, K.M., Ulbrich, U. and Leckebusch, G.C., 2014. Vb cyclones and associated rainfall extremes over central Europe under present day and climate change conditions. Meteorologische Zeitschrift, 22, 649–660. https://doi.org/10.1127/0941-2948/2013/0514.

Parker, W.S., 2016. Reanalyses and observations: What's the difference? Bulletin of the American Meteorological Society, 97, 1565–1572. https://doi.org/10.1175/BAMS-D-14-00226.1.

Ren, F., Cui, D., Gong, Z., Wang, Y., Zou, X., Li, Y., Wang, S. and Wang, X., 2012. An objective identification technique for regional extreme events. Journal of Climate, 25, 7015–7027. https://doi.org/10.1175/JCLI-D-11-00489.1.

Roberts, J.F., Champion, A.J., Dawkins, L.C., Hodges, K.I., Shaffrey, L.C., Stephenson, D.B., Stringer, M.A., Thornton, H.E., Youngman, B.D., 2014. The XWS open access catalogue of extreme European windstorms from 1979 to 2012. Natural Hazards and Earth System Sciences, 14, 2487–2501. https://doi.org/10.5194/nhess-14-2487-2014.

Schröter, K., Kunz, M., Elmer, F., Mühr, B., Merz, B., 2015. What made the June 2013 flood in Germany an exceptional event? A hydro-meteorological evaluation. Hydrology and Earth System Sciences, 19, 309–327. https://doi.org/10.5194/hess-19-309-2015.

Seibert, P., Frank, A., Hofmayer, H., 2007. Synoptic and regional patterns of heavy precipitation in Austria. Theoretical and Applied Climatology, 87, 139–153. https://doi.org/10.1007/s00704-006-0198-8.

Sodemann, H., Zubler, E., 2010. Seasonal and inter-annual variability of the moisture sources for Alpine precipitation during 1995–2002. International Journal of Climatology, 30, 947–961. https://doi.org/10.1002/joc.1932.

Smith, K., 2004. Environmental hazards: assessing risk and reducing disaster. 4th Edition. Routledge, 306 pp.

Sukovich, E.M., Ralph, F.M., Barthold, F.E., Reynolds, D.W., Novak, D.R., 2014. Extreme quantitative precipitation forecast performance at the Weather Prediction Center from 2001 to 2011. Weather and Forecasting, 29, 894–911. https://doi.org/10.1175/WAF-D-13-00061.1.

Šmídová, J., 2009. Analýza mechanismu vzniku povodní v povodí Opavy po profil Opava. Diplomová práce. Katedra fyzické geografie a geoekologie Přf UK, Praha.

Uhlemann, S., Thieken, A. H., Merz, B., 2010. A consistent set of trans-basin floods in Germany between 1952–2002, Hydrology and Earth System Sciences, 14, 1277–1295, https://doi.org/10.5194/hess-14-1277-2010.

Ulbrich, U., Brücher, T., Fink, A.H., Leckebusch, G.C., Krüger, A., Pinto, J.G., 2003a. The central European floods of August 2002: Part 1 – Rainfall periods and flood development. Weather, 58, 371–377. https://doi.org/10.1256/wea.61.03A.

Ulbrich, U., Brücher, T., Fink, A.H., Leckebusch, G.C., Krüger, A., and Pinto, J.G., 2003b. The central European floods of August 2002: Part 2 – Synoptic causes and considerations with respect to climate change. Weather, 58, 434–442. https://doi.org/10.1256/wea.61.03B.

Ulbrich, U., Fink, A., 1995. The January 1995 flood in Germany: Meteorological versus hydrological causes. Physics and Chemistry of the Earth, 20, 439–444. https://doi.org/10.1016/S0079-1946(96)00002-X.

Ustrnul, Z., Czekierda, D., 2001. Circulation background of the atmospheric precipitation in Central Europe (based on the Polish example). Meteorologische Zeitschrift, 10, 103–111. https://doi.org/10.1127/0941-2948/2001/0010-0103.

Ustrnul, Z., Wypych, A., Henek, E., Czekierda, D., Walawender, J., Kubacka, D., Pyrc, R., Czernecki, B., 2014. Meteorological hazard atlas of Poland. Kraków: Instytut Meteorologii i Gospodarki Wodnej, Wydawnictwo Attyka.

Valeriánová, A., Crhová, L., Holtanová, E., Kašpar, M., Müller, M., Pecho, J., 2017. High temperature extremes in The Czech Republic 1961–2010 and their synoptic variants. Theoretical and Applied Climatology, 127, 17–29. https://doi.org/10.1007/s00704-015-1614-8.

Valeriánová, A., Holtanová, E., Crhová, L., 2013. Klimatologie příčinných srážek červnové povodně v České republice v roci 2013. Meteorologické Zprávy, 66, 190–196.

van Bebber, W.J., 1891. Die Zugstrassen der barometrischen Minima nach den Bahnenkarten der deutschen Seewarte für den Zeitraum 1875–1890. Meteorologische Zeitschrift, 8, 361–366.

van den Besselaar, E.J.M., Klein Tank, A.M.G., Buishand, T.A., 2013. Trends in European precipitation extremes over 1951–2010. International Journal of Climatology, 33, 2682–2689. https://doi.org/10.1002/joc.3619.

Wilks, D.S., 2011. Statistical Methods in the Atmospheric Sciences. 3rd Edition. Elsevier, 676 pp.

Wypych, A., Ustrnul, Z., Czekierda, D., Palarz, A., Sulikowska, A., 2018. Extreme precipitation events in the Polish Carpathians and their synoptic determinants. Időjárás, 122, 145–158. https://doi.org/10.28974/idojaras.2018.2.3.

Zhang, X., Alexander, L., Hegerl, G.C., Jones, P., Klein Tank, A., Peterson, T.C., Trewin, B. and Zwiers, F.W., 2011. Indices for monitoring changes in extremes based on daily temperature and precipitation data. WIREs: Climate Change, 2, 851–870. https://doi.org/10.1002/wcc.147.